UNIVERSIDAD DE CONCEPCIÓN
FACULTAD DE CIENCIAS FÍSICAS Y MATEMÁTICAS

INDEFINITE CAUSAL ORDER TOWARDS CONTINUOUS-VARIABLE QUANTUM SYSTEMS

Por:

JORGE IGNACIO ANTONIO ESCANDÓN MONARDES

Tesis para optar al grado académico de
Doctor en Ciencias Físicas

Abril 2025
Concepción, Chile

Profesor Guía:

Dr. Stephen Patrick Walborn

A mis ancestros

AGRADECIMIENTOS

Aunque esta tesis está escrita en inglés, he decidido escribir esta pequeña sección en mi lengua materna, pues no sé si consiga expresar con la misma precisión en un segundo idioma mi gratitud hacia tantas personas que han sido parte de este proceso de formación que concluye con la presente tesis.

Mi formación de postgrado se inició formalmente en 2021 cuando comencé mis estudios doctorales, sin embargo el proceso comenzó mucho antes, cuando ya me había alejado de una carrera orientada a la investigación y decidí volver a ella tras varios años dedicado a la divulgación y a la pedagogía. Tras la decisión de perseguir estudios de postgrado, hubo una primera etapa de formación informal. Debo agradecer ante todo a Jorge Muñoz Soto, quien fue mi mentor y me acompañó durante la etapa previa al doctorado. Mi más profunda gratitud por todas las horas que dedicó a orientarme hasta encontrar el área de investigación que más me motivaba, por los métodos que me inculcó, modelando mi razonamiento con la paciencia de un artesano que esculpe una joya en bruto, a veces bastante en bruto. Me enseñó que la formación más valiosa es aquella que altera el "ser" de alguien, y aunque él no es físico, llegó el día en que por primera vez salieron de mi boca, como escapándose, las palabras "soy físico". Gracias profesor por ser el artífice de tan notable punto de inflexión en mi historia de vida y por transmitirme un modo de ser académico, el cual espero tener la capacidad de honrar y transmitir durante el resto mi carrera.

Debo agradecer también a Joquín Díaz de Valdés y Aldo Delgado, quienes creyeron en mí a mi regreso a la Universidad y me abrieron las puertas para retomar una carrera académica en la física y en la Universidad de Concepción. Su espaldarazo fue vital para quien en 2021 ya no era tan muchacho, pero tenía tantas dudas como un recién llegado.

Agradezco profundamente, y tal vez ni siquiera tenga palabras para agradecer como es debido, a mi supervisor Stephen P. Walborn, quien me acogió como su primer estudiante de doctorado desde que él arribase a la Universidad de Concepción. Su gozo por la física han sido motivación constante durante estos cuatro años y fracción, y su versatilidad para moverse entre la teoría, la técnica

experimental y las aplicaciones tecnológicas siguen siendo una inspiración. Gracias por ser un tutor presente y dedicado, por la retroalimentación constante que siempre consiguió elevar mi nivel de comprensión y ampliar mis horizontes en el área. Tengo confianza de que tras mi doctorado continuaremos colaborando decididamente en aquellos proyectos que tengamos en común.

Ignacio Ormazábal, con quien me reencontré en el doctorado después de muchos años, es otra persona que no puede faltar en los agradecimientos. Amigo, vecino, hermano mayor, compañero de compras. Unos años adelante en el doctorado en física y con una visión de planificación a futuro que no he conocido en nadie más. Frecuentemente me aconsejó acerca de cómo organizar mis tiempos y proyectar mi carrera, cómo "sacarle el jugo" a la beca y aprovechar al máximo los años del doctorado con miras a generar colaboraciones y una red que trascendiera mi alma mater. Sin sus consejos probablemente no habría alcanzado muchos de los hitos que marcaron mi paso por el postgrado.

El trabajo mancomunado con colegas, discutir ideas e intercambiar experiencias y métodos son de las facetas que más disfruto del trabajo académico. A todos mis compañeros de postgrado con quienes trabajamos en física cuántica, en especial a Leticia Tacca, Adheris Contreras, Felipe Quinteros, Kei Sawada, Nicolás Vera, Jorge Gidi, Katherine Muñoz, Mariano Uria, Nelson Villalba y Sebastián Ayala, muchas gracias por enriquecer la discusión y por compartir tantos buenos momentos dentro y fuera de la universidad.

Y si de colaboración se trata, Daniel Uzcátegui y Marco Rivera fueron los primeros con quienes discutimos ideas a profundidad y compartimos innumerables horas calculando en el pizarrón de su oficina, oficina que en muchas ocasiones fue incluso un refugio. ¡Cuántas horas dedicamos frente al computador programando juntos, ~~contabilizando los garabatos de Daniel~~ y editando hasta el más pequeño detalle de los artículos que luego publicaríamos! De desconocidos a colaboradores y de colaboradores a amigos. Les debo mucho del aprendizaje adquirido durante estos cuatro años (y del azúcar consumida también). Un millón de gracias por el apoyo académico, y un trillón por el apoyo moral y afectivo, por esas horas oscuras en que tuvieron la voluntad de escucharme y aconsejarme sobre temas que a veces poco tenían que ver con física.

En 2023 y 2024 "crucé el charco" a una ciudad que no existía en mi mapa mental y

de la cual terminaría por enamorarme: Gdańsk, Polonia. Debo agradecer a Stephen Walborn por la idea y especialmente a Marcin Pawłowski por recibirme dos veces para una pasantía doctoral en el Quantum Cybersecurity and Communications group en el International Centre for Theory of Quantum Technologies ICTQT. También a Łukasz Rudnicki, por el intercambio de ideas que, si bien no conseguimos que fueran más frecuentes, abrieron puertas insospechadas para el trabajo realizado durante el último año. Gracias también a Pedro Dieguez, por las valiosas discusiones sobre el quantum switch que resultaron en una serie de ideas para trabajo futuro que confío concretaremos más temprano que tarde. Y a todos los demás colegas y amigos de ICTQT, por recibirme tan cálidamente y hacerme sentir parte de ese lugar: Karthik Hosapete-Seshadri, Akshata Shenoy, Tushita Prasad, Chithra Ray, Lucas Pollyceno, Ekta Panwar, Anubhav Chaturvedi, Fernando Almaguer, Giovanni Scala, Giuseppe Viola, Luis Cort, Andre Malavazi, Marco Erba, Abhyoudai Shaleena y Aravinth Ravichandran. Mis disculpas si he olvidado a alguien en esta lista. Espero verlos pronto nuevamente.

Aún en Europa, debo agradecer a dos grandes mujeres que conocí estando allá y a los grupos de investigación de los que forman parte. Lina Vandré, gracias por ser la mejor anfitriona y por enseñarme que hacer física puede sentirse como un juego de niños. Aunque nuestra colaboración no está vinculada con esta tesis, tengo la confianza de que en el futuro volveremos a colaborar en algún nuevo tópico. De hecho, tenemos un experimento pendiente por implementar. Natália Móller, otra gran anfitriona y con gran experiencia en orden causal indefinido. Gracias por nutrir mis ideas con tu experiencia y proyectarlas más allá de lo que podía ver. Es un placer poder colaborar contigo y tengo muchas ansias de ver cómo los proyectos en los que ya estamos trabajando se desenvuelven. Sé que hay resultados muy interesantes aguardando por nuestro trabajo.

De regreso en Concepción, hay personas no vinculadas a la información cuántica que han acompañado todo el proceso de distintas formas. Lorena Sepúlveda, Pedro Contreras, José Huenchual y Nicolás Parra. Gracias por tantos almuerzos y risas. Sobre el alcohol no diré nada, sólo que ya no necesito el remedio para la hipertensión. Pero no se entusiasmen, no quiero arriesgar nuevos diagnósticos con métodos poco ortodoxos.

Respecto a la última etapa del doctorado, esta resultó ser la más solitaria, especialmente durante la escritura de esta tesis, la cual tuvo lugar durante mis

más recientes not-vacaciones. Y hubiese sido aún más solitaria si no fuera por Adheris Contreras y Constanza Rivas. Gracias por el apañe y el soporte durante este periodo crítico.

Gracias también a Carlos Baeza, mi psicólogo, que por motivos no académicos apareció en mi vida en 2021, y terminó siendo copiloto de un viaje de transformación gigante, cuyos efectos pudieron apreciarse también en el transcurso del doctorado. Quienes me conocieron antes de 2021 y me conocen hoy, sabrán reconocer las diferencias.

Y a mi familia. Gracias por creer siempre en mí. No hay minuto en que no sienta su apoyo y cariño.

Para finalizar, mis agradecimientos al programa de estudio Iniciativa Científica Milenio a través del Instituto Milenio de Investigación en Óptica MIRO, con el cual mantengo un convenio como becario colaborador, y a Agencia Nacional de Investigación y Desarrollo ANID, por financiar mis estudios a través de la Beca de Doctorado Nacional ANID Año Académico 2021 Folio 21211347. El trabajo contenido en esta tesis ha sido financiado también a través de Fondo Nacional de Desarrollo Científico y Tecnológico (ANID) N° 1200266, N° 1231940, N° 1230586, N° 3230427, N° 3230407, y ANID - Millennium Science Initiative Program - ICN17_012.

Gracias - Thanks - Dziękuję - Obrigado - Danke

Resumen

Orden causal indefinido ha atraído una creciente atención durante la última década, siendo el quantum switch su instancia más famosa. El quantum switch ha sido implementado en varios experimentos fotónicos y ha proporcionado ventajas computacionales en varias tareas. Sin embargo, orden causal indefinido ha sido apenas estudiado en sistemas cuánticos de variable continua. Esta tesis sugiere que las aplicaciones de orden causal indefinido en sistemas cuánticos de variable continua podrían ofrecer más amplias ventajas que utilizando sistemas cuánticos de dimensión finita. Nuestro enfoque es exploratorio, comparando el rendimiento del quantum switch con sistemas cuánticos de alta dimensión y de variable continua en algunas aplicaciones a computación y metrología cuánticas. En particular, utilizamos matrices de Hadamard complejas para introducir una familia generalizada de problemas de promesa, que se reduce a los conocidos problemas de promesa de Fourier y Hadamard como casos límite. Mostramos que el quantum switch proporciona ventaja tanto para el caso de varibale continua como discreta, y demostramos que sistemas de variable continua son necesarios para implementar el problema de promesa más general. Además, proponemos un procedimiento de estimación para transformaciones unitarias de dimensión d utilizando el quantum switch. Para $d > 2$, las transformaciones unitarias cercanas a la identidad se estiman saturando la cota cuántica de Cramér-Rao. Para $d = 2$, la estimación de todas las transformaciones unitarias es óptima en presencia de información previa. Remplazando la transformación unitaria por un canal cuántico arbitrario, mostramos que nuestro procedimiento codifica la matriz χ del canal en el estado de salida del sistema de control. Aunque orden causal indefinido no ofrece ventaja metrológica en nuestra propuesta, es importante señalar que una extensión al régimen de variable continua requeriría un sistema de control de dimensión infinita. Esto inspira la introducción del quantum switch de control continuo, dando lugar a nuevos fenómenos como el efecto acelerando/rallentando. Concluimos que el uso de sistemas de variable continua amplía el número de tareas que se benefician de orden causal indefinido y exhibe nuevos fenómenos dentro del área.

Keywords – Orden causal indefinido, quantum switch, fotónica, variable continua, problemas de promesa, metrología cuántica, transformaciones unitarias, ordenamiento temporal

Abstract

Indefinite causal order has attracted a growing attention during the last decade, with the quantum switch being its most prominent instance. The quantum switch has been implemented in several photonic experiments and has also provided computational advantages in several tasks. However, indefinite causal order on continuous-variable (CV) quantum systems has been barely studied. This thesis suggests that applications of indefinite causal order on CV quantum systems may offer broader advantages than using finite-dimensional quantum systems. We follow an exploratory approach comparing the performance of the quantum switch with high-dimensional and CV quantum systems in some applications to quantum computing and quantum metrology. In particular, we use Complex Hadamard matrices to introduce a generalised family of promise problems, which reduces to the known Fourier and Hadamard promise problems as limiting cases. We show that the quantum switch provides query advantage for both the continuous and discrete cases, and prove that a CV system is necessary for implementing the most general promise problem. In addition, we propose an estimation procedure for d-dimensional unitary transformations using the quantum switch. For $d > 2$, the unitary transformations close to the identity are estimated saturating the quantum Cramér-Rao bound. For $d = 2$, the estimation of all unitary transformations is also optimal with some prior information. We replace the unitary transformation by an arbitrary quantum channel and show that our procedure encodes the χ matrix of the channel in the output state of the control system. Although indefinite causal order does not offer metrological advantage in our proposal, it is worthy to note that an extension to the CV regime would require an infinite-dimensional control system. This inspires the introduction of the quantum switch with continuous control, which leads to new phenomena such as the accelerando/rallentando effect. We conclude that using CV systems enlarges the number of tasks benefited by indefinite causal order and exhibits new phenomena within the field.

Keywords – Indefinite causal order, quantum switch, photonics, continuous variable, promise problems, quantum metrology, unitary transformations, time-ordering

Contents

List of Tables

List of Figures

Chapter 1

Introduction

Let me invite you to listen to your favourite song. Please, look for it and press play. Reading this thesis can wait a few minutes.

Ready? Cool!

If you really played your favourite song, I could guess that you did not skip any part of it, you started listening from the first second of the recording until the last one. No pauses, no steps back and forth. A well defined sequence of sounds in a specific rhythm, carefully studied and performed by the artist. Now look for the album to which that song belongs. The order of the tracks in the album is most likely carefully designed as well, regardless you could choose the order in which you want to listen to them. If you want, you could randomly reshuffle the order of the tracks, although the whole experience would be a little different. Yes, you can reshuffle your playlist. But can you reshuffle the episodes of your life? Can you reshuffle the order of physical phenomena?

In Nature, some things cannot happen if another event, its cause, has not occurred beforehand. For example, we cannot expect a water leakage from a pipeline before the pipeline breaks, nor a plane to fly before being built. The effects cannot precede their causes. The order of the events is well defined and arranged in a timeline that runs from past to future, as in the best of musical compositions. We say that physical events are sorted in a *definite causal order*. By the way, the arrow of time is like a stubborn leader who does not wait nor turn back for us. We better give up trying to pause or remix the song of Nature!

Nevertheless, this thesis is about *indefinite causal order* (ICO). There are good reasons to explore the possibility of events without a definite order. The first of them is to examine the boundaries of the theories that we use to describe the universe. The second reason is plain: quantum mechanics allows for it.

In this introductory chapter we are going to present the concept of indefinite causal order and make a quick journey through its different flavours. We will start in Section 1.1 with a broad conceptual motivation for studying ICO, based on the approach of Lucien Hardy to quantum gravity. Then, we will introduce the quantum switch, which is a particular instance of ICO and the main character of this thesis, followed by the process matrices formalism and the gravitational quantum switch. In Section 1.1.5 we will comment on some ongoing debates within the field. In Section 1.2 we will notice a gap in the literature about indefinite causal order on continuous-variable quantum systems, what will lead us to define the objectives of this thesis in Section 1.3. Finally, in Section 1.4 we will outline the rest of the thesis. This chapter is intended as a conceptual introduction and we will avoid the use of equations whenever it is possible, though it is plenty of references for the interested reader. Technical details will be provided in further chapters when required.

Now let us start the trip and let the arrow of time flow.

1.1 Indefinite causal order

1.1.1 Hardy's program

Quantum theory and general relativity are the most succesful physical theories so far. They are able to explain together most of known physical phenomena. However, the golden dream of several physicists is to explain everything in one single theory involving both of them, that is, to achieve a sort of "quantum gravity" theory. The search for such a theory has been the motive for many researchers, Lucien Hardy among them. In 2007, introducing a very interesting approach, Hardy highligthed that general relativity is a deterministic theory where the causal structure is not predefined (it depends on the distribution of matter and energy), while quantum theory is a fundamentally probabilistic theory on a fixed

causal structure[1]. According to his reasoning, a quantum gravity theory should be expected to combine the radical aspects of both theories. In other words, it should be a *probabilistic theory with non-fixed causal structure* [1].

In a subsequent paper [2], Hardy discussed the consequences of an indefinite causal structure for computation. Algorithms, which are specific sequences of calculations, are the basic elements for computing. How could any algorithm be implemented or even defined when the causal structure and the order of events is non-fixed? Can an eventual quantum gravity computer outperform quantum and classical computers? By raising these questions Hardy implicitly invited the community of quantum information and quantum computation to join his research program.

Inspired by Hardy's ideas, at least three different approaches to indefinite causal order have been developed:

- **Quantum switch:** The first approach is based solely on quantum computation. It defines a higher-order operation, called the *quantum switch*, which consists in the application of two or more quantum operations in a coherent superposition of different orders, controlled by an ancillary system. The order of the operations remains indefinite unless the control system is measured in the computational basis. The quantum switch is a process allowed by quantum mechanics and has been already implemented in a number of experiments.

- **Process matrices framework:** In this approach, two parties are free to implement quantum operations on a quantum system according to the laws of quantum mechanics. Inside their labs there is a fixed Minkowski spacetime, but no causal structure is assumed out of the labs. Here, the connection between the outcomes and inputs of each lab is mediated by a *process matrix*. Physical processes such as state preparation, measurements and signalling from one lab to another can be fairly described by particular process matrices, but some non-physical processes are also allowed. Therefore, the process

[1]The causal structure of spacetime is usually understood as an order relation between spacetime points. Two points can be causally connected only if it is possible to send a signal from one to the other without surpassing the speed of light. We could say that the causal structure is a feature of the manifold describing spacetime, hence it depends on the distribution of matter and energy. In the case of quantum theory, we usually assume a fixed flat geometry, since quantum experiments are performed in a lab within a locally Minkowski spacetime.

matrices framework goes beyond quantum mechanics, although without dealing with gravity explicitly. One important feature of this approach is a precise definition of the notion of *causal nonseparability*, which is required to decide whether a given process is an instance of indefintie causal order or not. Actually, it has been shown, both theoretically and experimentally, that the quantum switch is a causally nonseparable process in this sense.

- **Superposition of causal structures:** The last approach is one that explicitly takes gravity into account. It postulates that spacetime can be treated as a quantum system and therefore can be assigned a quantum state. Particularly, any classical manifold can be related to a specific quantum state of the spacetime. Hence, an indefinite causal structure can be achieved just by superposing different manifolds. Interestingly, some particular gravitational scenarios can be devised in such a way that they reproduce the same effects as the quantum switch. This scenarios are naturally known as *gravitational quantum switches*.

In the following subsections we review these three different approaches to indefinite causal order. Although they raise relevant concerns regarding their physicality (see Section 1.1.5 for an overview on some ongoing debates), they push forward our understanding of quantum mechanics and explore what kind of phenomena we could expect in the realm of quantum gravity.

1.1.2 The quantum switch

1.1.2.1 Concept

The usual way to proceed in quantum computing is by encoding information in the state of a quantum system and then to process that information by performing certain quantum operations on the system. The final state of the quantum system is measured and hence the intended output of the computation is retrieved. This procedure is analogous to the evaluation of a function on a given input. But just like higher-order functions take other functions as input or output, we could define transformations which map quantum operations into quantum operations. Such higher-order maps are known as quantum supermaps and were introduced in Ref. [3] and extended to the notion of quantum combs in Ref. [4]. Operationally, these transformations can be seen as circuits with slots where

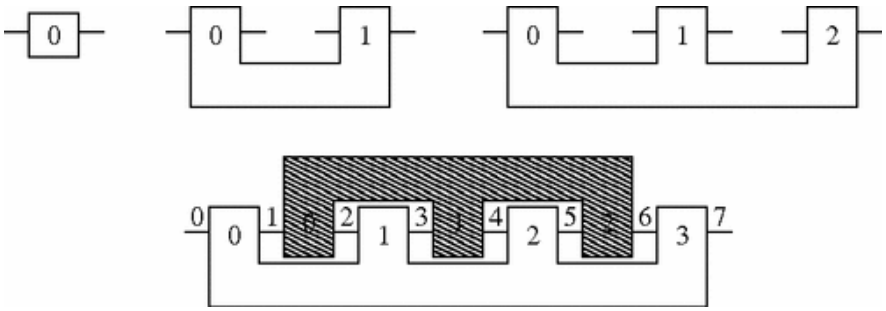

Figure 1.1.1: Quantum supermaps and quantum combs. A box represents a quantum operation or 1-comb (upper left); a diagram with two teeth represents a 2-comb, i.e., a supermap where a quantum box can be plugged (upper center); a diagram with three teeths represents a 3-comb where up to two boxes or one 2-comb can be plugged (upper right). When two combs are combined, the result is a new comb. For example, a 4-comb can take a 3-comb as input and transform it in a 1-comb as output (lower). Figure from Ref. [4].

the input operations, provided as black boxes or oracles, can be plugged. The resulting circuit corresponds to the output quantum operation (see Fig. 1.1.1).

The quantum switch, introduced in 2013 by Chiribella et al. [5], is a special example of quantum supermap. It consists in the application of two quantum channels $\mathcal{A}$ and $\mathcal{B}$ on a quantum system in one of two different orders, either $\mathcal{B} \circ \mathcal{A}$ or $\mathcal{A} \circ \mathcal{B}$. The order is coherently controlled by an ancillary qubit. Hereafter, the system on which $\mathcal{A}$ and $\mathcal{B}$ act will be called the *target system*, while the ancillary qubit will be called the *control system*. If the control is in state $|0\rangle$, $\mathcal{A}$ is applied before $\mathcal{B}$; conversely, if the control is in state $|1\rangle$, $\mathcal{B}$ is applied before $\mathcal{A}$ (see Fig. 1.1.2). Notice that this is a straightforward extension of a classical code where two subroutines are called in one specific order which depends on the truth value of an `if` statement. Here, the novelty is that the control system is characterized by a quantum state, which could be a superposition of $|0\rangle$ and $|1\rangle$, leading to a "superposition" of two different orders. For example, if the state of the control system is $|+\rangle = (|0\rangle + |1\rangle)/\sqrt{2}$, then the order of the operations will remain indefinite even after the application of both operations. Indeed, the order can be fixed in a later time by measuring the control system in the computational basis, with 50% of probability of getting one order or the other. Furthermore, the control system could be measured in a different basis, such as the σ_x eigenbasis, leading to an effective transformation on the target system that is not one of the two orders anymore. Particularly, if $\mathcal{A}$ and $\mathcal{B}$ are unitary operations, the target system will have undergone either the commutator or anticommutator of these

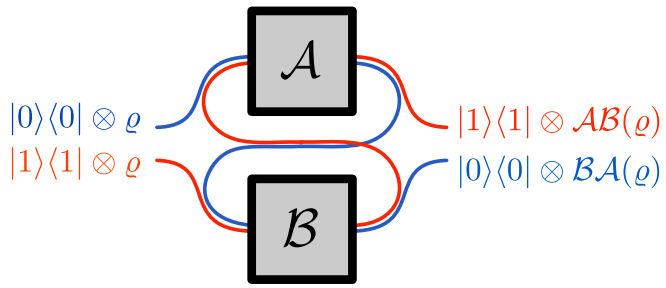

Figure 1.1.2: Quantum switch. The simplest quantum switch applies two gates in two different orders, which is coherently controlled by a control qubit. In photonic realizations, the order of the operations can be controlled by the path degree of freedom of photons, which we illustrate by colour wires. When the control is in a superposition of states, the order of the gates becomes indefinite.

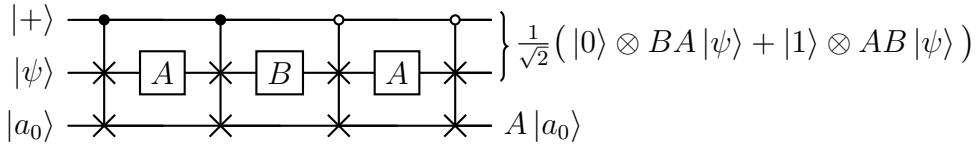

Figure 1.1.3: Fixed order circuit equivalent to the quantum switch. In order to implement the same transformation than the quantum switch in a fixed order circuit with unitary inputs A and B, at least one extra copy of one of the gates is required. Controlled-SWAP gates are used as a router to ensure the coherent control of the order of the operations.

operations.

In Ref. [5] the authors proved that the quantum switch "cannot be realized by inserting a single use of the input black box in a quantum circuit with fixed causal ordering of the gates". In other words, if we want to build a quantum circuit implementing this supermap, even in the simplest case of unitary gates, we would need to add at least one additional copy of one of the operations (see Fig. 1.1.3). Furthermore, for general quantum channels it is still unknown whether the quantum switch can be deterministically simulated with a finite number of copies of each channel [6]. This result strongly suggests two things: firstly, that the quantum switch may provide some computational advantages by reducing the number of queries to the quantum operations involved in some particular tasks (we will study exhaustively one of those tasks in Chapter 2), and secondly, that the quantum switch may be an instance of indefinite causal order, although a proper proof had to wait for a formal definition of causal nonseparability and the

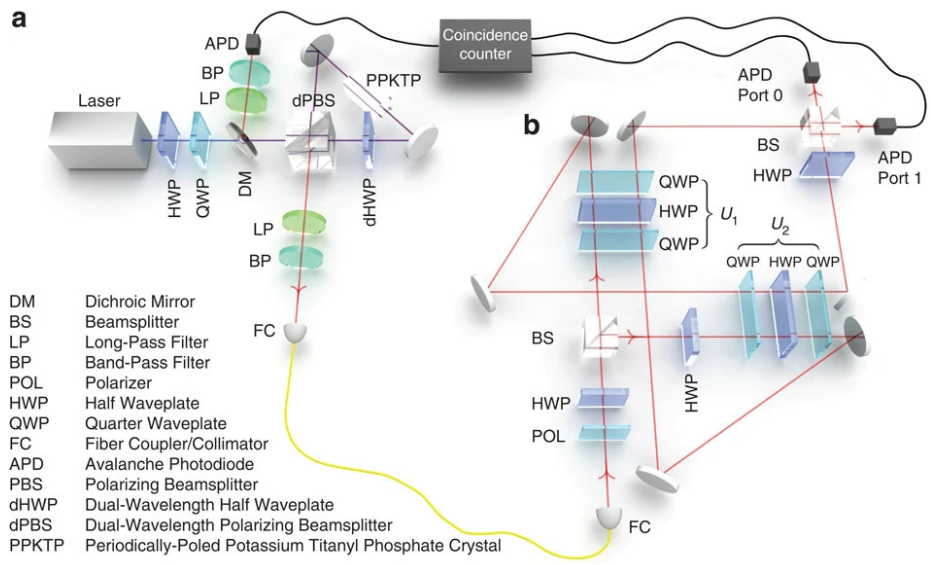

Figure 1.1.4: Photonic quantum switch by Procopio et al. (2015). (a) Source of entangled photons. One photon is used as a herald while the other is routed into a quantum switch. (b) Quantum switch. Unitaries U_1 and U_2, which act on the polarization degree of freedom, are applied on the photon in a superposition of two different orders, coherently controlled by the path degree of freedom. Figure from Ref. [7].

study of causal witnesses (cf. Section 1.1.3.2).

Despite the impossibility of implementing the quantum switch as a quantum circuit, it is still possible to build it as an interferometric setup. Indeed, as Fig. 1.1.2 suggests, if a given system can be routed through static devices in a superposition of two different paths, then the path followed by the system can act as control and some internal degree of freedom as target. This was the proposal by Procopio et al. in 2015, who reported the first experimental implementation of the quantum switch using a photonic platform [7]. In their experiment, the path of a photon is used as the control system and its polarization as the target. The superposition of paths is achieved using a balanced beam splitter and the operations acting on the polarization degree of freedom are unitary transformations implemented each one as a set of one half-wave and two quarter-wave plates. Then, a second beam splitter allows to measure the control system in the σ_x basis (see Fig. 1.1.4). The result of the measurement deterministically discriminates between commuting and anticommuting gates. Following this first experiment, many photonic implementations of the quantum switch have been reported, both for applications and certification of causal nonseparability [8–25].

The quantum switch has been also implemented on nuclear spins using nuclear magnetic resonance and coherently controlled interactions [26, 27]. For a thorough review on the experimental implementations of the quantum switch, see Ref. [28].

A generalization of the quantum switch to a larger number of gates, known as the *N-switch*, was introduced by Araújo, Costa and Brukner in 2014 [29]. It consists in the coherent control of the order of N transformations, although it is also possible to use only p of the $N!$ permutations of theses gates [30–32]. In Chapter 2 we will refer to this generalised quantum switch as (N, p)-*switch*[2]. The only experimental realization of a quantum switch with more than two gates so far was reported in 2021 by Taddei et al. [36] and was implemented at Universidad de Concepción.

1.1.2.2 Applications

Since its introduction, the quantum switch has seen a large amount of applications in several areas such as quantum computing, quantum communication, quantum thermodynamics and quantum metrology. Let us revisit some of them in this section.

1.1.2.2.1 Quantum computing. The first application of the quantum switch outperforming fixed order circuits was proposed by Giulio Chiribella in 2012. He showed that the quantum switch can deterministically discriminates between a pair of commuting and a pair of anticommuting unitaries, while fixed order circuits can only do this probabilistically [37]. This task was implemented experimentally in Refs. [7, 19] and extended and generalised as a family of promise problems using the (N, p)-switch in Refs. [29, 36, 38, 39]. We are going to talk extensively about these promise problems in Chapter 2.

Other application of the quantum switch for quantum computing is the inversion of a unitary evolution. A probabilistic protocol that takes an unknown unitary U and applies $U^\dagger$ on an arbitrary qubit was proposed in Ref. [40] and implemented using the quantum switch in Ref. [18]. It has been shown that some indefinite causal order processes can achieve greater success probability than any fixed order circuit for unitary inversion and unitary transposition when k copies of the

[2]Ref. [33] introduced a quantum switch of quantum switches, later generalised to higher-order quantum switches, also called *superswitches* [34, 35]. These nested quantum switches form a particular class of the (N, p)-*switch*.

unknown unitary are available, although these processes are different from the quantum switch and there is no clear intuition behind them [41–43].

The potential use of indefinite causal order processes for quantum computing has been also studied in connection with nonlocal quantum operations [44], Boolean functions [45], quantum machine learning [46], nonstabilizer operations [47] and distributed quantum computing [48].

1.1.2.2.2 Quantum communication. The first application of the quantum switch for quantum communication was introduced in Ref. [49]. There, it was proposed a tripartite communication task in which Charlie must calculate a function of two inputs provided by Alice and Bob. If the communication allowed between the parties is restricted to two bits, then the probability of success using fixed order processes is less than one, while the quantum switch allows the parties to succeed with probability 1. In a subsequent work, the same authors showed a similar task where the quantum switch offers an exponential saving in communication in the asymptotic limit [50]. This advantage was experimentally demonstrated in 2019 in the first implementation of the quantum switch with a high-dimensional target system [10].

The quantum switch admits general quantum channels as input and not only unitary transformations, which are just a particular class of quantum channels. Regarding noisy channels, Ebler, Salek and Chiribella showed in 2018 one of the most striking uses of the quantum switch: the activation of channel capacity. This phenomenon consists in an increase of the amount of information that a quantum channel can transmit. In particular, they showed that if two completely depolarizing channels, which have zero capacity, are applied in a superposition of two different orders, then some amount of information can now be transmitted [51]. The capacity activation mediated by the quantum switch is a phenomenon that appears also in the more general case of N partially depolarizing channels in a superposition of $p \leq N!$ orders [30–32, 52–54]. Furthermore, the phenomenon has been studied for general Pauli channels [33, 35, 55, 56], thermalizing channels [57] and amplitude damping channels [58]. One outstanding result was provided in Ref. [56], where it was shown that two copies of a specific entanglement-breaking channel in a quantum switch exhibit perfect transmission of quantum information if it is heralded by a measurement on the control system.

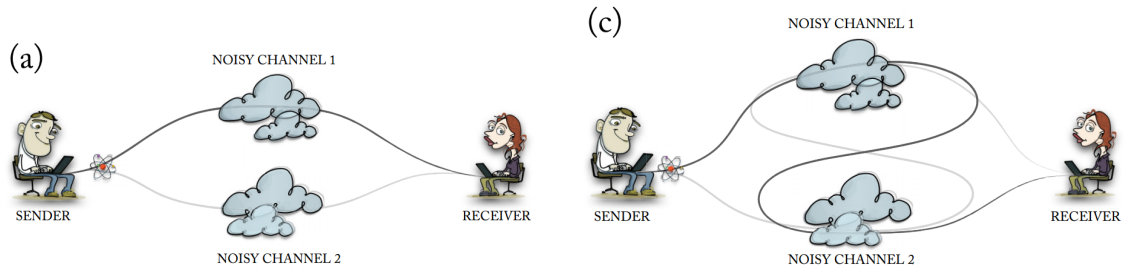

Figure 1.1.5: Coherent control of operations versus coherent control of orders. In the coherent control of operations (left), also called "superposition of quantum channels", two quantum channels are applied on a target system, each one in a different arm of an interferometer. Instead, in the quantum switch, or coherent control of order (right), both channels are applied in a sequence whose order depends on the path followed by the target system. Figure from Ref. [13]. The original figure also shows two additional arrays of two quantum channels, not discussed in this thesis.

The first experimental demonstration of the activation of channel capacity was reported in 2020 by two independent groups, both of them implementing two Pauli channels in a photonic quantum switch, although using different degrees of freedom of the photons [11, 12]. Perfect transmission through noisy channels in a quantum switch was reported in Refs. [13] and the quantum switch of thermal channels was recently implemented in a photonic setup [25] and in a nuclear magnetic resonance experiment [27].

The capacity activation of noisy channels using the quantum switch is a major result that has been shown to enhance the performance of several communication tasks, such as entanglement distribution [59, 60], teleportation [61–63], superdense coding [64], quantum random access codes [65], quantum steering [65], quantum state discrimination [34] and quantum key distribution [66]. Notwithstanding, this effect is not based solely on indefinite causal order. Indeed, Ref. [67] showed that it is possible to obtain an activation of the channel capacity also in a scenario where two noisy channels are coherently controlled, that is, when each channel is located in a different arm of an interferometer, such that one of them is applied on the target when the control system is in state $|0\rangle$ and the other is applied when the state of the control is $|1\rangle$ (see Fig. 1.1.5). However, this scenario has subtle differences with the quantum switch. As showed by Abbott et al. in Ref. [68], additional information regarding the implementation of the quantum channels is required in the coherent control of operations, since the capacity of the

effective channel can be different for different implementations of the same noisy channels, while in the quantum switch the effect is independent of their particular implementations. Another difference was highlighted in Ref. [69], where it was shown numerically that the coherent control of quantum channels always provide a communication advantage, while the quantum switch can give either an advantage or disadvantage depending on which the input channels are. Interestingly, for some particular cases the quantum switch can achieve perfect transmission, what was proved to be impossible for the coherent control of noisy channels [56]. An experimental comparison of these two scenarios was implemented in Ref. [13]. Also, the effect of using different implementations of the same quantum channels with a coherent control was experimentally studied in Ref. [70]. It is important to notice that a third scenario was also proposed in Ref. [71], in which two noisy channels are implemented in a fixed order, but adding controlled unitaries before them, after them and/or in between. Although this third scenario also offers perfect transmission, as far as we known it has not been further explored. All these works are part of an ongoing debate on the role of indefinite causal order in the activation of channel capacity. In some of them it is claimed that the resource that allows capacity activation is the coherence of the control system. Indeed, the advantages provided by the quantum switch are affected by decoherence on the control system, as firstly noticed in Ref. [65] and further studied in Ref. [72]. Summarizing, the activation of quantum channels capacity is the result of a combination of three factors: indefinite causal order, coherent control of operations and the particular implementation of the quantum channels.

In addition to this important application of the quantum switch, other communication tasks using the quantum switch have been studied. In particular, entanglement generation with local operations in indefinite order was proposed in Ref. [73], a protocol for entanglement distillation was devised in Ref. [74] and a key distribution protocol assisted by the quantum switch was studied in Ref. [75]. A new cryptographic task called *local-data-hiding* was proposed in Ref. [76], showing that causally nonseparable processes outperform fixed order circuits, although these processes are different from the quantum switch.

1.1.2.2.3 Quantum thermodynamics. Another striking application of the quantum switch was suggested by Felce and Vedral in Ref. [77]. They considered two copies of a thermalizing channel applied in a superposition of two different

orders as in the quantum switch. While the application of these channels in a fixed order always leads to an output thermal state in the same temperature as the thermal baths, the quantum switch allows the target to get a higher or lower temperature than the baths depending on the result of the measurement performed on the control. The authors use this result to build a refrigeration cycle that extracts energy from a cold reservoir while consuming coherence of the control system. This effect was experimentally implemented in 2022 in two independent works, one of them using a photonic setup [14] and the other one being the first realization of the quantum switch using nuclear magnetic resonance [26]. The effect of decoherence of the control in this task was studied in Ref. [72].

1.1.2.2.4 Quantum metrology. Other important avenue for applications of the quantum switch is quantum metrology. One of the first metrological tasks using the quantum switch was proposed in Ref. [78], where the goal was to estimate the strength of a depolarizing channel. To achieve the goal, two copies of the same depolarizing channel are applied on the target system in a superposition of orders. By comparing the quantum Fisher information, it was shown that the strategy using the quantum switch can reach a better precision than strategies applying the operations in a fixed order. A similar idea was also proposed in Ref. [79], where the aim was to measure the temperature of two copies of a thermal bath. These two instances of single parameter estimation using the quantum switch showed that the quantum switch can offer a metrological advantage compared to fixed order strategies. Further instances of single parameter estimation with enhanced precision via the quantum switch are the estimation of the product of two displacements in the phase space[20, 80], estimation of the phase of a noisy unitary gate[22, 81–84], estimation of the phase of an ideal unitary gate sorrounded by two noisy channels in a superposition of orders [85, 86], estimation of the rotation angle in an orbital angular momentum state [24] and estimation of an area on the Bloch sphere [87]. Some of these tasks have been demonstrated in photonic experiments [20, 22, 24]. A proposal for using the quantum switch for multiparameter estimation, again showing an improvement in the precision of the estimation, was studied in Ref. [88].

1.1.2.2.5 Others. The list of applications of the quantum switch also includes charging quantum batteries [21], applying non-gaussian operations [89] and

measuring the incompatibility of observables [90]. The topic is becoming popular with a larger amount of research being performed in this subject every year.

1.1.3 Process matrices

1.1.3.1 Concept

The quantum switch was introduced following a strictly computational motivation, inspired by the research program of Lucien Hardy. But does quantum mechanics allow other schemes with no definite causal order? Contemporarily to the introduction of the quantum switch, Ref. [91] proposed the framework of process matrices, which describes all the correlations that two parties can observe in their laboratories when quantum mechanics is valid within each lab, but without making any assumption about the causal structure out of the labs. Each party, let us call them Alice and Bob, receives a quantum system as input, on which they perform some local quantum operations (see Fig. 1.1.6). Given a fixed set of operations, the set of joint probabilities that Alice and Bob produce as outcome is called a *process*. Each process is represented by a matrix W, which must satisfy some conditions to be a valid process matrix: it must 1) be positive semidefinite in order to ensure that probabilities are non-negative, and 2) satisfy a completeness relation guaranteeing that the sum of all probabilities is 1. If we also assume that the global causal structure forbids signaling from one of the parties to the other one, then an extra condition must be imposed on W, which becomes a channel with memory as defined in Ref. [4]. A process where Alice cannot signal to Bob, what means that Alice is not in the causal past of Bob, is denoted by $W^{A \not\prec B}$. Similarly, $W^{B \not\prec A}$ denotes a process where Bob cannot signal to Alice. Using this notation, Ref. [91] introduced the notion of *causal non-separability*, formalizing the definition of indefinite causal order. A process W is said to be *causally separable* if it can be written as a convex combination $W = qW^{A \not\prec B} + (1-q)W^{B \not\prec A}$, where $q \in [0, 1]$. Conversely, if W cannot be written in this form, i.e. if it cannot be decomposed as a mixture of definite order processes, it is said to be *causally non-separable*.

In addition to the introduction of the process matrices framework and the definition of causal non-separability, Ref. [91] also introduced a particular example of causally

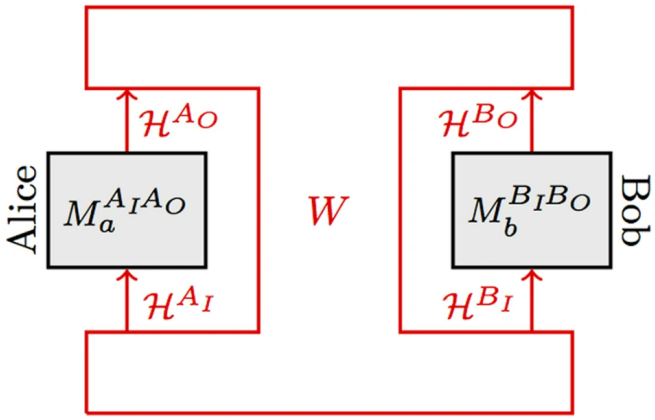

Figure 1.1.6: Bipartite process matrix. Alice and Bob perform quantum operations acting on some input systems and obtain outcomes a and b. Their labs are connected by an unknown causal structure represented by a process matrix W, which may be causally non-separable. The joint probabilities $P(a, b)$ depend on a combination of W and the operations performed by the parties. Figure from Ref. [92].

non-separable process, later called the "OCB process"[3]. The proof of its causal non-separability consists in the violation of a "causal inequality", similar to the violation of a Bell inequality for proving that a given bipartite quantum state is entangled. The proof can be summarized as follows: when Alice and Bob are connected by a causally separable process, their success probability in the "Guess Your Neighbour Input" game is always less than 3/4, while the OCB process allows the parties to exceed this bound; thus, the OCB process must be causally non-separable.

It is important to note that Ref. [91] did not offer a way to implement the OCB process, letting open the question about its physicality. Furthermore, it rose the question about which processes in the framework are physically implementable and which are not. This question was addressed in Refs. [93] and [94], which proposed some demarcation criteria for the implementability of general processes. Additionally, Ref. [95] showed that the probabilities arising from standard quantum theory do not violate causal inequalities of the type violated by the OCB process, what means that the OCB process cannot be physically implemented according to quantum theory and thus confirms that the process matrices framework goes beyond quantum mechanics. However, the proof in Ref. [95] does not consider the possibility of realizing indefinite causal order in time-delocalized subsystems

[3]"OCB" refers to the authors of Ref. [91], namely Oreshkov, Costa and Brukner.

as suggested by Ref. [94]; moreover, there exist tripartite processes which admit such a realization and also violate causal inequalities [96]. Thus, the question about the implementability of general processes remains open.

Regarding the quantum switch, it has been shown that it is a causally non-separable process that does not violate any causal inequality [97]. However, and despite its several experimental implementations, there is still an active debate concerning its physicality. Indeed, some authors claim that the reported experiments are just simulations instead of genuine implementations of the quantum switch [98, 99]. We are going to postpone this debate for later (cf. 1.1.4).

In the search for physically implementable processes with indefinite causal order others than the quantum switch, Ref. [100] characterised a broad class of implementable processes called "Quantum circuits with coherent control". The quantum switch is an instance of this family, while processes violating causal inequalities, such as the OCB process, cannot be described by it. A novel example of causal non-separable process within this class is a tripartite process that involves dynamical control of the causal order [100]. To the best of our knowledge, this process, known as the "Grenoble process", has not been implemented in any experiment so far.

Now let us comment some extensions of the process matrices framework. First of all, the extension to multipartite scenarios was not as straightforward as originally thought by Oreshkov, Costa and Brukner in their seminal work [91]. Actually, the multipartite scenario exhibits a richer causal structure than the bipartite case. For example, in the multipartite case the result of an operation performed by one party could influence the order of the operations performed by other two parties [101], a dynamical feature which is absent in the bipartite case. Also, an N-partite causally non-separable process is not necessarily genuinely N-partite non-causal, since the parties could eventually be grouped in smaller sets with a definite causal order between the sets [102]. Another difference between the bipartite and multipartite cases relates to the restriction to classical parties. While all the correlations between two parties that only perform classical operations can be explained by causally separable processes [91], this is not true in the multipartite case [103, 104]. For a discussion on the definition of multipartite causal nonseparability, see Ref. [105].

The process matrices formalism and its multipartite extension was introduced originally for finite dimensional systems. Its continuous-variable (CV) version, i.e. with parties performing operations on CV quantum systems, was studied in Ref. [106], but only for the bipartite case. That work showed that the quantum switch is a causal non-separable process also in the CV regime. However, to our knowledge, no certification strategy has been proposed for this scenario. The extension of the process matrices framework to the CV multipartite case, with its expected richer structure, is lacking as well.

Finally, we can mention a few further developments on the process matrices framework. For instance, Ref. [107] studied the possibility of composing process matrices, Ref. [108] addressed the discrimination of process matrices and Ref. [23] proposed and implemented a scheme for process matrix tomography. The possibility of process matrices evolving in time was studied in Ref. [109]. Lastly, Refs. [110, 111] studied the so called "causal reference frames", i.e., how a process is observed from the perspective of each party involved in the process.

1.1.3.2 Certification of causal non-separability

How can we certify that a given quantum process or experiment is an instance of indefinite causal order? In this subsection we are going to take a glance at the different strategies that answer this question, which mimic the methods for entanglement certification.

We mentioned above that some causally non-separable processes violate some causal inequalities. Causal inequalities allow for a device-independent certification of indefinite causal order, since they, as well as Bell inequalities, rely solely on the outcome probabilities of the operations performed by each party involved in the process. In the case of entanglement, tight Bell inequalities are the facets of the "Local Polytope", wich is the set of probabilities compatible with local hidden variable models [112]. In analogy to this description, Ref. [113] characterized the "Causal Polytope" for bipartite processes, that is the set of correlations compatible with definite causal order. The facets of the causal polytope define causal inequalities which can be violated for some causally non-separable processes. The causal polytope for the tripartite scenario was characterised in Ref. [114]. In entanglement certification, the extent to which a Bell inequality can be violated has been shown to have an upper limit given by the Tsirelson bound [115].

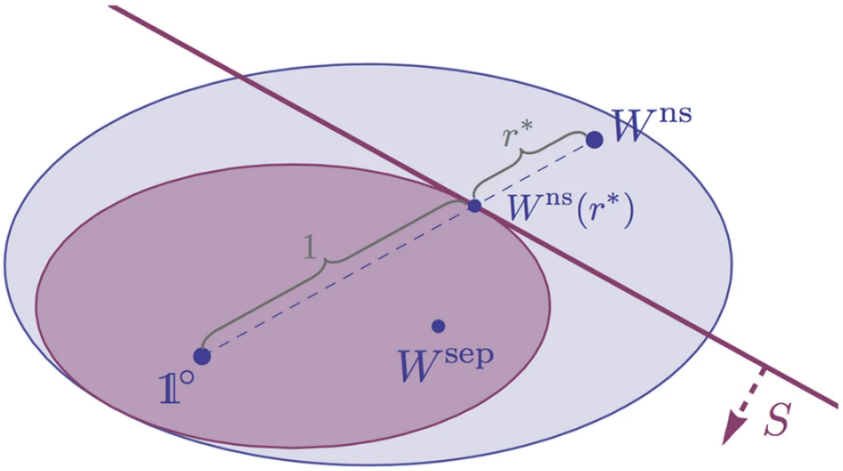

Figure 1.1.7: Causal Witness. The inner ellipse represents the set of causally separable processes and the bigger ellipse represents the set of all process matrices. For every causally non-separable process W^{ns}, it can be defined a hyperplane S (a causal witness) that separates W^{ns} from the set of causally separable processes. Figure from Ref. [92].

Similarly, a Tsirelson-like bound for the violation of causal inequalities was shown in Refs. [116, 117]. We have also mentioned above that there exist causally non-separable processes, like the quantum switch, that do not violate causal inequalities. Notwithstanding, by adding an extra party it is possible to build some inequalities that can be violated by the quantum switch. For instance, Ref. [118] proposed an inequality for a quantum switch whose control is entangled with a qubit sent to a space-like separated party who performs measurements on it. This proposal shows that device-independent certification of indefinite causal order is possible.

One of the most important methods to certify entanglement is the measurement of entanglement witnessess [112]. For different quantum states, different witnesses must be build, and their implementation requires prior knowledge about the particular state and the functioning of the devices used by the parties; hence, it is a device-dependent certification strategy. Again, it is possible to mimic this method and build "causal witnesses" for certifiyng causal non-separability [92, 97]. Indeed, given that the set of causally separable processes is a convex set, it is possible to define an hyperplane separating this set from the specific causally nonseparable process to be certified (see Fig. 1.1.7). The main advantage of this approach is that a causal witness can be translated into a number of operational

settings to be implemented by the parties. In particular, a causal witness for the quantum switch was derived using semidefinite programming in Ref. [97] and Refs. [8] and [9] independently demonstrated that the quantum switch is an instance of indefinite causal order by measuring a causal witness in photonic experiments.

An intermediate approach, known as semi-device-independent certification of causal non-separability, was formulated in Ref. [119]. There, one of the parties is trusted, meaning that their operations are fully characterised, while the other one is untrusted and only their outcome probabilities are known. Correlations certified this way are stronger than those certified only by device-dependent strategies. The causal non-separability of the quantum switch can be certified using this method [119] and has been demonstrated experimentally [16]. An alternative semi-device-independent method was proposed in Ref. [120], where all the parties remain uncharachterised, but they are given trusted quantum inputs instead of classical ones. By adding new uncharacterised parties, although connected in a particular network, this semi-device-independent with quantum inputs strategy becomes a network-device-independent certification of causal non-separability. [121].

Lastly, a possibilistic proof of causal non-separability of the quantum switch has been recently introduced [122] in analogy to the possibilistic proof of nonlocality by Peres and Mermin [123, 124].

Summarizing, different tools used for proving nonlocality of quantum states, both probabilistic and possibilistic, have been translated for certifying causal non-separability of process matrices. This spectrum of strategies also shows that quantum processes can be sorted in a hierarchy with different causal non-separability strengths, although, to our knowledge, no measure of causal non-separability has been proposed within this framework.

1.1.4 Superposition of causal structures

The purpose of the Hardy's program is to build a theory of quantum gravity, but neither the quantum switch nor the process matrices framework deal with gravity explicitly. Alternatively, Ref. [125] put features from both gravity and quantum theory together, by assuming the possibility of a superposition of causal structures. The idea is the following: let us suppose that each metric defining a manifold

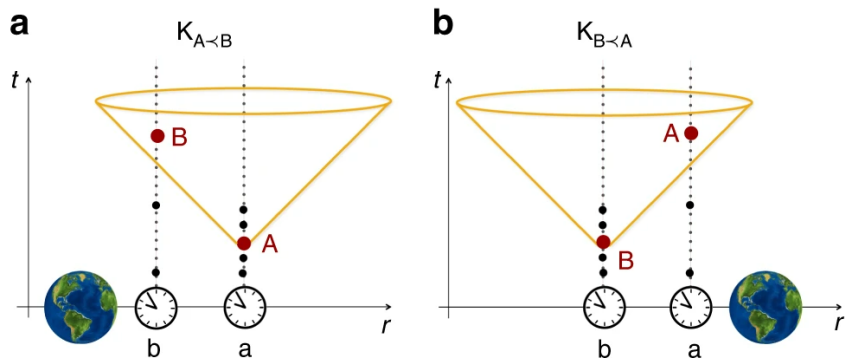

Figure 1.1.8: Gravitational quantum switch. A massive body is in a superposition of two different locations, while two clocks are in fixed locations. Due to gravitational time dilation, an event defined in one clock can be in the causal past of an event defined in the other clock. The order of the events depends on the branch of the superposition; an indefinite location of the massive body generates an indefinite causal structure realising a gravitational version of the quantum switch. Figure from Ref. [125].

$\mathcal{M}$ can be assigned a quantum state $|\mathcal{M}\rangle$, with orthogonal states representing macroscopically distinguishable spacetimes; then, we assume that a superposition of different manifolds, such as $(|\mathcal{M}_1\rangle + |\mathcal{M}_2\rangle)/\sqrt{2}$, is a valid state for the geometry of spacetime. We could guess that a theory of quantum gravity would eventually admit this kind of composition. If so, what kind of phenomena should we expect from such a superposition of causal structures?

Ref. [125] studied a particular scenario where a massive body is in a superposition of two different locations. There, the gravitational field is naturally in a superposition of two different geometries. As seen in Fig. 1.1.8, we could locate two clocks in fixed positions respect to a far-away observer, such that in one configuration one of the clocks will be closer to the massive body, while in the other branch of the superposition the other clock will be the one closer to the source of the gravitational field. For a given proper time τ the clocks define corresponding events A and B. However, for each configuration, if the clocks start synchronised as seen from the far-away observer, after a while their proper times will be different due to gravitational time dilation. Hence, one of the events will be in the causal past of the other. For the superposition of the two geometries, the result will be a superposition of order of the events, as in the quantum switch. Moreover, the quantum switch can be implemented in this scenario by locating a target system together with one of the clocks and applying on it local quantum

operations triggered by a signal emmited from each clock at its proper time τ. This version of the quantum switch, where the control system is the gravitational field prepared in a superposition of classical manifolds, is usually called a *gravitational quantum switch*. An alternative realization of the gravitational quantum switch, where the source of the gravitational field is a superposition of spherical mass shells, was proposed in Ref. [126].

Notice that in the scenario described in the previous paragraph there are two parties or labs with their own clocks either applying or triggering quantum operations on a target system. According to the reference frame of each lab there is one quantum operation applied in a definite time while the other operation appears to be time-delocalised. This observation led to the concept of "time reference frames", i.e., quantum reference frames associated to gravitating clocks, studied in Ref. [127]. Other realizations of the gravitational quantum switch consider agents in a superposition of paths [128] or with entangled acceleration [129] in a fixed spacetime, although these scenarios are different to the superposition of causal structures that we are reviewing here.

In Section 1.1.3.1 we mentioned that some authors claim that the photonic experiments implementing the quantum switch are just simulations of this process [98]. According to them, only the gravitational quantum switch can be a genuine implementation of the quantum switch. The reason for that comes from the fact that all the photonic experiments implementing the quantum switch are performed within a laboratory immersed in a fixed Minkowski spacetime. As shown in Fig. 1.1.9, in a photonic experiment the target system is split in a superposition of paths, with one of them reaching Alice's lab at time t_1 and then going to Bob's lab at time t_2, while in the other arm of this array the photon goes first to Bob's lab at time t_1 and then to Alice's in time t_2. Strictly speaking, there are two controlled operations (A and A' in Fig. 1.1.9), which happen to be equal, performed in Alice's side at different times. The same occurs at Bob's. Thus, the photonic implentation of the quantum switch is just a simulation, since it considers four events in spacetime instead of two as a genuine quantum switch, like the gravitational one, would do. Four controlled operations are explicitly applied also in nuclear magnetic resonance implementations of the quantum switch.

A different analysis leading to a similar conclusion was carried out in Refs. [99, 130], where it was discussed that there are two different notions of causality

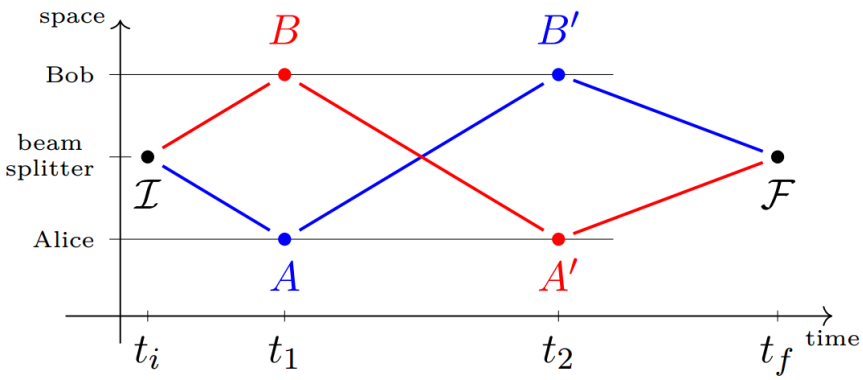

Figure 1.1.9: Photonic quantum switch embedded in spacetime. The implementation of the photonic quantum switch comprises four points in spacetime. A genuine quantum switch should comprise only two events. Figure from Ref. [98].

involved in the study of the quantum switch. One of them is an information-theoretic concept of causality and the other one is spacetime causality. The latter demands an acyclic spacetime structure in order to satisfy relativistic causality principles such as the impossibility of superluminal signaling. By introducing the concept of "fine-graining", Refs. [99, 130] showed that cyclic information-theoretic structures are embedded in acyclic spacetime structures, reconciling both notions. Furthermore, they showed that causally nonseparable processes are compatible with cyclic causal structures, therefore they admit a realization in an acyclic spacetime at a fine-grained level as fixed order processes. In particular, since the photonic experiments of the quantum switch are implemented in a definite Minkowski spacetime (acyclic structure satisfying relativistic causality), they must be instances of a fixed order process. The question about how to make general processes compatible with spacetime in the fine-grained level was studied in Ref. [131].

Nevertheless, the criticism against a faithful realisation of the quantum switch in photonic experiments strongly relies on the notion of *event* understood as a *point in spacetime*. Although the concept is uncontroversial when the spacetime is definite, it must be revisited when a superposition of causal structures is considered. Indeed, Ref. [132] advocates for a rather operational definition of an event as a *coincidence of worldlines*, notion further discussed in Ref. [133]. For each branch of the superposition of manifolds (see Fig. 1.1.10), it is possible to draw the worldlines of the target system and the agents Alice and Bob. The application

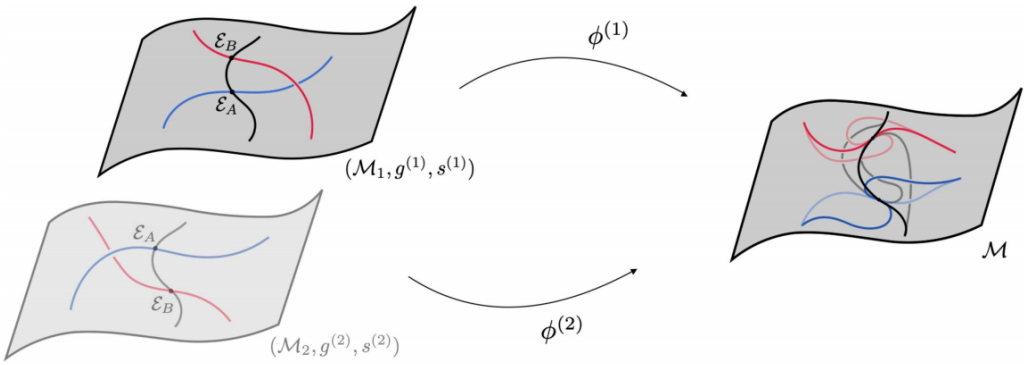

Figure 1.1.10: Superposition of causal structures. In the superposition of classical manifolds, an event is a crossing of worldlines. For each branch, the corresponding events are identified via a quantum controlled diffeomorphism. Figure from Ref. [132].

of a quantum operation on the target occurs when the target's worldline meets the worldine of one of the agents. However, since there is a superposition of causal structures, the events of each branch must be identified. This identification can be achieved via a quantum controlled diffeomorphism [132]. According to this operational view, the photonic implementation of the quantum switch is as genuine as its gravitational version, provided a superposition of causal structures is involved.

The superposition of causal structures is still a new approach with room for further developments. We can mention a few works on this line. For example, some quantifiers for indefinite causal order have been defined in Refs. [132, 134]. Besides, Ref. [135] studied the operational effects of a superposition of Minkowski spacetimes with periodic boundary conditions while Ref. [136] analyses the influence of a superposition of diamond spacetimes on quantum entanglement. Also, it has been shown that superposition of spacetimes related by coordinates transformations can be expressed as a single definite spacetime with matter in a superposition of configurations [137]. Actually, this is the case of the scenario considered in Ref. [125] with a massive body in a superposition of two locations and two clocks in fixed positions, which is equivalent to a massive body in a fixed position and two clocks with entangled positions. Anyway, there are much more questions to solve in this approach. For instance, if quantum states are assigned to classical manifolds, in which Hilbert space do those states live? How do they evolve? How can the state of a classical manifold be projected onto a superposition

of geometries or viceversa? How to identify events when two worldlines meet in one of the branches but not in the other one? As we mentioned earlier, while the superposition of causal structures is a rather speculative approach, it is an interesting avenue to explore new phenomena that could eventually appear in a theory of quantum gravity and therefore in regimes where both quantum and gravitational effects are relevant.

1.1.5 Ongoing debates

We have seen that indefinite causal order is a research topic that embraces from foundational research to applications, linking quantum gravity with quantum information communities. Different approaches have been explored in the last decade in order to formalize the concept and a number of experiments have been already implemented. However, there are still major ongoing debates, which we summarize here.

1. **On the advantages of the quantum switch:** The quantum switch offers interesting advantages when compared to fixed order circuits. However, it is not completely clear which is the resource behind those advantages. Is it indefinite causal order or the coherent control of operations? Or maybe is it the non-commutativity of operators? Or a mixture of all of them? Besides, some of the advantages have been shown either in *ad hoc* tasks for the quantum switch or in impractical scenarios. Can they be transferred to real-world problems in order to provide practical solutions?

2. **On the physicality of process matrices:** The process matrices framework includes processes that violate causal inequalities. However, they seem to be non-physical processes. Which is the boundary between physically implementable processes and non-physical ones? Can those processes forbidden by standard quantum mechanics be relevant processes in a quantum gravity scenario? In other words, can some of them be still allowed by Nature in some extreme conditions?

3. **On the faithfulness of ICO realisations:** The notion of event is still controversial and it is the key when interpreting current experiments on indefinite causal order. Are the experiments realising the quantum switch genuine instances of indefinite causal order or are they just simulations

instead?

4. **On the definition of quasi-classical manifolds:** The superposition of causal structures is an approach that needs to be further developed. Is the Hilbert space of the states assigned to classical manifolds well defined? How much more structure from quantum theory can be added to this approach?

All these questions are quite interesting, and there are more open questions on each of the specific topics reviewed along this section. Notwithstanding, there is still another gap that we consider important to fill. We will take a closer look at it in the next section, as it will motivate the objectives of this thesis.

1.2 Indefinite causal order in the continuos-variable regime

Most of the literature we have reviewed above considers a target system which lives in a finite-dimensional Hilbert space. In this section, let us recapitulate what is already known about indefinite causal order, but in the continuous-variable (CV) regime.

Regarding applications of the quantum switch on CV systems, the majority of them concern quantum metrology. The most famous work in this regard is Ref. [80], which showed that the quantum switch can estimate the product of the averages of two sets of displacements in phase space, with one set corresponding to displacements along the X quadrature and the other set corresponding to displacements along the P quadrature. Interestingly, the estimation is achieved by measuring the qubit control system alone, while discarding the target. Moreover, the target ends in a state which is the result of applying the total displacement to its initial state. In other words, the target undergoes all the displacements while the relevant information about these operations is retrieved from the ancillary qubit. Additionally, the authors claim that the use of the quantum switch provides a super-Heisenberg scaling in the precision of the estimated parameter, although this seems to be due to averaging each set of displacements rather than because of the use of indefinite causal order. Actually, the same scaling can be achieved via a coherent superposition of the displacements, though with a different effective transformation on the target system [138]. A photonic implementation of this

work was reported in Ref. [20], which is the first experiment of the quantum switch on a CV target system.

A different scenario was studied in Ref. [86], which considers two thermalizing channels acting on a qumode and one phase shift operation implemented between them. The goal is to estimate the phase introduced by the phase shift. If the operations are applied in a fixed order, the last thermalizing channel erases all information about the phase. Instead, by using the quantum switch it is still possible to estimate the phase, with the amount of information available in the target depending on the result of a measurement performed on the control qubit. Similarly, Ref. [24] considers three operations but acting on the orbital angular momentum of a photon. One operation is a rotation characterized by an azimuthal angle and the other two operations increase or reduce the orbital angular momentum. In their experiment, measuring the qubit control is enough to estimate the angle of the rotation with a higher precision than in experiments without indefinite causal order.

In other surprising application of the quantum switch, Ref. [89] showed that a non-gaussian state can be prepared starting from the single-mode vacuum state by applying two gaussian operations, specifically one displacement and one squeezing, in a superposition of two different orders. The non-gaussianity and non-classicality of the final state appears deterministically after post-selection on the control system, and their amount can be engineered since they depend on the displacement and squeezing parameters of the operations.

There is also one application of the quantum switch to quantum communication. In particular, Ref. [62] studied the effect of the quantum switch in the teleportation of a CV state when the entangled pair required for this task has been distributed through two thermalizing channels in a superposition of orders. Lastly, Ref. [139] studied the quantum switch as a resource for thermodynamics and considered a qumode among their study cases.

Finally, regarding the process matrices framework, it was shown in Ref. [106] that the bipartite quantum switch with operations on CV quantum systems is an instance of indefinite causal order. However, to our knowledge, no certification strategy nor an extension to multipartite scenarios have been studied.

As we can see, works on indefinite causal order with a CV target system are

comparatively few compared to the amount of literature that we reviewed in the previous section. We speculate that focusing on CV systems or at least trying to extend the field in that direction may bring some novelties which deserve to be discussed.

1.3 Objectives and methodology

At what extent can applications of indefinite causal order and its certification strategies be extended to the CV regime? This thesis tries to address this question, led by the following

Hypothesis:

Applications of indefinite causal order on CV quantum systems offer broader advantages than using finite-dimensional quantum systems.

The tasks reviewed in Section 1.2 exhibit particular features suggesting that they are indeed causally non-separable instances. Among them, engineering non-gaussian states from gaussian operations applied in indefinite order on the vacuum state [89] is perhaps the only task qualitatively different to what is achievable using finite-dimensional systems and can be considered as support to our hypothesis. We aim to provide further and stronger support by pursuing the following goals:

General objective:

To show that the quantum switch provides broader advantages for quantum information processing when the target system is a CV quantum system rather than finite-dimensional.

Specific objectives:

(*i*) To assess the performance of the quantum switch in the solution of promise problems for high-dimensional and CV quantum systems.

(*ii*) To assess the performance of the quantum switch in multiparameter estimation using high-dimensional and CV quantum systems.

Because of the few works regarding indefinite causal order on CV systems so

far, this thesis is rather exploratory. Our work follows a theoretical approach, although we also discuss possible experimental realizations of the proposed tasks.

The general plan is to study new applications of the quantum switch while comparing its performance in finite higher-dimensional and CV target systems. This comparison may give a better intuition about what is new when taking indefinite causal order to the CV regime. In particular, we will study one application of the quantum switch in quantum computing and one in quantum metrology. The methodological approach to each specific objective is the following:

(i) To achieve objective (i), we will study a family of promise problems where the goal is to discriminate between a set of properties of a given set of unitary gates. It has been shown that the quantum switch can reduce the number of gate queries required for solving promise problems, what we denote as "query advantage". Known promise problems where the quantum switch provides query advantage are the discrimination between commuting and anticommuting gates [37], the Fourier promise problem [29] and the Hadamard promise problem [36, 38]. While the first one is well defined for every dimension of the target, the other two have severe restrictions in the dimension of the target and control systems. We propose to extend the family of promise problem such that they could be defined in every finite dimension and also in CV systems. To this aim, we will use Butson-Hadamard matrices [140] and complex Hadamard matrices [141], which are more general than the Fourier and Hadamard matrices. We will assess the query advantage of the quantum switch in solving this generalised family of promise problems.

(ii) To address objective (ii), we propose to apply the quantum switch to the estimation of unitary transformations. We will start with qubit unitary gates, scenario where the precision of the estimation can be compared with related works [142] using the quantum Fisher information matrix [143] as figure of merit. Then, we will extend the protocol to higher dimensions and non-unitary transformations before trying to extend the proposal to CV systems.

Details regarding the methods used for tackling each objective are included within each chapter.

1.4 Outline

Chapters 2 and 3 address specific objectives (*i*) and (*ii*), respectively. In particular, Chapter 2 studies a generalised family of promise problems that can be solved using the quantum switch, including a special analysis for CV target systems, and Chapter 3 is dedicated to the estimation of unitary gates using the quantum switch and an extension of the protocol to arbitrary quantum channels. The attempt to extend the latter task to the CV regime will suggest the introduction of the quantum switch with continuous control, a novel process which opens new unexpected avenues for indefinite causal order. The quantum switch with continuous control is sketched out in Chapter 4, after drawing our conclusions and some open questions.

The results of this thesis have been communicated in the following scientific publications and conferences:

Publications:

- J. Escandón-Monardes, A. Delgado and S. P. Walborn, "Practical computational advantage from the quantum switch on a generalized family of promise problems", *Quantum* **7**, 945 (2023).
- J. Escandón-Monardes, D. Uzcátegui, M. Rivera-Tapia, S. P. Walborn and A. Delgado, "Estimation of high-dimensional unitary transformations saturating the Quantum Cramér-Rao bound", *Quantum* **8**, 1405 (2024).

Conferences:

- Workshop MIRO 2022, Millennium Institute for Research in Optics, Universidad de Los Andes, Santiago, Chile. 5th - 7th October 2022. **Poster: "Estimation of unitary gates using the quantum switch"**.
- XXIII Simposio Chileno de Física SOCHIFI 2022, Universidad Técnica Federico Santa María, Valparaíso, Chile. 22nd - 24th November 2022. **Talk: "Computational advantage from the quantum switch"**.
- VIII Paraty Quantum Information School and Workshop, Paraty, Rio de Janeiro, Brazil. 7th - 18th August 2023. **Talk: "Computational**

advantage from the quantum switch on a generalized family of promise problems".

- Workshop MIRO 2023, Millennium Institute for Research in Optics, Pontificia Universidad Católica de Chile, Santiago, Chile. 10th - 13th October 2023. **Talk: "Quantum channel to quantum state converter"**.
- XV Symposium KCIK-ICTQT on Quantum Information, Sopot, Poland. 15th - 18th May 2024. **Poster: "Transcribing quantum channels into quantum states"**.
- 19th Central European Quantum Information Processing Workshop, Skalica, Slovakia. 3rd - 6th June 2024. **Poster: "Transcribing quantum channels into quantum states"**.
- Time in Quantum Theory 2024, Smolenice Castle, Slovakia. 10th - 13th September 2024. **Poster: "Quantum switch with continuous control"**.
- 2024 INAQT Network Meeting (International Network for Acausal Quantum Technologies), Vienna, Austria. 4th - 6th November 2024. **Poster: "Quantum switch with continuous control"**.
- Quantum Optics X, Puerto Varas, Chile. 9th - 13th December 2024. **Poster: "Quantum switch with continuous control"**.

Chapter 2

Practical computational advantage from the quantum switch on a generalized family of promise problems

The quantum switch provides computational advantage by reducing the number of queries of unknown quantum channels in a family of tasks, of which the simplest known case is to decide whether a pair of unitary gates commute or anticommute [7, 37]. This can be achieved using the quantum switch with a single use of each gate, whilst a fixed-order circuit demands one extra query to one of them. This task has been generalised to the so-called Fourier Promise Problem (FPP). There, a quantum switch of N unitary gates (N-`switch`) deterministically discriminates between a set of $N!$ properties that a set of gates is promised to satisfy upon permutation [29]. The N-`switch` coherently applies the $N!$ different orders of the gates such that the permutation property can be determined with a single use of each unitary. On the contrary, the best known fixed-order circuit simulating the quantum switch requires a total of $\mathcal{O}(N^2)$ gate queries [144]. An alternative solution to the FPP using a fixed-order circuit has a query complexity of $\mathcal{O}(N \log N)$, with the cost of using extra ancillary systems [145].

The quantum switch has been experimentally implemented to solve the FPP for $N = 2$ qubit gates [7, 8]. However, implementation for $N > 2$ is technically difficult

due to the unfavorable scaling of the dimension of the target system, which must have dimension at least $N!$ [29]. While photons do indeed have accessible degrees of freedom with large dimension, such as orbital angular momentum [146] and other types of spatial modes [147, 148], producing the required transformations even for the smallest dimensional case of 3! is challenging. One possible path towards more practical realizations of promise problems was provided in Ref. [36], where the Hadamard Promise Problem (HPP) was introduced, with an explicit solution experimentally demonstrated using a quantum switch that applied four sequences of four gates to a qubit target system. A more general definition of HPPs using N gates was introduced in Ref. [38], with the same distinctive feature of requiring just a qubit as the target system. Both the FPP and HPP can be cast as the task of determining which column of a matrix describes the permutation properties of a set of unitaries, relating the promise satisfied by the set of unitaries to the entries of a Fourier or Hadamard matrix.

In this chapter, we introduce a generalized set of promise problems, which in addition to providing much more freedom in regards to the dimension of the target system, uncouples the order of the matrix and the number of quantum gates, offering more parameters to explore. To achieve this, we turn to the more general Complex Hadamard (CH) matrices to define the Complex Hadamard Promise Problem (CHPP), providing a large family of promise problems. The CHPP reduces to the FPP or HPP as limiting cases. In regard to discrete variable target systems, our approach removes the unfavorable factorial scaling of the FPP, and we find that CHPPs exist for every finite dimension with some additional constraints on the entries of the CH matrix. In addition, the entire family of CHPPs can be defined for continuous variable (CV) target systems. Moreover, some CHPPs are exclusively defined for CV systems, which could possibly lead to new applications. For a comparison with related works on these features, see Table 2.0.1. Looking towards implementation, we show how the quantum switch solves the CHPP and offers computational advantage compared to the best known fixed-order circuits for both discrete and continuous variable target systems. This result renders new flexibility to the design of experiments using the quantum switch to solve promise problems and opens the possibility of using CV platforms to this end.

The structure of the chapter is as follows. Section 2.1 introduces Complex

Parameter	Chiribella [37]	Araújo, Costa, Brukner[29]	Taddei et al. [36]	Renner, Brukner [38]	This work
Matrix M	H_2	F	H_4	H	CH
Number N of gates	2	$N \geq 2$	4	$N \geq 2$	$N \geq 2$
Dimension d of the target system	2	multiple of $N!$	2	2	$d \geq 2$ and CV
Number p of permutations	2	$N!$	4	2^{N-1}	$p \leq N!$
Subclass	HPP, FPP	FPP	HPP	HPP	BHPP, CHPP

Table 2.0.1: Promise problems in the literature. Comparison between different promise problems and explicit solutions using the quantum switch. The last row shows the subclass of promise problems covered in each related work.

Hadamard matrices and some relevant properties. The Complex Hadamard Promise Problem (CHPP) is defined in Section 2.2 and shown to be well defined for every dimension, with some restrictions on the Complex Hadamard (CH) matrices. Section 2.3 shows the solution of the CHPP using the quantum switch and Section 2.4 assesses the computational advantage of the quantum switch against the best known fixed-order solutions. A discussion on possible experimental implementations is found in Section 2.5, and concluding remarks are drawn in Section 2.6.

The results of this chapter have been published in

- Jorge Escandón-Monardes, Aldo Delgado and Stephen P. Walborn, "Practical computational advantage from the quantum switch on a generalized family of promise problems", *Quantum* **7**, 945 (2023).

2.1 Complex Hadamard matrices

A square matrix M of size p is called a *Complex Hadamard* (CH) matrix if its entries are unimodular ($|M_{jk}| = 1$) and $MM^\dagger = pI$, where I is the identity matrix of size p (for further details see [141]). We denote the set of complex Hadamard matrices of size p as $CH(p)$. It is clear from the definition that if $M \in CH(p)$, then $M/\sqrt{p}$ is unitary, and that any two columns or rows of M are orthogonal. If the entries of a complex Hadamard matrix in the first column and the first row are all equal to one, we say that the matrix is in its *dephased* form. Any

$M \in CH(p)$ can be cast in dephased form[1].

Since the entries of a complex Hadamard matrix are unimodular, they can be written as

$$M_{jk} = e^{i\phi_{jk}} \ . \tag{2.1.1}$$

The phases $\phi_{jk} \in [0, 2\pi)$ are the entries of a matrix ϕ known as a *log-Hadamard* matrix. For example, if M is dephased, then all the entries of the first row and first column of the corresponding log-Hadamard matrix are equal to zero.

A special subset of complex Hadamard matrices is the set of *Butson-type complex Hadamard matrices*, or Butson-Hadamard (BH) matrices for short [140]. They satisfy the additional condition that all their entries are roots of unity. We say that $M \in CH(p)$ is a BH matrix of *complexity* d if all its entries are d-th roots of unity, what we denote as $M \in BH(p, d)$. Notice that the log-Hadamard elements associated to a BH matrix of complexity d have the form $\phi_{jk} = 2\pi q_{jk}/d$, with $q_{jk} \in \{0, 1, ..., d-1\}$.

Particular examples of BH matrices are Fourier matrices F_d, belonging to $BH(d, d)$ with entries

$$(F_d)_{jk} = e^{i\frac{2\pi jk}{d}} \ , \tag{2.1.2}$$

where we have dropped the normalizing constant. Another known family of BH matrices is the set of *real Hadamard* matrices, with entries equal to ± 1, hence corresponding exactly to the set $BH(p, 2)$.

It is important to notice that not every CH matrix is BH. As an example, let us consider the case of CH matrices of size 4. Every matrix in $CH(4)$ is equivalent [2] to a matrix in the family

$$F_4^{(1)}(a) = \begin{pmatrix} 1 & 1 & 1 & 1 \\ 1 & ie^{ia} & -1 & -ie^{ia} \\ 1 & -1 & 1 & -1 \\ 1 & -ie^{ia} & -1 & ie^{ia} \end{pmatrix}, \tag{2.1.3}$$

with $a \in [0, \pi)$. Conversely, every matrix in this family is a CH. Notice that

[1] For any Complex Hadamard matrix M, there exist diagonal unitary matrices D_1 and D_2 such that $D_1 M D_2$ is dephased.

[2] Two complex Hadamard matrices M_1 and M_2 are said to be equivalent if there are permutation matrices P_1, P_2 and diagonal matrices D_1, D_2 such that $M_1 = D_1 P_1 M_2 P_2 D_2$.

$F_4^{(1)}(0)$ is the Fourier matrix of size 4, F_4, while $F_4^{(1)}(\pi/2)$ is a real Hadamard matrix. To get a CH matrix which is not BH, it is enough to write $a = 2\pi\nu$ and fix ν as an irrational number.

2.2 Complex Hadamard Promise Problem

2.2.1 The Problem

In this section we introduce the Complex Hadamard Promise Problem (CHPP). Our definitions follow those laid out in Ref. [29].

Let M be a $CH(p)$ matrix in its dephased form and consider a set of N unknown unitary gates $U_0, ..., U_{N-1}$. We define the product $\Pi_0 = U_{N-1}U_{N-2}...U_0$ and denote different permutations of the same gates by $\Pi_1, ..., \Pi_{p-1}$. The Complex Hadamard Promise states that the set of unitaries satisfies the following property for one of the columns of M:

$$\forall j \in \{0, ...p-1\} : \Pi_j = M_{jk} \cdot \Pi_0. \tag{2.2.1}$$

The problem is to find the column k.

Notice that the size p of the matrix defines the number of permutations that will be considered. This sets a lower bound for the number of unitaries N, which must be such that:

$$p \leq N!. \tag{2.2.2}$$

2.2.2 Existence of unitaries satisfying the promise: Finite dimensional target

The definition of the CHPP does not garantee the existence of a set of unitaries satisfying the promise under some permutations for a given CH matrix. Here, we prove that those unitaries do exist, but some restrictions appear on the CH matrices if we choose unitary gates acting on finite dimensional systems.

Let us consider a D-dimensional target system. In that case, gates are $D \times D$ unitary matrices. We can follow a similar approach as in Ref. [29] to find that $M_{jk}^D = 1$, due to $\det\Pi_j = M_{jk}^D \det\Pi_0$ and $\det\Pi_j = \det\Pi_0$, for any j and k. Consequently, M must be a BH matrix. More specifically, a CHPP can be implemented in finite dimensional systems only if the CH matrix specifying the

promise is Butson-type with complexity $d = D/m$ for some positive integer m. Moreover, if a CHPP can be formulated for a d-dimensional target, it can also be formulated for any system with dimension that is a multiple of d. This follows from the definition of BH matrices, which implies that $BH(p, d) \subseteq BH(p, md)$. For the canonical case of a qubit target, the CHPP must be specified by a real Hadamard matrix, i.e., the CHPP gets restricted to the HPP already introduced in Refs. [36, 38], which may also be implemented in any even dimensional target system.

It is useful to set some nomenclature at this point. We will refer to particular classes of CHPPs, such as Butson-Hadamard Promise Problems (BHPPs), Fourier Promise Problems (FPPs) and Hadamard Promise Problems (HPPs), when the CH matrices specifying them are Butson-type, Fourier and Hadamard, respectively. Notice that the original definition of the FPP [29] uses all possible permutations of N unitaries, hence the dimension of the target must be a multiple of $d = N!$. Since we are loosening the number of permutations required for the promise, our definition allows the FPP to be formulated with Fourier matrices whose size, and therefore the dimension of the target system, does not need to be as large as the factorial of the number of unitaries, allowing for more realistic experimental scenarios. Similarly, Ref. [38] introduced a method to construct HPPs from simpler HPPs. It leads to specific relations between p and N depending on the fundamental HPP considered. Their explicit construction is based on Chiribella's task [37] and leads to $p = 2^{N-1}$, which is included in Table 2.0.1. It can be proven that Taddei et al.'s task [36] is also fundamental in this sense, providing a different scaling for p in terms of N. With our approach instead, we shall be able to build solutions for every HPP, be it fundamental or not.

Now, let us show that any BHPP is well defined on a target with compatible dimension, i.e. we can always find sets of unitary gates fulfilling the promise when the dimension of the target is multiple of the complexity of the BH matrix. The construction is as follows:

Let us consider the generalized Pauli X and Z gates, defined as:

$$X := \sum_{j=0}^{d-1} |j \oplus 1\rangle \langle j| \,, \tag{2.2.3}$$

$$Z := \sum_{j=0}^{d-1} \omega_d^j |j\rangle \langle j| \,, \tag{2.2.4}$$

where $\oplus$ denotes sum modulo d and $\omega_d = \exp(2\pi i/d)$ is the primitive d-th root of unity. These unitary operators satisfy $X^d = Z^d = I_d$ and the commutation relation

$$ZX = \omega_d XZ \ , \tag{2.2.5}$$

which can be extended using mathematical induction to

$$Z^j X^k = \omega_d^{jk} X^k Z^j \ . \tag{2.2.6}$$

Now, let us define the following p unitaries:

$$\begin{array}{rcl} U_0 & = & X \ , \\ U_j & = & Z^{q_j} \ , \quad \forall j = 1, ..., p-1 \ , \end{array} \tag{2.2.7}$$

where q_j are integers, and consider the following p permutations, where U_0 is shifted one position to the left each time:

$$\begin{array}{rcl} \Pi_0 & = & U_{p-1}U_{p-2}\cdots U_1 U_0 \ , \\ \Pi_1 & = & U_{p-1}U_{p-2}\cdots U_0 U_1 \ , \\ \vdots & & \vdots \\ \Pi_{p-2} & = & U_{p-1}U_0\cdots U_2 U_1 \ , \\ \Pi_{p-1} & = & U_0 U_{p-1}\cdots U_2 U_1 \ . \end{array} \tag{2.2.8}$$

Using the commutation relation (2.2.6) it is easy to show that

$$\Pi_j = e^{i\frac{2\pi}{d}(q_1+q_2+...+q_j)}\Pi_0 \ , \ \forall j = 1, ..., p-1 \ . \tag{2.2.9}$$

Hence, given $M \in BH(p,d)$ dephased and an arbitrary column

$$M_{*,k} = (1, e^{i\frac{2\pi}{d}q_{1k}}, e^{i\frac{2\pi}{d}q_{2k}}, \cdots, e^{i\frac{2\pi}{d}q_{(p-1)k}})^T \tag{2.2.10}$$

of M, we just need to choose $q_j = q_{jk} - q_{(j-1)k}$ for $j = 1, ..., p-1$ to obtain a set of p unitaries satisfying the promise, as we wanted to show.

2.2.3 Existence of unitaries satisfying the promise: Continuous variable target

As mentioned in Section 2.1, there are Complex Hadamard matrices which are not Butson-type. Consequently, they do not define valid CHPPs on finite dimensional target systems. Interestingly, the restriction imposed by the determinant in the finite dimensional case is dropped in the continuous variable (CV) regime. Moreover, as we next prove, unitary gates satisfying the promise do exist for every CH matrix in its dephased form and for each of its columns, thus the CHPP is always well defined for CV target systems.

The construction of unitaries is analogous to that in previous section. Now let us consider the displacement operators

$$\begin{aligned} X_\alpha &= e^{-i\alpha\hat{p}} \quad , \\ Z_{\beta\gamma} &= e^{i(\beta\hat{x}+\gamma\hat{p})} \quad , \end{aligned} \tag{2.2.11}$$

where α, β, γ are real numbers, while $\hat{x}$ and $\hat{p}$ are position and momentum operators satisfying $[\hat{x}, \hat{p}] = iI$. Using the Baker-Campbell-Hausdorff formula we have

$$Z_{\beta\gamma} X_\alpha = e^{i\alpha\beta} X_\alpha Z_{\beta\gamma} \ . \tag{2.2.12}$$

Setting the gates

$$\begin{aligned} U_0 &= X_\alpha \ , \\ U_j &= Z_{\beta_j\gamma_j} \ , \quad \forall j = 1, ..., p-1 \ , \end{aligned} \tag{2.2.13}$$

and considering the same p permutations of (2.2.8), it can be shown that

$$\Pi_j = e^{i\alpha(\beta_1+\beta_2+...+\beta_j)} \Pi_0 \ , \ \forall j = 1, ..., p-1 \ . \tag{2.2.14}$$

Given M dephased and an arbitrary column

$$M_{*,k} = (1, e^{i\phi_{1k}}, e^{i\phi_{2k}}, \cdots, e^{i\phi_{(p-1)k}})^T \tag{2.2.15}$$

of M, we can choose $\alpha \neq 0$, $\beta_j = (\phi_{jk} - \phi_{(j-1)k})/\alpha$ and γ_j arbitrary for $j = 1, ..., p-1$

to have a set of unitaries satisfying the promise.

Notice that if $\{U_j\}$ is a set of unitaries satisfying a specific promise and V is any unitary gate, then the set $\{VU_jV^\dagger\}$ fulfills the same promise.

2.2.4 Existence of unitaries satisfying the promise: Minimal sets

From the definition of the problem, we already know that the number of unitaries N required to satisfy a promise specified by a $CH(p)$ matrix is such that $p \leq N!$. We will say that a set of unitaries satisfying the promise is *minimal* if the number of unitaries is the minimum N such that $p \leq N!$. In this section we discuss the following question: is it possible to define a minimal set of unitaries satisfying a given promise?

Some examples are already known. Indeed, Ref. [29] shows minimal sets of unitaries for some FPPs; since they consider only matrices of order $N!$, their construction of unitaries is trivially minimal. Also, in Ref. [38] a specific HPP is considered for any N, with a construction of unitaries that is minimal for $N = 2$, 3 and 4, but not for larger N. Meanwhile, our construction above is minimal only for matrices of size $p = 2$ and 3.

We also investigated the case of a CHPP specified by a $CH(4)$ matrix. In particular, we considered an arbitrary member of the parameterised family defined in Eq. (2.1.3). Since this family includes matrices which are not Butson-type, we required unitary gates acting on a CV system. This promise consists on four permutations; therefore, a minimal set of unitaries must have three gates: U_0, U_1 and U_2. We chose $\Pi_0 = U_2U_1U_0$, $\Pi_1 = U_2U_0U_1$, $\Pi_2 = U_0U_2U_1$ and $\Pi_3 = U_0U_1U_2$, and the ansatz $U_0 = X_{\alpha_0}Z_{\beta_0}$, $U_1 = X_{\alpha_1}Z_{\beta_1}$ and $U_2 = X_{\alpha_2}Z_{\beta_2}$. Solving for α_j and β_j, we found solutions for each column and any $a \in [0, \pi)$. Some solutions are the following:

- **For column $k = 0$:** $\alpha_j = 0$ and β_j arbitrary for every j.
- **For column $k = 1$:** $\alpha_0 = 0$, $\alpha_1 \neq 0$ arbitrary, $\alpha_2 = (\pi - 2a)\alpha_1/(\pi + 2a)$, $\beta_0 = (\pi + 2a)/2\alpha_1$, β_1 arbitrary and $\beta_2 = (3\pi + 2\alpha_2\beta_1 - 2a)/2\alpha_1$.
- **For column $k = 2$:** $\alpha_0 = 0$, $\alpha_1 \neq 0$ arbitrary, $\alpha_2 = -\alpha_1$, $\beta_0 = \pi/\alpha_1$, β_1 arbitrary, and $\beta_2 = -\beta_0 - \beta_1$.

- **For column $k = 3$:** If $a = \pi/2$, then $\alpha_0 \neq 0$ arbitrary, $\alpha_1 = 0$, α_2 arbitrary, β_0 arbitrary, $\beta_1 = 0$, $\beta_2 = (-\pi + \alpha_2\beta_0)/\alpha_0$. If $a \neq \pi/2$, then $\alpha_0 = 0$, $\alpha_1 \neq 0$ arbitrary, $\alpha_2 = (-3\pi + 2a)\alpha_1/(\pi - 2a)$, $\beta_0 = (-\pi + 2a)/2\alpha_1$, β_1 arbitrary, and $\beta_2 = (\pi + 2\alpha_2\beta_1 - 2a)/2\alpha_1$.

Thus, for every CHPP of size 4, minimal sets of unitaries satisfying the promise do exist.

We conjecture that minimal sets of unitaries satisfying a CHPP exist for every size p. However, they may require joint systems as target, just like the construction in Ref. [29]. That is, for some p, keeping the number of unitaries low would demand an increase in the dimension of the target.

2.3 Solution using the quantum switch

The quantum switch S is a device that applies a set of unknown gates on a target quantum system in different orders that are determined by a control quantum system. For each basis state $|j\rangle$ of the control, a corresponding permutation Π_j of the gates is applied on the target, which is prepared in some arbitrary initial state $|\psi\rangle$. Mathematically, the action of the quantum switch for unitary gates is described by the joint unitary

$$S = \sum_{j=0}^{p-1} \Pi_j \otimes |j\rangle\langle j| \ , \tag{2.3.1}$$

where the first operation in the tensor product acts on the target system and the second one acts on the control. Hence,

$$S\left(|\psi\rangle \otimes |j\rangle\right) = \Pi_j |\psi\rangle \otimes |j\rangle \ . \tag{2.3.2}$$

If the control is in a superposition of states, then the gates are applied in a superposition of orders (see Fig. 2.3.1).

In the literature, it is common to find the expression "N-`switch`" for a quantum switch of N gates. As we mentioned above, we do not necessarily require all possible permutations, so it makes sense to refer to an (N, p)-`switch`, i.e., a quantum switch of N gates applied in p different orders. Of course, since there are different combinations of p permutations of N elements, the expression "(N, p)-

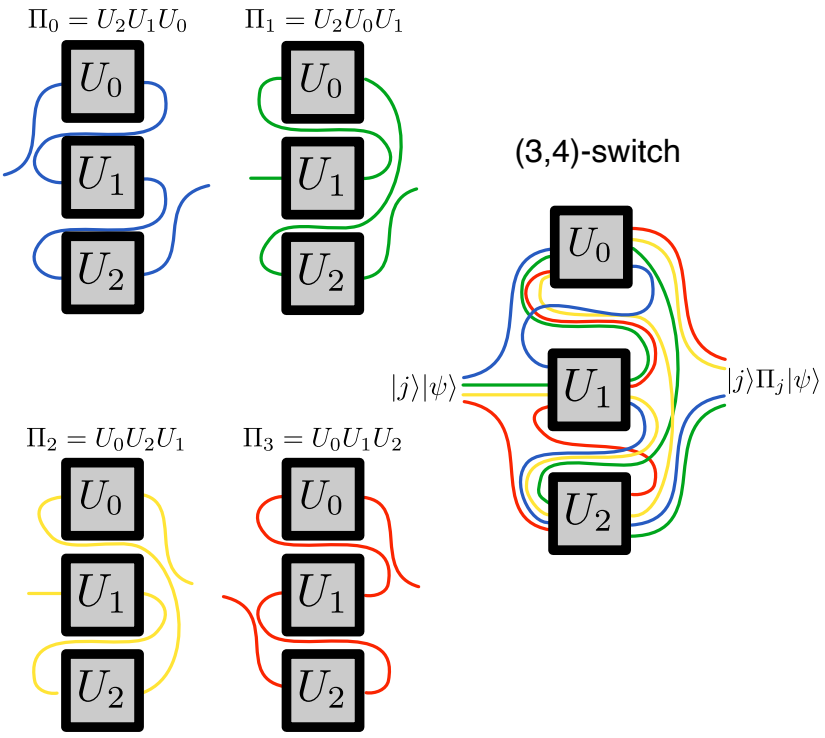

Figure 2.3.1: Example of (N, p)-`switch`. An (N, p)-`switch` applies N unitaries in p different orders. In the image we show a $(3, 4)$-`switch`, where the colour wires represent the states of the control system.

`switch`" properly denotes a *class* of quantum switches. Therefore, the N-`switch` considering all the $N!$ permutations, as originally introduced in Ref. [29], is the only quantum switch in the class of $(N, N!)$-`switches`. Rigorously speaking, the HPP implemented in Ref. [36] is solved using a $(4, 4)$-`switch` and the scaling method proposed in Ref. [38] uses $(N, 2^{N-1})$-`switches` that can be described as nested $(2, 2)$-`switches`[3]. Note that the exploration of different combinations of permutations of channels was also highlighted in Refs. [30–32].

The quantum switch plays a key role in the quantum approach to solving the CHPP, which is a straightforward extension of the protocol for solving the FPP in Ref. [29]. It is as follows: First, consider a CHPP specified by a matrix $M \in CH(p)$ and a set of p permutations $\{\Pi_j\}$ of N unitaries. Suppose the unitaries satisfy the promise for the k-th column of M. Now initialize a control system of dimension p in the state $|0\rangle$, and a target system of dimension compatible with the problem in an arbitrary state $|\psi\rangle$. The unitary gate $M/\sqrt{p}$ is applied on the control system.

[3]Cf. footnote 2.

Since M must be in its dephased form, the joint state becomes

$$\left(I \otimes \frac{1}{\sqrt{p}} M\right) (|\psi\rangle \otimes |0\rangle) = |\psi\rangle \otimes \frac{1}{\sqrt{p}} \sum_{j=0}^{p-1} |j\rangle \ . \tag{2.3.3}$$

Then, applying the corresponding quantum switch we get

$$\begin{aligned} S\left(|\psi\rangle \otimes \frac{1}{\sqrt{p}} \sum_{j=0}^{p-1} |j\rangle\right) &= \frac{1}{\sqrt{p}} \sum_{j=0}^{p-1} S\left(|\psi\rangle \otimes |j\rangle\right) \\ &= \frac{1}{\sqrt{p}} \sum_{j=0}^{p-1} \Pi_j |\psi\rangle \otimes |j\rangle \end{aligned} \tag{2.3.4}$$

where we used Eq. (2.3.2). Using now the definition of the promise (2.2.1) and recognizing the matrix multiplication, we have

$$\begin{aligned} S\left(|\psi\rangle \otimes \frac{1}{\sqrt{p}} \sum_{j=0}^{p-1} |j\rangle\right) &= \frac{1}{\sqrt{p}} \sum_{j=0}^{p-1} \Pi_0 |\psi\rangle \otimes M_{jk} |j\rangle \\ &= \frac{1}{\sqrt{p}} \Pi_0 |\psi\rangle \otimes M |k\rangle \ . \end{aligned} \tag{2.3.5}$$

Applying the inverse $M^\dagger/\sqrt{p}$ on the control, the number k of the column becomes encoded on the control system:

$$\left(I \otimes \frac{1}{\sqrt{p}} M^\dagger\right) \left(\frac{1}{\sqrt{p}} \Pi_0 |\psi\rangle \otimes M |k\rangle\right) = \Pi_0 |\psi\rangle \otimes |k\rangle \, . \tag{2.3.6}$$

Finally, a projective measurement on the control system gives us the solution of the problem deterministically.

The solution of the CHPP using the quantum switch only requires a single use of each gate. Indeed, this can be shown by coupling one high-dimensional ancilla state $|f\rangle$ as "counter" to each gate [29], whose state evolves from $|f\rangle$ to $|f+1\rangle$ each time the corresponding gate is used, with $f \in \mathbb{N}$. More specifically, if the counters are initialized in state $|0\rangle$, then the state of each counter becomes $|1\rangle$ after applying the quantum switch, since the unitaries are coherently controlled. The solution using the quantum switch is the most efficient solution known to the CHPP, as we discuss in next section.

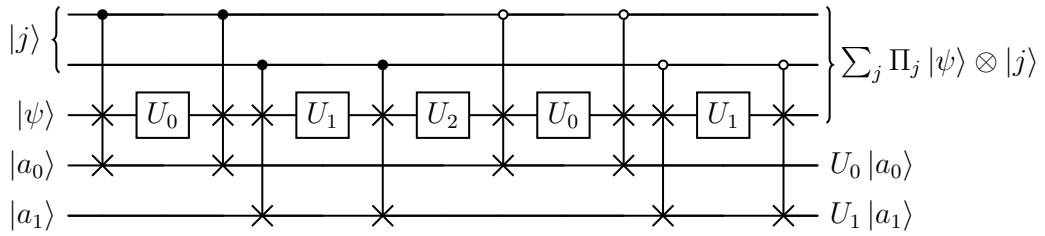

Figure 2.4.1: Fixed-order simulation of a $(3,4)$-switch. The arrangement of the U_i gates in the circuit is the shortest one containing the permutations 012, 021, 120 and 201. This circuit has a two-qubit control register, one target and two ancillary systems. The state $|j\rangle$ of the control defines which permutation will be applied to the target system $|\psi\rangle$. The target is routed with the aid of controlled-swap gates which interchange the target and one of the ancillas $|a_i\rangle$.

2.4 Solution using fixed-order circuits

The CHPP can also be solved using fixed-order circuits. However, as we discuss next, the solution using the quantum switch requires a fewer number of gate queries than the best known fixed-order alternatives, which is referred to as *query complexity advantage*.

2.4.1 Simulation of the quantum switch

A first way to solve the CHPP using a fixed-order circuit is by simulating the quantum switch in the circuit model [144, 149]. The best simulation known requires as many gates as elements are in the shortest common supersequence (SCS)[4] of the permutations involved [144]. The circuit consists of a target and a p-dimensional control system. The gates are applied in the order specified by the SCS and for each extra use of a unitary gate an ancillary system with the same dimension of the target is added [36]. Controlled-swap gates route the target in such a way that it undergoes the required permutation of the gates. Furthermore, the ancillas are used in such a way that they end up being disentangled from the rest of the system. See Fig. 2.4.1 for a $(3,4)$-`switch` fixed-order simulation example.

In order to assess the query advantage of the quantum switch against its fixed-order

[4]Given a set of sequences $s_1, ..., s_r$, a supersequence s' is a sequence such that every s_i can be recovered by deleting some elements from s'. A SCS is a supersequence of minimal length and may not be unique. For example, $s' = 0120210$ is a SCS for the set of sequences $\{012, 021, 102, 120, 201, 210\}$.

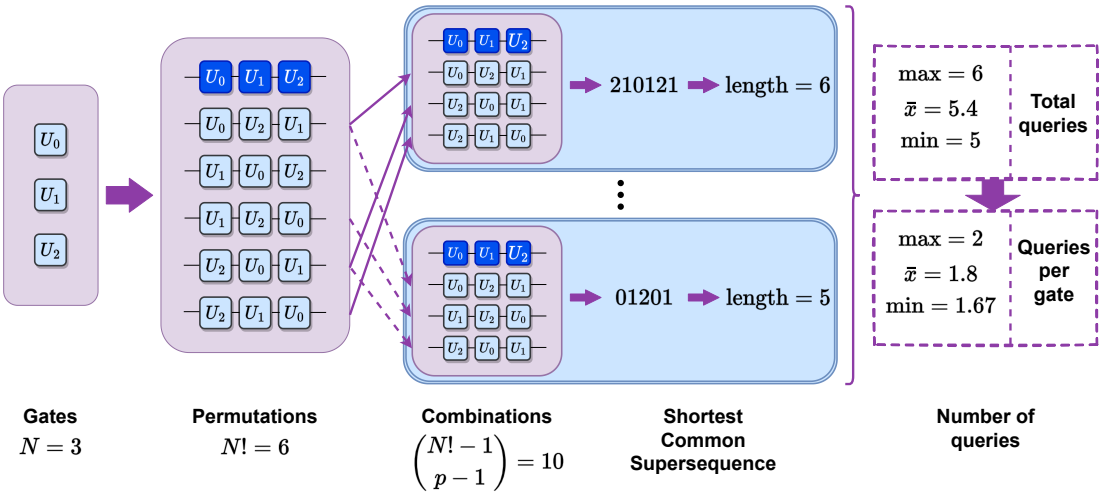

Figure 2.4.2: Number of gate queries in a fixed-order simulation. We illustrate how to calculate numerically the number of queries required by the simulation of a $(3, 4)$-`switch`. Firstly, all the permutations of the gates and all the combinations of p permutations are computed. We demand the combinations to include $\Pi_0 = U_{N-1}...U_1U_0$, otherwise the gates are relabeled. Then, one SCS for each combination is found numerically and their lengths are averaged.

simulation, we have to find the length of the corresponding SCS, which will be equal to the total number of queries. However, the problem of finding a SCS has been proved to be NP-complete [150] and some approximate algorithms have been reported in the literature (for further details see Ref. [151]). In the case of the SCS containing all the $N!$ permutations of N elements, its length grows with $\mathcal{O}(N^2)$ [144] and an upper bound is set by the length of the Koutas-Hu supersequence [152]. In this work, we deal with a broader scenario considering $p \leq N!$ permutations, hence the SCS may be shorter. To find it, we proceed by numerical exhaustive search, i.e., we list and sort by length all the sequences shorter than the Koutas-Hu supersequence and for each one we decide if it contains or not the desired set of permutations; the search halts when the first supersequence is found and its length is recorded. In this fashion, we explored the cases $N = 3$ and $N = 4$ with varying p, confirming that the total number of queries depends on both N and p, and also on the specific set of permutations. For example, simulating a $(3, 4)$-`switch` demands 5 or 6 gate uses, which depends on the set of chosen permutations, with an average of 5.4 queries (see Fig. 2.4.2). For the case of the $(3, 3!)$-`switch`, 7 calls to the gates are required. Similarly, simulating a $(4, 4)$-`switch` requires a number of gate uses in a range from 6 to 9, with an average of 7.43, while simulating all the permutations of 4 gates demands 12 queries.

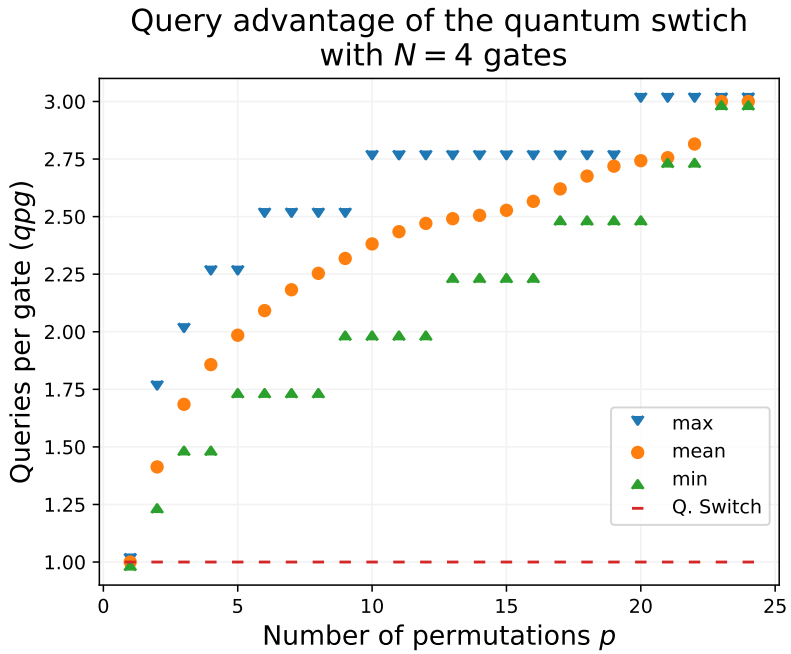

Figure 2.4.3: Queries per gate in fixed-order simulations for $N = 4$ gates. The graph shows the minimum, maximum and average queries per gate (qpg) of a fixed-order simulation of an (N, p)-`switch`, for $N = 4$ and varying p. The dashed line shows the performance of the quantum switch.

In Refs. [29, 38], each promise problem is specified by the number of gates N. Here, we have seen that the same CHPP can be defined for different values of N. As a consequence, the total number of queries may not be the best parameter to assess the computational advantage of the quantum switch over solutions based on fixed-order circuits solving the same task. We find it useful to introduce the average number of *queries per gate* (qpg) as a parameter for query complexity advantage. The quantum switch has a constant value of $qpg_{switch} = 1$ for every CHPP, while its simulation via the shortest common supersequence grows with $qpg = \mathcal{O}(N)$. The simulations of the $(3, 4)$- and $(4, 4)$-`switches` described in the previous paragraph have averages $qpg_{(3,4)} = 1.8$ and $qpg_{(4,4)} = 1.86$, respectively, and if we consider all the permutations of 3 and 4 gates, the corresponding simulations of the quantum switch will be $qpg_{(3,3!)} = 2.33$ and $qpg_{(4,4!)} = 3$. A thorough description for the case $N = 4$ is shown in Fig. 2.4.3. It can be seen that the quantum switch offers advantage for every $p \geq 2$ with the greatest difference for $p = N!$.

2.4.2 Other approaches

We could ask whether different approaches using fixed-order circuits could solve any arbitrary CHPP as well. In particular, tomographic reconstruction of the gates is discussed in Ref. [36], with cubically worse performance in N than with the quantum switch; similarly, direct reconstruction of the permutations is still quadratically worse than the quantum switch. Alternatively, the authors of Ref. [145] proposed a causal circuit which solves the original FPP with $\mathcal{O}(N \log N)$ queries to the gates ($qpg = \mathcal{O}(\log N)$), and in Ref. [38] they extended it to solve the HPP. That is the best fixed-order circuit known to solve these particular tasks for large N and it is conjectured that no causal algorithm can solve them more efficiently. It is an open question whether this approach can be extended to the general CHPP.

There is one additional scenario that deserves special attention, since it could solve the CHPP also with $qpg = 1$. It is known from the d-dimensional dense coding protocol that we can send a 2-dit message using 1 qudit system when a maximally entangled high-dimensional channel has been previously shared. This information is encoded by applying a generalized Pauli gate on the system and retrieved at the end in a Bell-state measurement [153]. Retrieving the message is equivalent to discriminating which Pauli gate was applied. Consequently, to solve a CHPP where the unitary gates are known to be a certain set of Pauli gates, we could identify each unitary by using it to perform a dense coding protocol and then calculate their permutations; it would solve the CHPP with a single query to each gate, the same as the quantum switch. Notwithstanding, this approach consumes N pairs of maximally entangled qudits (one for each unitary) and requires prior information about the gates. Also, the Bell-state measurement must be performed with respect to the correct basis. Instead, the quantum switch based solution does not consume entanglement nor need prior information about the gates.

2.5 Remarks on possible experimental realizations

The introduction of the more general CHPP opens the possibility for experimental realizations of the computational advantage of the quantum switch in higher

dimensions, both in terms of the number of permutations and the dimension of the target system. In addition, the more general description via CH matrices should allow these problems to be more readily adapted to different experimental platforms that do not necessarily implement a Fourier or Hadamard transformation directly.

Most of photonic implementations of the quantum switch have exploited the polarization degree of freedom as either the control or target system [7–10, 12, 36]. For higher-dimensional target systems, implementations of the BHPP with the quantum switch requires two photonic degrees of freedom (DOF) with dimension greater than two. Due to the fact that arbitrary $d \times d$ unitary operations can be constructed from 2×2 beam splitters and phase shifters [154], the path DOF is a natural candidate for the control system. Moreover, multiport beam splitters can be used to implement Hadamard and/or Fourier transformations directly [155, 156]. For the target system, a number of transverse DOFs could be used. For example, Weyl-Heisenberg operators can be implemented on the orbital angular momentum of photons using spiral wave plates and other linear devices [157]. D-dimensional states and unitaries can also be implemented using gratings and near-field diffraction via the Talbot effect [158], an approach which could also apply to matter waves [159]. Regarding the implementation of the most general CHPP, a CV target system is required. Particularly, simple photonic realizations could exploit the continuous transverse position/momentum of photons [20], where the appropriate Weyl-Heisenberg operators can be implemented using lenses and phase devices [160].

Our results might also inspire exploration of promise problems and the quantum switch using non-photonic systems. As noted in Ref. [80], there are a number of systems with continuous degrees of freedom that could be candidates for the quantum switch, including trapped ions or cavity QED systems.

Generalization of the Fourier and Hadamard promise problem to the CHPP also inspires further study from a fundamental point of view. Causal non-separability of the quantum switch has been experimentally confirmed for the case of two gates acting on a qubit target [8, 9, 16], but a similar proof with gates acting on either higher-dimensional or CV systems is still lacking. Furthermore, as far as we are aware, nor has experimental demonstration of causal non-separability of the (N, p)-`switch` been reported.

2.6 Conclusions

We have introduced the Complex Hadamard Promise Problem, a family of computational tasks that includes the previously defined Fourier Promise Problem [29] and Hadamard Promise Problem [36] as limiting cases, and shown how it can be solved using the quantum switch. This generalization allows for the definition of promise problems that can be solved in a wider array of physical control and target systems, including continuous variable target systems. Moreover, it uncouples the size p of the Complex Hadamard matrix and the number of quantum gates N, requiring only that $p \leq N!$.

Restricting to the case of finite dimensional target systems, we have shown that these generalized promise problems are restricted to the sub-class of Butson-Hadamard Promise Problems. In that case, the dimension of the target must be compatible with the complexity of the Butson-Hadamard matrix defining the problem. In particular, all Complex Hadamard Promise Problems reduces to the Hadamard Promise Problem when the target system is a qubit. A comparison with related work is summarized in Table 2.0.1.

Also, we have proved that using a more general class of (N, p)-`switches` to solve the Complex Hadamard Promise Problem provides computational advantages against known fixed-order algorithms in both discrete and continuous variable target systems. To best highlight this advantage, we have introduced the "query per gate" parameter. The lowest value of this parameter is reached by the quantum switch, which has a fixed $qpg_{switch} = 1$, suggesting that the quantum switch could be considered a benchmark for query complexity.

Our work opens the possibility for experimental implementations of promise problems in new platforms, such as CV photonic systems, trapped ions or cavity QED. Regarding differences between using finite-dimensional and CV quantum systems, we remark that some CHPPs are exclusively defined for CV systems, since the restrictions imposed by the dimension of the system are lifted in the CV regime. Finally, we highlight the necessity of further study on the (N, p)-`switch` as an indefinite causal order instance and its possible application to other computational tasks.

Chapter 3

Estimation of unitary transformations using the quantum switch

The continuous advancement in the ability to control quantum systems and its application to the development of quantum technologies has driven the search for high-precision measurements and estimation methods. Quantum metrology aims to develop methods and tools that achieve the ultimate precision in parameter estimation.

An instance of multiparameter estimation is the estimation of d-dimensional unitary transformations. Several methods to accomplish this task have been studied [161, 162], particularly standard quantum process tomography (SQPT) [163], which has been successfully implemented for reconstructing quantum gates on ion traps [164], superconducting circuits [165], among many others [166, 167].

This chapter explores the application of the quantum switch to estimation of unitary gates. It starts with a brief introduction to quantum parameter estimation in Section 3.1. In Section 3.2 we show how to estimate qubit unitary gates using a $(3, 4)$-switch and saturating the quantum Cramér-Rao bound. We draw an equivalent fixed-order circuit and perform numerical simulations comparing it with SQPT. Then, in Section 3.3 we extend the circuit to higher dimensions and show that our estimation procedure saturates the quantum Cramér-Rao bound for unitaries close to the identity. In Section 3.4 we replace the unknown unitary

transformation by an arbitrary quantum channel and discuss some features of the circuit. Finally, we summarise our results in Section 3.5 and discuss how the proposed circuit inspires the introduction of the quantum switch with continuous control when trying to extend it to the CV regime.

Part of the results of this chapter have been published in

- J. Escandón-Monardes, D. Uzcátegui, M. Rivera-Tapia, S. P. Walborn and A. Delgado, "Estimation of high-dimensional unitary transformations saturating the Quantum Cramér-Rao bound", *Quantum* **8**, 1405 (2024).

3.1 Quantum parameter estimation

Parameter estimation, either classical or quantum, consists of four stages [143]:

(1) **Preparation:** A *probe* system is initialized in a particular state ρ_0.

(2) **Parameterization:** The probe interacts with some device or natural process which alters the state of the probe in a way that the final state of the probe depends on a parameter vector $\mathbf{t}$.

(3) **Measurement:** The probe in its final state is measured, generating a probability distribution $P(y|\mathbf{t})$, where y is the observed value in an experiment for a given parameter vector $\mathbf{t}$.

(4) **Classical estimation:** An estimator $\hat{\mathbf{t}}$ provides an estimated value of $\mathbf{t}$ based on the results of the measurement.

The precision of the estimation is described by the Fisher information. The classical Fisher information for the estimation of a single parameter t is given by

$$\mathcal{I} = \sum_y \frac{1}{P(y|t)} \left[\frac{\partial P(y|t)}{\partial t}\right]^2, \tag{3.1.1}$$

which is a measure of the sensitivity of the probability distribution to variations in the parameter t. Its extension to the multiparameter case is the classical Fisher information matrix defined by its entries as:

$$\mathcal{I}_{ab} = \sum_y \frac{1}{P(y|\mathbf{t})} \left[\frac{\partial P(y|\mathbf{t})}{\partial t_a}\right] \left[\frac{\partial P(y|\mathbf{t})}{\partial t_b}\right]. \tag{3.1.2}$$

The significance of the Fisher information in classical estimation theory is better understood in the light of the Cramér-Rao bound. The classical Cramér-Rao bound states that the covariance matrix $cov(\hat{\mathbf{t}})$ of an unbiased estimator $\hat{\mathbf{t}}$ of a parameter vector $\mathbf{t}$ is bounded below by the inverse of Fisher information matrix $\mathcal{I}(\mathbf{t})$, that is, for n repetitions of the experiment,

$$cov(\hat{\mathbf{t}}) \geq \frac{1}{n}\mathcal{I}^{-1}(\mathbf{t}). \tag{3.1.3}$$

In quantum metrology, the probe system is a quantum state and the measurement performed on it is a POVM. The probability distribution $P(y|\mathbf{t})$ depends on the measurement performed, which leads to different Fisher information matrices. Moreover, it is possible to derive (see Appendix H in Ref. [143]) a new bound known as the quantum Cramér-Rao bound [168, 169] given by

$$cov(\hat{\mathbf{t}}) \geq \frac{1}{n}\mathcal{I}^{-1}(\mathbf{t}) \geq \frac{1}{n}\mathcal{F}^{-1}(\mathbf{t}), \tag{3.1.4}$$

where $\mathcal{F}$ is the quantum Fisher information matrix. Eq. (3.1.4) sets a bound to the achievable precision in the estimation of a set of parameters in the context of quantum mechanics for a fixed probe ρ_0. For single parameter estimation, the quantum Fisher information is just the classical Fisher information optimised over the set of all POVMs. In the case of estimating a set of parameters encoded in a unitary transformation U that acts onto a pure probe state $|\phi\rangle$, the quantum Fisher information matrix can be calculated as [143]

$$\mathcal{F}_{a,b} = 2\langle\phi|\{H_a, H_b\}|\phi\rangle - 4\langle\phi|H_a|\phi\rangle\langle\phi|H_b|\phi\rangle, \tag{3.1.5}$$

where $H_a = i(\partial_a U^\dagger)U$.

The enhancement provided by quantum metrology depends not only on the quantum measurement, but also on the probe state. Indeed, the optimal probe state for single parameter estimation depends on the process that encodes the parameter; while a given state may be optimal regarding one process, it may be useless for a different encoding.

Due to its intrinsic difficulty [143], the multiparameter case has remained less explored than the single parameter scenario. In particular, the optimal measurements for different parameters are often incompatible [170] and the optimal

probe states for different parameters can typically be different. Furthermore, in the multiparameter estimation, the quantum Cramér-Rao bound is generally not achievable even asymptotically [171, 172]. However, there are other Cramér-Rao type bounds, which are defined considering a weighted trace of the covariance matrix and are attainable in some scenarios [173–177].

Parameter estimation and the quantum switch

Is it possible to use the quantum switch for parameter estimation getting any advantage in precision when compared with fixed order circuits? We have seen in Section 1.1.2.2.4 that several works have shown this advantage in the single parameter case, particularly in the estimation of a parameter that characterises a noisy channel and the estimation of the phase of a unitary transformation surrounded by a noisy environment. The advantage is often shown by using the Fisher information as figure of merit. Nonetheless, it is important to note that the advantage provided by indefinite causal order in single parameter estimation disappears in the asymptotic limit [178].

Here, we propose to use the quantum switch for a multiparameter estimation task, namely the estimation of a d-dimensional unitary transformation U. In paralel to this work, Ref. [88] studied a different scenario to the one developed in the rest of this chapter. To the best of our knowledge, Ref. [88] is the only reported application of the quantum switch to multiparameter estimation.

3.2 Estimation of qubit unitary transformations

3.2.1 Qubit unitary transformations

Let us start considering the case of 2-dimensional unitary transformations. These can be written as [179]

$$U = \exp(-i\alpha\hat{n}\cdot\hat{\sigma}), \tag{3.2.1}$$

where $\hat{\sigma} = (X, Y, Z)^T$ is the Pauli vector, $\alpha \in [0, \pi/2]$, and $\hat{n} \in \mathbb{R}^3$ is a real unitary vector. After carrying out the exponentiation, we obtain the representation

$$U = u_{00}I + u_{10}X + u_{11}XZ + u_{01}Z, \tag{3.2.2}$$

where we replaced $Y = iXZ$, and the coefficients are given by

$$\begin{aligned} u_{00} &= \cos(\alpha), \\ u_{10} &= -i\sin(\alpha)\sin(\theta)\cos(\phi), \\ u_{11} &= \sin(\alpha)\sin(\theta)\sin(\phi), \\ u_{01} &= -i\sin(\alpha)\cos(\theta), \end{aligned} \tag{3.2.3}$$

with $\theta \in [0, \pi]$ and $\phi \in [0, 2\pi[$ being the spherical coordinates for $\hat{n}$, and I the 2×2 identity matrix. Notice that u_{00} is always non-negative, whereas the signs of u_{10}, u_{11}, u_{01} depend on the octant in which the vector $\hat{n}$ points. Estimating an unknown two-dimensional unitary transformation U is thus equivalent to estimating the values of the angles (α, θ, ϕ).

3.2.2 Protocol

Let us consider a $(3, 4)$-switch, that is a quantum switch with three gates applied in a superposition of four different orders. The three gates are one copy of the unknown unitary U, one fixed Pauli gate X and one fixed Pauli gate Z. The four orders (see. Fig. 3.2.1) are:

$$\begin{aligned} \Pi_{00} &= XUZ\ , \\ \Pi_{01} &= UZX\ , \\ \Pi_{10} &= XZU\ , \\ \Pi_{11} &= ZUX\ . \end{aligned} \tag{3.2.4}$$

The control system is a four dimensional system, but for convenience we denote it as a two-qubits system and use a pair of subindexes accordingly. The operation applied by the quantum switch is the unitary

$$U_{switch} = \sum_{i,j=0}^{1} \Pi_{ij} \otimes |ij\rangle\langle ij|\ , \tag{3.2.5}$$

with the first operation in each tensor product acting on the target system and the second operation acting on the control system.

Let us initialise the target system in an arbitrary pure state $|\psi\rangle$ and the control

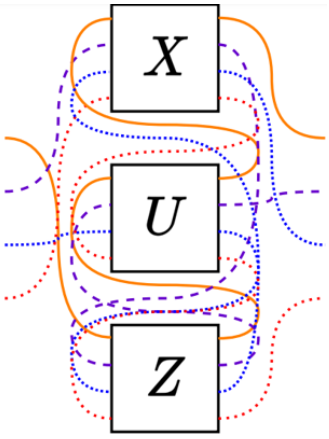

Figure 3.2.1: $(3,4)$**-switch for estimation of qubit unitary.** In our proposal, one unknown unitary U and fixed unitaries X and Z are inserted in a quantum switch of three gates and four coherently controlled orders.

system in the state $|{+}{+}\rangle = \sum_{i,j=0}^{1} |ij\rangle /2$. After the application of the quantum switch, the joint system is in a superposition of four orders, which are then combined by applying a Hadamard gate on each control qubit, getting the state

$$|\Phi\rangle = u_{01} X |\psi\rangle \otimes |00\rangle + u_{00} XZ |\psi\rangle \otimes |01\rangle + u_{11} |\psi\rangle \otimes |10\rangle + u_{10} Z |\psi\rangle \otimes |11\rangle \ . \quad (3.2.6)$$

Notice that additional controlled Pauli gates X, ZX, I and Z can be applied on the target, respectively for each state of the control, disentangling the control and target systems. Additionally, if an X gate is applied on the second control qubit, then the subindexes of the coefficients would match the corresponding states of the control. Consequently, the final state is

$$|\Phi'\rangle = |\psi\rangle \otimes (u_{00} |00\rangle + u_{01} |01\rangle + u_{10} |10\rangle + u_{11} |11\rangle) \ . \quad (3.2.7)$$

Thus, a projective measurement of control qubits in the computational basis leads to probabilities

$$P_{00} = \cos^2(\alpha), \quad (3.2.8)$$

$$P_{10} = \sin^2(\alpha) \sin^2(\theta) \cos^2(\phi), \quad (3.2.9)$$

$$P_{11} = \sin^2(\alpha) \sin^2(\theta) \sin^2(\phi), \quad (3.2.10)$$

$$P_{01} = \sin^2(\alpha) \cos^2(\theta). \quad (3.2.11)$$

It follows that

$$\begin{aligned}\cos^2(\alpha) &= P_{00},\\ \cos^2(\theta) &= \frac{P_{01}}{1-P_{00}},\\ \cos^2(\phi) &= \frac{P_{10}}{P_{11}+P_{10}}.\end{aligned} \tag{3.2.12}$$

These relations allow for estimating the value of α, which is always in the interval $[0, \pi/2]$. However, parameters θ and ϕ remain ambiguous, since u_{01}, u_{10}, u_{11} are determined up to a sign. This ambiguity is removed when the octant pointed to by $\hat{n}$ is known beforehand, in which case our estimation procedure characterizes the unknown unitary transformation. Furthermore, it can be shown by direct algebra that our estimation procedure fulfills the equality $\mathcal{I} = \mathcal{F}$ where

$$\mathcal{F} = 4\begin{pmatrix} 1 & 0 & 0 \\ 0 & \sin^2(\alpha) & 0 \\ 0 & 0 & \sin^2(\alpha)\sin^2(\theta) \end{pmatrix}, \tag{3.2.13}$$

and therefore our proposal saturates the quantum Cramér-Rao bound. Moreover, $\mathcal{F}$ is diagonal, hence our circuit is optimal in the sense that the three parameters defining U can be estimated simultaneously with the highest possible precision. The quantum Fisher information matrix in Eq. (3.2.13) was also obtained in other works [142, 180, 181]. Thus, in terms of precision, our protocol is as good as the best of known fixed order strategies for the same number of queries to the unknown transformation U.

The lack of a priori information does not prevent the use of our estimation procedure. As we show through numerical simulations in section 3.2.5, our procedure can be complemented with additional measurements and at the same time achieves better estimation accuracy than that obtained by SQPT.

3.2.3 Experimental proposal

A photonic quantum switch of four gates and four paths based on multicore fibers technology was implemented in Ref. [36]. There, the polarization degree of freedom of a photon is used as the target qubit while its path degree of freedom acts as control. In the setup, shown in Fig. 3.2.2, a four-core fiber beam splitter (4CF-BS)

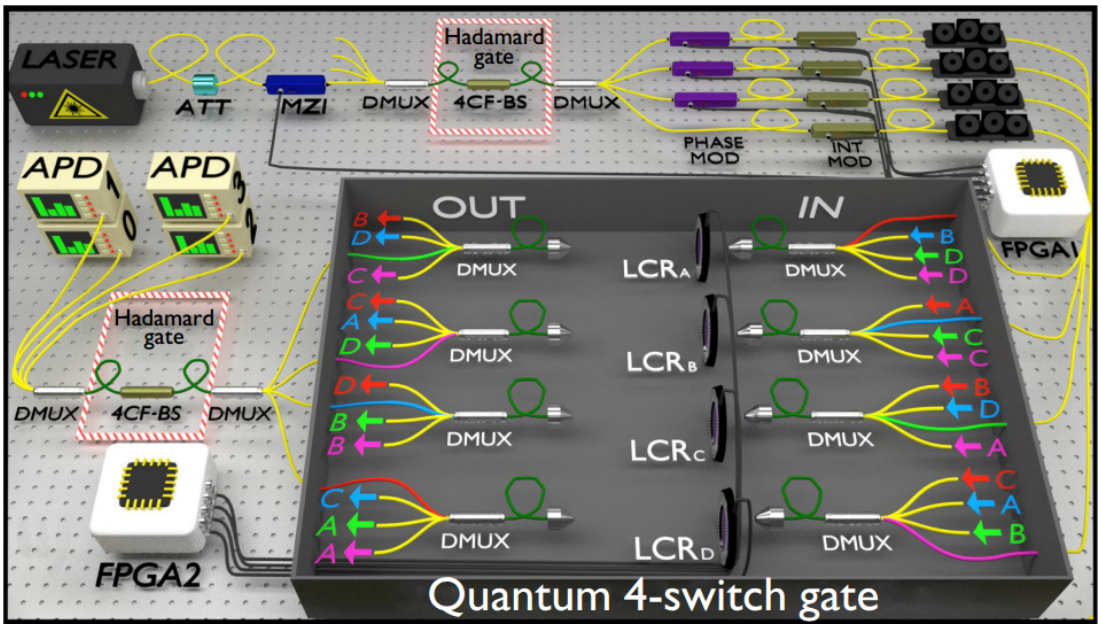

Figure 3.2.2: Experimental setup of a $(4,4)$**-switch.** Experimental setup for a photonic quantum switch using four-core-fiber beam splitters (4CF-BS) and controllable liquid crystal retarders (LCRs). This setup can be adapted to implement an optimal estimation of a unitary transformation on polarization. Figure from Ref. [36]

performs a four-dimensional Hadamard gate on the control. This operation is described by the matrix

$$H_4 = \begin{pmatrix} 1 & 1 & 1 & 1 \\ 1 & 1 & -1 & -1 \\ 1 & -1 & -1 & 1 \\ 1 & -1 & 1 & -1 \end{pmatrix}, \tag{3.2.14}$$

which is equivalent to the tensor product $H \otimes H$ of two qubit-Hadamard gates up to a relabeling of the computational basis. Before entering the quantum switch, a demultiplexer (DMUX) couples each core of the multicore fiber (green fibers) to a different single-mode fiber (yellow fibers). Four controllable liquid crystal retarders (LCRs) implement desired unitary transformations on the polarization of the photon. The photon is routed through the LCRs in the desired order by the single-mode fiber corresponding to each path. Finally, a second 4CF-BS recombines the paths and a projective measurement of the control is performed using a single-photon detector (APD) at the end of each path.

The same technology can be used to devise an experimental setup realizing our scheme. Indeed, as in Fig. 3.2.2, a photon can be initialised in an arbitrary state of polarization and coupled to a single-core fiber. After going through a 4CF-BS, the photon will be in the desired state of superposition of paths. The quantum switch in Fig. 3.2.2 can be modified in such a way that unitaries are fixed to be X, Z, I and the arbitrary unknown U. The order of the operations is adapted to the permutations in Eq. (3.2.4) by reconnecting the single-mode fibers that route the photon. Finally, the second 4CF-BS recombines the paths and the measurement of the control is performed as before. This proposal leads to the same probabilities from Eqs. (3.2.11) up to a relabeling. Hence, the estimation of a polarization transformation can be achieved with the highest precision using just two 4CF-BSs, one copy of U and two extra auxiliary unitaries.

3.2.4 Equivalent fixed-order circuit

The protocol proposed in Section 3.2.2 can be also implemented using the fixed-order circuit shown in Fig. 3.2.3, leading exactly to the same results. The circuit consists in one target qubit (qubit 0) and two control qubits (qubits 1 and 2). The target is initialised in an arbitrary state $|\psi\rangle_0$ and the control qubits in state $|00\rangle_{12}$. A Hadamard gate is applied on each control qubit, leading to the desired superposition state. Controlled Pauli operations are applied before and after U mimicking the quantum switch. Then, Hadamard gates are applied again on the control qubits to combine the different orders. The joint state $|\Phi^7\rangle_{012}$, where the superindex indicates the time step in the circuit, is exactly the state derived in Eq. 3.2.6. Extra controlled operations disentangle the target from the control and a final X gate on the second control qubit is applied just for convenience. The final state is the tensor product $|\psi\rangle_0 \otimes |\varphi\rangle_{12}$, where

$$|\varphi\rangle_{12} = u_{00}\,|00\rangle + u_{01}\,|01\rangle + u_{10}\,|10\rangle + u_{11}\,|11\rangle \ . \tag{3.2.15}$$

Interestingly, the final state of the target system is exactly the same as it was initialised, while all the information of U is now available in the control.

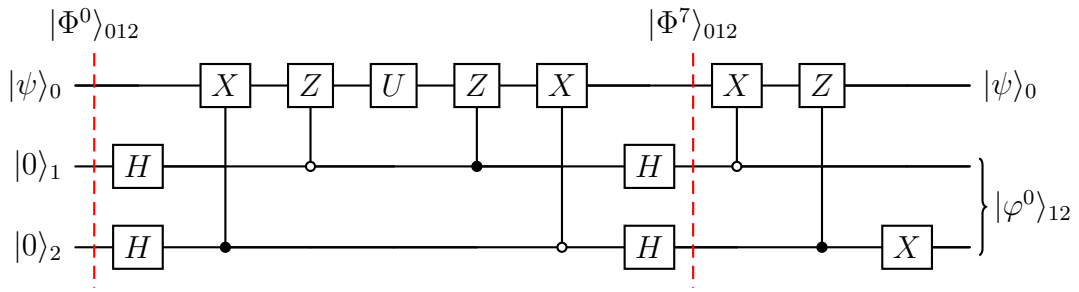

Figure 3.2.3: Fixed-order circuit for estimation of qubit unitary. The circuit is equivalent to the quantum switch proposed in Section 3.2.2. All the information related to U is transcribed to the final state of the control system.

3.2.5 Numerical simulations

In this section we study the performance of our estimation procedure for the case of qubit gates without prior information. This is achieved by measuring the quantum state in Eq. (3.2.15) in three different bases. The resulting statistics completely characterizes the unknown unitary transformation, as shown in Appendix A.

We simulate the fixed-order realization of our estimation procedure with Qiskit [182], IBM's software development platform for quantum processors, and compare its performance against the built-in function for SQPT. Since the output of SQPT is a quantum channel that is not necessarily unitary, contrary to our procedure which guarantees unitarity, we use as figure of merit the average gate fidelity, which compares a general quantum channel with a unitary quantum transformation [183]. We generate a set of 200 single-qubit unitary matrices, which are randomly drawn from a uniform Haar distribution. Each unitary transformation is reconstructed 1000 times using our estimation procedure and additionally SQPT. In both strategies we calculate the average gate fidelity respect to the ideal unitary gate. This is repeated using increasing number of shots (or ensemble sizes) to simulate the measurement results. Finally, we also perform simulations considering various error sources (see Appendix B) and readout error mitigation. The code implementing this method is available in a Github repository [184].

Figure 3.2.4 shows the simulation results for our estimation procedure (green solid dots) and SQPT (red solid dots). Figures (a) and (c) show mean and median gate fidelity, respectively, as functions of the number of shots obtained in absence of error sources, that is, when the operations required by the estimation procedures

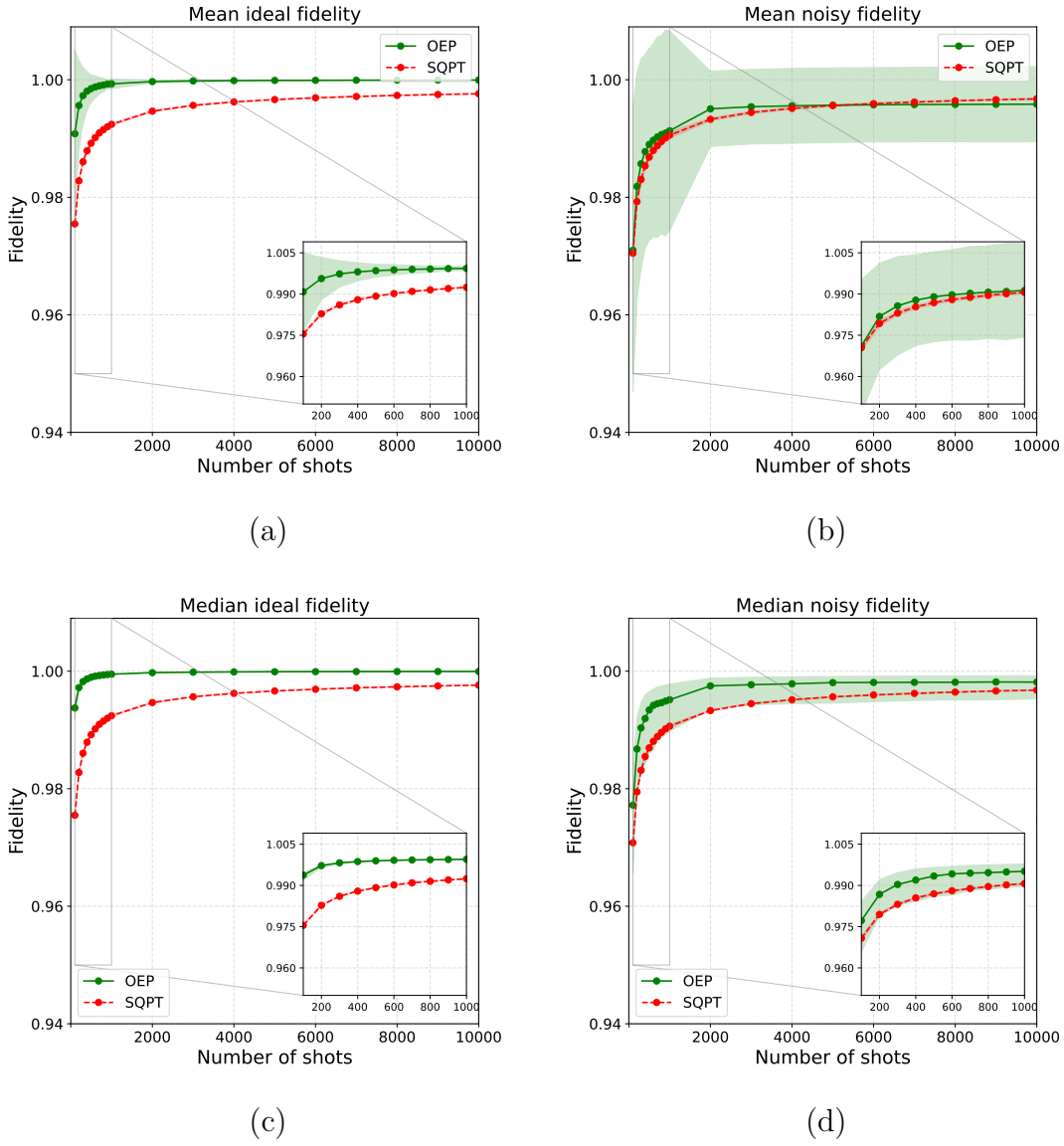

Figure 3.2.4: Mean and median gate fidelities - Noiseless and full noise. Plots (a) and (b) show the mean and plots (c) and (d) show the median gate fidelities as functions of the number of shots for both our estimation procedure (solid green dots) and SQPT (solid red dots). The left and right plots represent the noiseless and noisy cases, respectively. Shaded areas represent standard deviation or interquartile range. The insets illustrate the low number of shots regime.

are carried out perfectly. Figures (b) and (d) show results considering experiments with errors affecting single qubit gates, conditional gates, thermal relaxation, and measurements, a scenario that we call *full noise model*. This situation corresponds to a unitary gate embedded in a noisy device. Insets illustrate the behavior of estimation procedures in the small number of shots regime. Shaded areas show

standard deviation in Figs. (a) and (b) and interquartile range in Figs. (c) and (d).

In the noiseless case, according to Figs. (a) and (c), both our estimation procedure and SQPT are characterized by almost indistinguishable mean and median average gate fidelity. In addition, in regime of a large number of shots, both estimation procedures exhibit extremely narrow standard deviation and interquartile range. In the small number of shots regime, our estimation procedure has a very rapidly narrowing standard deviation and interquartile range. Therefore, our estimation procedure and SQPT lead to an average gate fidelity that is independent of the unitary transformation. Figures (a) and (c) show that our estimation procedure achieves near-unit gate fidelity for ensemble sizes as small as 2×10^3 clearly outperforming SQPT.

Simulations show that the presence of noise affects the estimation of our procedure, decreasing the mean and median average gate fidelity with respect to their noiseless values, as exhibited in Figs. (b) and (d). The mean average gate fidelity of both estimation procedures becomes very similar, while the median gate fidelity of our estimation procedure is above that of SQPT, although standard deviation and interquartile range of our estimation procedure become wider.

In Fig. 3.2.5 we study the impact of different error sources on our estimation procedure and compare it to SQPT. Figures (a) and (b) show the mean and median average gate fidelity, respectively, for the noiseless case (solid green dots), noisy control-not gate (solid red pentagons), full noise with ideal control-not gate (solid blue diamonds) and full noise (solid pink squares) for our estimation procedure, and SQPT with full noise (black crosses). All simulations consider readout error mitigation as described in Qiskit documentation [182]. The noise models and values used correspond to the `ibmq_quito` processor, and are provided in Appendix B. Insets depict the small ensemble regime. As expected, Fig. 3.2.5 shows that the full noise model leads to the the biggest decrease in the mean and median average gate fidelity. In the small ensemble regime, the estimation considering noisy control-not gates leads to a better mean and median gate fidelity than the estimation considering other error sources. However, as the ensemble size increases, the estimation procedure is clearly more affected by noisy control-not gates. Also, in this regime mean and median average gate fidelity become constant and the increase in the ensemble has no impact in the estimation accuracy.

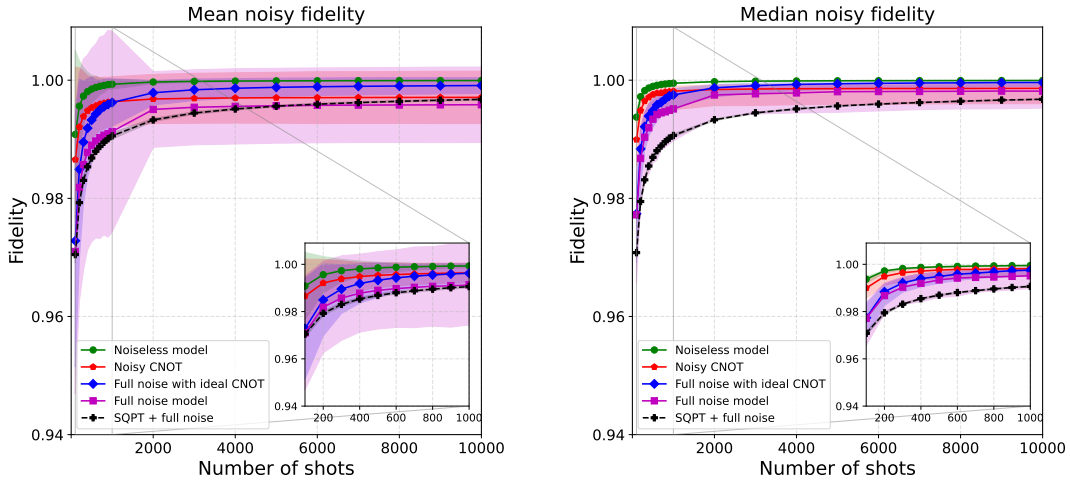

Figure 3.2.5: Mean and median gate fidelities - Different noise models. Mean (a) and median (b) gate fidelities as functions of the number of shots for our estimation procedure with different noise models and SQPT with full noise. Shaded areas represent standard deviation or interquartile range.

3.2.6 Discussion

Which is the role of indefinite causal order in our protocol? Is there any advantage provided by the quantum switch in this task? Unfortunately, indefinite causal order plays no role in this task.

It is clear from Section 3.2.4 that the outcome state from the quantum switch can be obtained from a fixed-order circuit using a single query of U. Hence, no query advantage is exhibited. Moreover, this conclusion agrees with Theorem 1 in Ref. [3], which states that every deterministic supermap (i.e. every transformation of a quantum channel into a quantum channel) can be realised as a quantum circuit where the input operation (in this case the unitary U) is inserted between two isometries (in this case all the unitary transformations before and after U in Fig. 3.2.3). In other words, if only one operation is unknown while all the rest are fixed, there is no query advantage compared to fixed-order circuits; the quantum switch can only provide query advantage when two or more unknown operations are inserted on it.

Notwithstanding, the quantum switch is still an alternative setup for estimation of unitary transformations, offering a saving in the number of auxiliary gates. Indeed,

in Section 3.2.3 we have proposed a photonic experiment realising estimation of a unitary transformation acting on the polarization degree of freedom of a photon. A comparable experiment has been performed in Ref. [142], which includes repetition of U and feedback further improving the precision of the estimation procedure. To make a fair comparison, we may remove feedback and fix the number of repetitions of U per round to $N = 1$. In that case, the implementation in Ref. [142] requires 10 half wave plates and 3 quarter wave plates as auxiliary gates on polarization, together with 3 beam displacers. Instead, our experimental proposal requires just 4 auxiliary gates in total. For a better precision, feedback and repetitions of U can be added without changing the number of auxiliary gates, thus keeping the advantage of the quantum switch in terms of number of auxiliary gates.

Regarding precision of the estimation procedure, we proved that our squeme saturates the quantum Cramér-Rao bound, being as good as the best fixed-order circuit. This is again a consequence of being a deterministic supermap. In experimental implementations, the precision achievable by our proposal, its fixed-order equivalent circuit or any other proposal, will be affected by noise. Thus, precision will depend more on the development of the chosen technology than on the presence of indefinite causal order.

For getting a real advantage in precision from indefinite causal order, it is needed to move to scenarios such as those studied in Ref. [88], where different parameters are encoded by different operations. In the next section we will follow a rather different direction, extending our protocol to higher dimensions and proving that it saturates the quantum Cramér-Rao bound for estimating high-dimensional unitary transformations close to the identity.

3.3 Estimation of high-dimensional unitary transformations saturating the Quantum Cramér-Rao bound

3.3.1 Unitary transformations

An arbitrary d-dimensional unitary transformation U can be expanded in the Weyl-Heisenberg basis as

$$U = \sum_{m,n=0}^{d-1} u_{m,n} X^m Z^n, \tag{3.3.1}$$

where X and Z are the shift and phase operators, respectively. These act onto the canonical basis $\{|k\rangle\}$ with $k = 0, \ldots, d-1$ as $X|k\rangle = |k \oplus 1\rangle$ and $Z|k\rangle = \omega^k |k\rangle$ with $\omega = \exp(2i\pi/d)$. The set $\{u_{m,n} = r_{m,n} e^{i\phi_{m,n}}\}$ of d^2 complex coefficients satisfies the unitarity constraint and characterizes U. With this, a general unitary can be written

$$U = r_{0,0} I + \sum_{\substack{m,n=0 \\ (m,n)\neq(0,0)}}^{d-1} r_{m,n} e^{i\phi_{m,n}} X^m Z^n. \tag{3.3.2}$$

where we set $\phi_{0,0} = 0$ without loss of generality.

3.3.2 General procedure

To estimate a d-dimensional unitary operation U, we propose a procedure which uses the quantum circuit shown in Fig. 3.3.1, which for dimension $d = 2$ reduces to the circuit in Fig. 3.2.3. This circuit is applied to the following initial quantum state of three qudits

$$|\Phi^0\rangle_{012} = |\psi\rangle_0 \otimes |00\rangle_{12}, \tag{3.3.3}$$

where the target qudit is in the arbitrary state $|\psi\rangle_0$, and the qudits labeled 1 and 2 are the control states. The superscript i in $|\Phi^i\rangle_{012}$ indicates the time step in the circuit. Each control qudit is subject to the action of a Fourier transform $F|k\rangle = (1/\sqrt{d}) \sum \omega^{mk} |m\rangle$, followed by the sequence of controlled shift and phase

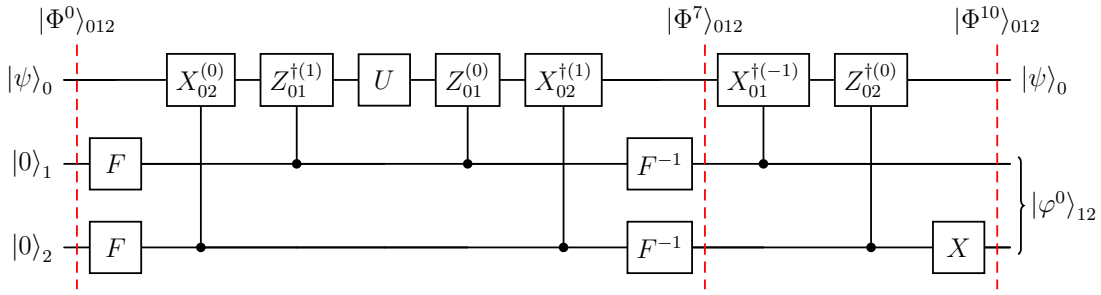

Figure 3.3.1: Quantum circuit implementation of our estimation procedure. F are d-dimensional Fourier transforms acting on control qudits 1 and 2, $X_{tc}^{(i)}$ and $Z_{tc}^{(i)}$ are controlled gates defined in Eq. (3.3.4), and U is the unitary transformation to be estimated. State tomography of the control system leads to complete estimation of U.

operators $X_{02}^{(0)}$ and $Z_{01}^{\dagger(1)}$ defined by

$$X_{tc}^{(i)} = \sum_{m=0}^{d-1} X_t^m \otimes |m \ominus i\rangle_c\langle m \ominus i|,$$
$$Z_{tc}^{(i)} = \sum_{m=0}^{d-1} Z_t^m \otimes |m \ominus i\rangle_c\langle m \ominus i|. \tag{3.3.4}$$

The action of the previous transformations leads to the probe state

$$\left|\Phi^3\right\rangle_{012} = \frac{1}{d}\sum_{j_1,j_2=0}^{d-1} Z_0^{-j_1-1} X_0^{j_2} \left|\psi\right\rangle_0 \otimes \left|j_1\right\rangle_1 \otimes \left|j_2\right\rangle_2 . \tag{3.3.5}$$

The unitary transformation U to be estimated acts on the target qudit followed by the sequence $Z_{01}^{(0)}$ and then $X_{02}^{\dagger(1)}$ and inverse Fourier transforms acting on each control qudit. Thereby, the initial state is transformed into the state

$$|\Phi^7\rangle_{012} = \sum_{m,n=0}^{d-1} u_{m,n+1}(X^{m-1}Z^n|\psi\rangle_0) \otimes |m\rangle_1 \otimes |n\rangle_2, \tag{3.3.6}$$

then $X_{01}^{\dagger(-1)}$ and $Z_{02}^{\dagger(0)}$ disentangles the target qudit from the control qudits, followed by X_2 which correlates the indexes of the coefficients with the computational basis of both control qudits. The final state (see Appendix C for details) is

$$|\Phi^{10}\rangle_{012} = |\psi\rangle_0 \otimes |\varphi^0\rangle_{12}, \tag{3.3.7}$$

where

$$\left|\varphi^0\right\rangle_{12} = \sum_{m,n=0}^{d-1} u_{m,n}|m\rangle_1 \otimes |n\rangle_2. \tag{3.3.8}$$

The coefficients $u_{m,n}$ entering in Eq. (3.3.1) are now in a one-to-one relation with the states in the canonical basis of the control qudits. Thus, the estimation of state $|\varphi^0\rangle_{12}$ by any quantum tomographic scheme for pure states leads to the estimation of the unknown unitary transformation U. Moreover, simpler measurement schemes can be used, provided that a pure state of two qudits is defined by a set of $2d^2 - 2$ independent real parameters while a unitary transformation acting on a single qudit is characterized only by $d^2 - 1$ real parameters. Some specific cases are studied below.

3.3.3 Unitary transformations close to the identity

In order to estimate a higher-dimensional unitary transformation we need a clear dependence of U in terms of $d^2 - 1$ independent real parameters. For example, U can be parametrized in a similar fashion to Eq. (3.2.1) as $U = \exp\left(i\sum_{j=1}^{d^2-1}\lambda_j T_j\right)$, where T_j are the generalized Gell-Mann matrices and λ_j are the independent real parameters. For $d = 2$ we expanded this expression in the Weyl-Heisenberg basis as in Eq. (3.2.2), where the complex coefficients $u_{m,n}$ explicitly depend on the corresponding parameters λ_j (see Eq. (3.2.3)). However, it is not possible to obtain equivalent relations for $d > 2$ analytically, leading to difficulties in both the estimation of λ_j and the calculation of the classical and quantum Fisher information matrices. Furthermore, finding a convenient parametrization that facilitates these calculations is an open problem. In this work, we consider the expansion of U from Eq. (3.3.2) where the elements in $\{r_{m,n}, \phi_{m,n}\}$ are not independent from each other. We restrict the analysis to unitary transformations that are close to the identity, since this approximation uncouples the parameters and allows us to obtain analytically both the classical and quantum Fisher information matrices.

To simplify the notation, we denote the coefficients $u_{p_x,p_z} \equiv u_p = r_p e^{i\phi_p}$, where we have defined a single index $p = (p_x, p_z)$. These coefficients are constrained by the conditions

$$\sum_{m\in\mathbb{Z}_d^2} r_m^2 = 1 \tag{3.3.9}$$

and

$$\sum_{m\in\mathbb{Z}_d^2} r_m r_{p\oplus m} e^{i(\phi_{p\oplus m}-\phi_m)}\omega^{-m_x p_z} = 0,\ \forall\ p\neq(0,0), \tag{3.3.10}$$

which enforce unitarity (see Appendix D). For unitary transformations close to the identity we have that $r_m/r_0 \ll 1$ for $m \neq (0,0)$. With this approximation, the only terms contributing in Eq. (3.3.10) are those where $m = (0,0)$ and $m = \ominus p \equiv (d-p_x, d-p_z)$. Thus, Eq. (3.3.10) becomes

$$r_p e^{i\phi_p} \approx r_{\ominus p} e^{-i\phi_{\ominus p}+i\frac{2\pi}{d}p_x p_z+i\pi}, \tag{3.3.11}$$

where we set $\phi_{0,0} = 0$ without loss of generality. From the previous equation we obtain

$$r_p \approx r_{\ominus p} \tag{3.3.12}$$

and

$$\phi_p \approx -\phi_{\ominus p} + \frac{2\pi}{d}p_x p_z + (2n+1)\pi\ \text{, with } n\in\mathbb{Z}. \tag{3.3.13}$$

These conditions show that the amplitudes and phases of the coefficients u_p are related in pairs. In the case $p = \ominus p$, Eq. (3.3.13) ties the phase to a discrete set, that is,

$$\phi_p \approx \frac{\pi}{d}p_x p_z + \frac{2n+1}{2}\pi\ \text{, with } n\in\mathbb{Z}. \tag{3.3.14}$$

Notice that the last restriction on the phases only occurs when d is even, and only for $p = (d/2, 0)$, $p = (0, d/2)$ and $p = (d/2, d/2)$. Therefore, in the case $d = 2$, the three coefficients have a fixed phase up to a difference of π.

The constraints in Eqs. (3.3.12) and (3.3.13) allow us to recognize the d^2-1 parameters that characterizes U in the close-to-the-identity approximation. These are, for $d = 2$, three unpaired amplitudes r_p. For $d > 2$ odd, all the coefficients are paired, implying that the relevant parameters are $(d^2-1)/2$ amplitudes r_p and the same number of phases ϕ_p. For $d > 2$ even, we have the three unpaired amplitudes $r_{(d/2,0)}$, $r_{(0,d/2)}$ and $r_{(d/2,d/2)}$, and $(d^2-4)/2$ other amplitudes and equal number of phases.

To handle these three cases at once we introduce the following partition of the set $\mathbb{Z}_d^2$ of indexes:

$$\mathbb{Z}_d^2 = S_0 \cup S_u \cup S_+ \cup S_-\ , \tag{3.3.15}$$

where $S_0 = \{(0,0)\}$, $S_u = \{(d/2,0),(0,d/2),(d/2,d/2)\}$, and S_+ and S_- are any

partition such that $p \in S_+$ if and only if $\ominus p \in S_-$. In this way, we can easily identify the set of parameters defining U:

$$\texttt{Par}_U = \{r_f\}_{f\in S_u} \cup \{r_a, \phi_a\}_{a\in S_+} \,. \tag{3.3.16}$$

Notice that every r_a and ϕ_a with $a \in S_+$ is respectively paired with $r_{\ominus a}$ and $\phi_{\ominus a}$, with $\ominus a \in S_-$, via Eqs. (3.3.12) and (3.3.13). Here and in what follows we use indexes $f, g \in S_u$ to label unpaired amplitudes and $a, b \in S_+$ to label paired amplitudes and phases.

Let us introduce the notation $|f\rangle = |f_x\rangle_1 \otimes |f_z\rangle_2$ for index $f = (f_x, f_z)$, and similarly for $a = (a_x, a_z)$. Then, using partition (3.3.15), the state $|\varphi^0\rangle_{12}$ in Eq. (3.3.8) becomes

$$\begin{aligned} |\varphi^0\rangle_{12} = r_0\,|0\rangle + \sum_{f\in S_u} r_f e^{i\phi_f}\,|f\rangle \\ + \sum_{a\in S_+} r_a \left(e^{i\phi_a}\,|a\rangle + e^{i\phi_{\ominus a}}\,|\ominus a\rangle\right), \end{aligned} \tag{3.3.17}$$

where $r_0 = (1 - \sum_{n\neq(0,0)} r_n^2)^{1/2}$.

Now, consider the following two-qudit operation

$$\tilde{H}\,|n\rangle = \begin{cases} |n\rangle & \text{, for } n = 0 \text{ and } n \in S_u. \\ \frac{1}{\sqrt{2}}\left(|n\rangle + |\ominus n\rangle\right) & \text{, for } n \in S_+. \\ \frac{1}{\sqrt{2}}\left(|\ominus n\rangle - |n\rangle\right) & \text{, for } n \in S_-. \end{cases} \tag{3.3.18}$$

This operation can be understood as a set of Hadamard gates each acting in a subspace labeled with paired indexes, while acting as an identity on the other subspaces. Applying $\tilde{H}$ on $|\varphi^0\rangle_{12}$ we obtain the state

$$\begin{aligned} |\varphi^1\rangle_{12} = r_0\,|0\rangle + \sum_{f\in S_u} r_f e^{i\phi_f}\,|f\rangle \\ + \sum_{a\in S_+} \frac{r_a}{\sqrt{2}}\left(e^{i\phi_a} + e^{i\phi_{\ominus a}}\right)|a\rangle \\ + \sum_{a\in S_+} \frac{r_a}{\sqrt{2}}\left(e^{i\phi_a} - e^{i\phi_{\ominus a}}\right)|\ominus a\rangle\,. \end{aligned} \tag{3.3.19}$$

Projective measurements on the computational basis for both qudits leads to the

probabilities

$$\begin{aligned} P_0 &= r_0^2, \\ P_f &= r_f^2, \\ P_a &= r_a^2(1+\cos(\Delta_a)), \\ P_{\ominus a} &= r_a^2(1-\cos(\Delta_a)), \end{aligned} \tag{3.3.20}$$

where $\Delta_a = \phi_a - \phi_{\ominus a}$ is given by the expression

$$\Delta_a = 2\phi_a - \frac{2\pi}{d} a_x a_z - (2n+1)\pi \text{ , with } n \in \mathbb{Z}. \tag{3.3.21}$$

These probabilities lead to the estimates for the amplitudes

$$\begin{aligned} r_f &= \sqrt{P_f} \\ r_a &= \sqrt{\frac{P_a + P_{\ominus a}}{2}}, \end{aligned} \tag{3.3.22}$$

and for the phases

$$\begin{aligned} \phi_a = &\pm \frac{1}{2} \arccos\left(\frac{P_a - P_{\ominus a}}{P_a + P_{\ominus a}}\right) + \frac{\pi}{d} a_x a_z \\ &+ (n + \frac{1}{2})\pi \text{ , with } n \in \mathbb{Z}. \end{aligned} \tag{3.3.23}$$

Thus, our proposal estimates the amplitudes and phases that characterize any d-dimensional close-to-the-identity unitary gate. In any case, the phases are estimated up to a set of four candidates, as implied by Eq. (3.3.23) and in agreement with the 2-dimensional case. The discrimination of the candidates requires prior information or additional experiments.

For dimension d even, the quantum Fisher information matrix characterizing our process is given (see Appendix E for details) by the block matrix

$$\mathcal{F}_{even} = \begin{pmatrix} \mathbf{A} & \mathbf{B} & \mathbf{0} \\ \mathbf{B}^T & \mathbf{C} & \mathbf{0} \\ \mathbf{0} & \mathbf{0} & \mathbf{D} \end{pmatrix}, \tag{3.3.24}$$

where the ordering in the block matrix $\mathcal{F}_{even}$ is given by $(\{r_f\}, \{r_a\}, \{\phi_a\})$, with

$f \in S_u$ and $a \in S_+$, and the explicit form of each block is

$$\mathbf{A}_{f,g} = 4\frac{r_f r_g}{r_0^2} + 4\delta_{f,g} \tag{3.3.25}$$

$$\mathbf{B}_{f,a} = 8\frac{r_f r_a}{r_0^2} \tag{3.3.26}$$

$$\mathbf{C}_{a,b} = 16\frac{r_a r_b}{r_0^2} + 8\delta_{a,b} \tag{3.3.27}$$

$$\mathbf{D}_{a,b} = 8r_a^2\delta_{a,b}\ , \tag{3.3.28}$$

being $\delta_{x,y}$ the Kronecker delta. In particular, for $d = 2$, the unitary transformation is characterized by three unpaired amplitudes, i.e., S_+ and S_- are empty. Hence, the quantum Fisher information matrix reduces to the upper left block as

$$\mathcal{F}_2 = \mathbf{A}\ . \tag{3.3.29}$$

In the case of dimension d odd all amplitudes and phases are paired, hence S_u is empty. Thus, the quantum Fisher information matrix is given by

$$\mathcal{F}_{odd} = \begin{pmatrix} \mathbf{C} & \mathbf{0} \\ \mathbf{0} & \mathbf{D} \end{pmatrix}. \tag{3.3.30}$$

In this way, we have obtained the quantum Fisher information matrix $\mathcal{F}_d$ for estimating close-to-the-identity unitary transformations in every dimension. Furthermore, we show in Appendix F that the classical Fisher information matrix $\mathcal{I}_d$ is equal to $\mathcal{F}_d$. Thus, our estimation procedure saturates the quantum Cramér-Rao inequality for close-to-the-identity unitary transformations. Let us note that within the approximation $r_m/r_0 \ll 1$ the non-diagonal terms in $\mathcal{F}_{even}$ are $O((r_m/r_0)^2)$, hence they can be neglected and consequently all the Fisher information matrices are nearly diagonal. In this way, in the case of odd dimension, the amplitudes can be estimated independently of each other and with equal precision. For even dimension, the amplitudes are also estimated independently; however, unpaired amplitudes are estimated with half the precision of paired amplitudes. Lastly, the precision in the estimation of the phases is severely restricted since it is proportional to the inverse of the square of the corresponding amplitude.

We must emphasize that our result is only valid within the close-to-the-identity

approximation, where the parameters in the Weyl-Heisenberg expansion of d-dimensional unitary matrices, namely the phases $\{\phi_p\}$ and the amplitudes $\{r_p\}$, are approximately independent between each other. In the case far from the identity, where the parameters are strongly correlated, the above does not hold: even a slight variation in one of the amplitudes, which produces slight variations in the other ones because of the normalization, leads to violation of the unitarity conditions. Since the relation between the parameters for the general case is not clear, it is not possible to calculate, even numerically, the partial derivatives required to obtain the classical and quantum Fisher information matrices. In Appendix G we use a different parametrization to compare these matrices, showing that the distance between them increases as U is further from the identity.

3.3.4 Discussion

In this section we extended the analysis of the circuit proposed in Section 3.2.4 to higher dimensions and proved analytically that our procedure is optimal for unitary gates close to the identity in any finite dimension. In Ref. [180] it was shown that the quantum Cramér-Rao bound can be achieved for unitary transformations close to the identity, but no explicit protocol was proposed; our procedure accomplishes this task. Far from the identity our procedure still estimates the amplitudes r_p of the coefficients, but the assessment of the precision of this estimation is an open problem.

Notice that part of the circuit in Fig. 3.3.1 can be described by a quantum switch. Indeed, if the control system is the path degree of freedom of a photon and the target system is any high-dimensional degree of freedom, then the Fourier and inverse Fourier transforms correspond to multiport beam splitters. The controlled operations acting before U have the form of a gate $Z^{d-m-1}X^n$ when the control is in state $|mn\rangle$. Meanwhile, the controlled operations after U and before the inverse Fourier transforms for the same control state become the operation $X^{d-n-1}Z^m$. Hence, to get the state $|\Phi^7\rangle_{012}$, a total of $d-1$ copies of X, $d-1$ copies of Z and one copy of U need to be applied on the target system in a different order in each path. Thus, it is equivalent to a $(2d-1, d^2)$-switch. As discussed in the previous section, since only one of these gates is unknown, no role is expected for indefinite causal order in this protocol other than being an alternative setup for estimation of high-dimensional unitary gates.

Although indefinite causal order is not relevant in the behaviour of the circuit, our circuit exhibits some surprising features. Firstly, it transcribes the coefficients of the gate in the Weyl-Heisenberg basis into probability amplitudes of two control qudits. And secondly, the initial state of the target system is kept the same at the end of the procedure. These characteristics will be further discussed in the next section, where we replace the unitary operation U by an arbitrary quantum channel $\mathcal{E}$.

3.4 Transcribing quantum channels into quantum states

3.4.1 Process matrix of a quantum channel

In this section, we show that when U is replaced by an arbitrary quantum channel $\mathcal{E}$, the circuit in Fig. 3.3.1 encodes the process matrix of $\mathcal{E}$ in the output state of the control, while the original state ρ_0 of the target is obtained as output, unaffected by the channel. Here, we denote as "process matrix" one of the different representations of a quantum channel and must not be confused with the process matrices framework reviewed in Section 1.1.3.1. Also, notice that for dealing with arbitrary channels, quantum states must be now described by density matrices instead of unitary vectors. Let us start this section briefly introducing quantum channels and their process matrix representation.

Let $\mathcal{H}$ be a d-dimensional Hilbert space, $\mathcal{L}(\mathcal{H})$ the space of linear operators on $\mathcal{H}$ and $\mathcal{E} : \mathcal{L}(\mathcal{H}) \to \mathcal{L}(\mathcal{H})$ an arbitrary quantum channel, i.e., a linear map taking quantum states into quantum states. The map $\mathcal{E}$ is a quantum channel if and only if it is a completely positive and trace preserving (CPTP) linear map or, equivalently, its action on an input state ρ can be written in the Kraus representation [179, 185] as

$$\mathcal{E}(\rho) = \sum_i E_i \rho E_i^\dagger, \tag{3.4.1}$$

where the E_i are linear operators on $\mathcal{H}$ satisfying the completeness relation

$$\sum_i E_i^\dagger E_i = I, \tag{3.4.2}$$

with I the identity operator. Given a basis $\mathcal{B} = \{\tilde{E}_j\}_{j=1}^{d^2}$ for the space $\mathcal{L}(\mathcal{H})$, Kraus operators can be spanned as the linear combination

$$E_i = \sum_j e_{ij} \tilde{E}_j \ , \tag{3.4.3}$$

where e_{ij} are complex coefficients. Then, the action of the channel can be written as

$$\mathcal{E}(\rho) = \sum_{jk} \chi_{jk} \tilde{E}_j \rho \tilde{E}_k^\dagger \ , \tag{3.4.4}$$

where

$$\chi_{jk} := \sum_i e_{ij} e_{ik}^* \tag{3.4.5}$$

are the elements of a $d^2 \times d^2$ matrix χ, known as *process matrix* [163]. It can be seen from Eq. (3.4.4) that χ completely describes the action of $\mathcal{E}$ on any quantum state, provided a basis for $\mathcal{L}(\mathcal{H})$.

If the operators $\tilde{E}_j \in \mathcal{B}$ satisfy the orthogonality relation

$$Tr[\tilde{E}_j{}^\dagger \tilde{E}_k] = d\delta_{jk} \ , \tag{3.4.6}$$

where δ_{jk} is the Kronecker delta, then χ is a positive semi-definite matrix with trace equal to 1 (see Appendix H for details). In other words, the process matrix χ is a valid d^2-dimensional quantum state.

A basis for $\mathcal{L}(\mathcal{H})$ satisfying relation (3.4.6) is the set of Weyl-Heisenberg operators[1]

$$\mathcal{B} = \{X^j Z^k\}_{j,k=0}^{d-1} \ . \tag{3.4.7}$$

Hereafter, we will only consider the process matrix χ of a quantum channel relative to the Weyl-Heisenberg basis.

3.4.2 The circuit

Fig. 3.4.1 depicts the circuit that transcribes the process matrix of an arbitrary quantum channel $\mathcal{E}$ onto an auxiliary output system. This circuit consists in one

[1] Cf. Eq. C.7.

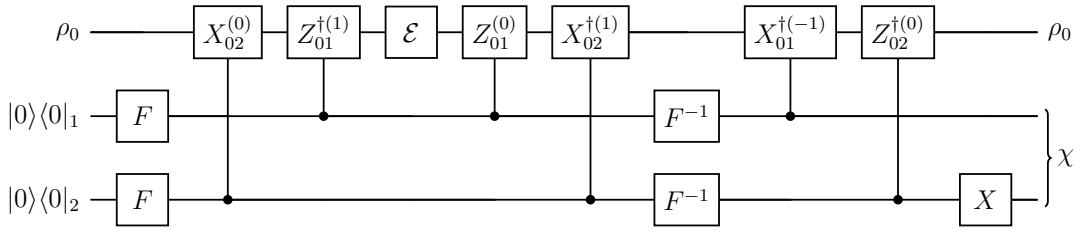

Figure 3.4.1: Circuit that transcribes the process matrix χ of an arbitrary quantum channel $\mathcal{E}$ into the state of an auxiliary quantum system. The circuit does not alter the state ρ_0 of the target system. F are d-dimensional Fourier transforms acting on control qudits 1 and 2, and $X_{tc}^{(i)}$ and $Z_{tc}^{(i)}$ are controlled gates with shift in the control.

target and two control qudits initialized in the state

$$\rho_{in} = \rho_0 \otimes |0\rangle\langle 0|_1 \otimes |0\rangle\langle 0|_2 \,, \tag{3.4.8}$$

where ρ_0 is an arbitrary initial state for the target qudit. Let us briefly review the action of the circuit. First, Fourier transforms

$$F = \frac{1}{\sqrt{d}} \sum_{j,k=0}^{d-1} \omega^{jk} |j\rangle\langle k| \tag{3.4.9}$$

act on the control qudits, transforming them into maximal superposition states. Then, controlled operations $X_{02}^{(0)}$ and $Z_{01}^{\dagger(1)}$ are applied creating entanglement between the target and control systems. These controlled operations are particular cases of what we call *controlled operators with shifted control*, which are generally defined as

$$V_{tc}^{(i)} := \sum_{k=0}^{d-1} V_t^k \otimes |k \ominus i\rangle\langle k \ominus i|_c \,, \tag{3.4.10}$$

where V_t^k is the k-th power of the operator V applied on the target system t, and i indicates a shift in the control system c, with $\ominus$ denoting difference modulo d. Then, an arbitrary quantum channel

$$\mathcal{E}(\rho) = \sum_i E_i \rho E_i^\dagger \tag{3.4.11}$$

is applied on the target system followed by controlled operations $Z_{01}^{(0)}$ and $X_{02}^{\dagger(1)}$. Inverse Fourier transforms then act on the control qudits. At this point, the joint

state of the system may remain entangled, so new controlled operations $X_{01}^{\dagger(-1)}$ and $Z_{02}^{\dagger(0)}$ are implemented in order to separate the target from the control. Finally, an X gate is applied to the second control qudit in order to more conveniently pair the coefficients that characterize the quantum channel with the computational basis of the control register.

Notice that the evolution of the joint system before the application of $\mathcal{E}$ is unitary. Hence, we can group the operations preceding $\mathcal{E}$ as

$$V = (Z_{01}^{\dagger(1)} \otimes I_2)(X_{02}^{(0)} \otimes I_1)(I_0 \otimes F_1 \otimes F_2) \ . \tag{3.4.12}$$

Similarly, we can group the unitary operations applied after $\mathcal{E}$ in the gate

$$W = (I_0 \otimes I_1 \otimes X_2)(Z_{02}^{\dagger(0)} \otimes I_1)(X_{01}^{\dagger(-1)} \otimes I_2)(I_0 \otimes F_1^\dagger \otimes F_2^\dagger)(X_{02}^{\dagger(1)} \otimes I_1)(Z_{01}^{(0)} \otimes I_2) \ . \tag{3.4.13}$$

Thus, the action of the circuit can be written shortly as

$$\rho_{out} = \sum_i W E_i V \rho_{in} V^\dagger E_i^\dagger W^\dagger \ , \tag{3.4.14}$$

or

$$\rho_{out} = \sum_i K_i \rho_{in} K_i^\dagger \ , \tag{3.4.15}$$

with

$$K_i = W E_i V \ . \tag{3.4.16}$$

In other words, we can consider our circuit as transforming a d-dimensional quantum channel with Kraus operators E_i into a d^3-dimensional quantum channel with Kraus operators $K_i = W E_i V$.

As shown in Appendix I, these final Kraus operators are

$$K_i = \sum_{n \in \mathbb{Z}_d^2} \sum_{k_1,k_2=0}^{d-1} e_{in} \omega^{k_1(k_2+n_z-1)} X_0^{-k_1} Z_0^{-k_2} \otimes |k_1 \oplus n_x\rangle \langle k_1|_1 \otimes |k_2 \oplus n_z\rangle \langle k_2|_2 \ . \tag{3.4.17}$$

Here we use a notation with ordered pairs $n = (n_x, n_z) \in \mathbb{Z}_d^2$ as indexes for the elements in $\mathcal{B}$, such that e_{in} is the component of E_i along $X^{n_x} Z^{n_z}$.

Applied to ρ_{in}, the output state of the circuit is

$$\begin{aligned}\rho_{out} &= \sum_i K_i \rho_{in} K_i^\dagger \\ &= \rho_0 \otimes \chi \ , \end{aligned} \tag{3.4.18}$$

i.e., the circuit keeps the initial target state invariant and outputs the process matrix χ associated to $\mathcal{E}$ as the state of the control system. For brevity and convenience, we refer to this process as "transcription".

In the following, let us briefly discuss some aspects of the circuit.

3.4.3 Some features of the circuit

3.4.3.1 Correlations between target and external systems is maintained

Suppose that the target system is coupled to an extra arbitrarily large system A, with their joint initial state being ρ_{A0} and $\rho_0 = Tr_A[\rho_{A0}]$. If the target system enters in the circuit as before while the system A undergoes an identity evolution, then the initial state ρ_{A0} is again recovered. Indeed, linearity of quantum channels implies that the output state of the circuit will be $\rho_{A0} \otimes \chi$. This indicates that not only the initial state of the target, but also its entanglement and other types of correlations with other systems get protected against the action of noisy channels.

3.4.3.2 Initial state can be recovered even if target qudit is lost

Suppose the target qudit gets lost in the region immediately before or immediately after the application of $\mathcal{E}$. We could replace the lost qudit by a new qudit in an arbitrary state σ and continue with the remaining operations of the circuit. This action is equivalent to the application of the map $\mathcal{M} = Tr[\rho]\sigma$ instead of $\mathcal{E}$. Since $\mathcal{M}$ is also a quantum channel, the output of the circuit will be still the tensor product of the initial state of the target and the process matrix χ, but now χ being the process matrix associated to $\mathcal{M}$.

The previous observation suggests that the initial state of the target system is transferred to the control qudits before applying $\mathcal{E}$, from where it is retrieved afterwards. This can be interpreted as the action of an "asymmetric SWAP" operation between the target and control systems, which also explains why

entanglement between the target and external systems is protected by the circuit.

3.4.3.3 Information available in sub-systems

Finally, let us see what the reduced density matrices of each qudit right after the application of $\mathcal{E}$ are. Denoting the joint state of the system at this stage as $\rho^{(4)}$ (right after the fourth step in the circuit), we obtain

$$\rho_0^{(4)} = Tr_{12}[\rho^{(4)}] = \frac{\mathcal{E}(I)}{d} , \tag{3.4.19}$$

$$\rho_1^{(4)} = Tr_{02}[\rho^{(4)}] = \frac{I}{d} , \tag{3.4.20}$$

$$\rho_2^{(4)} = Tr_{01}[\rho^{(4)}] = \frac{1}{d}\sum_{m,n=0}^{d-1} \rho_{mn} X^{n-m} , \tag{3.4.21}$$

where ρ_{mn} are the matrix elements of ρ_0. That is, the first control qudit alone has no information concerning ρ_0 while the second control qudit exhibits partial information. In particular, if ρ_0 is an eigenstate of X, then $\rho_2^{(4)}$ is also an eigenstate of X, specifically the one with conjugate eigenvalue; instead, if ρ_0 is diagonal in the computational basis, then $\rho_2^{(4)} = I/d$ (for details, see Appendix J). Thus, although the information about ρ_0 is safe in the control register, whose state at this point is given by

$$\rho_{12}^{(4)} = \frac{1}{d^2}\sum_{p,q,m,n,k=0}^{d-1} \rho_{mn}\omega^{k(q-p)} \left|p\right\rangle \left\langle q\right|_1 \otimes \left|k \ominus m\right\rangle \left\langle k \ominus n\right|_2 , \tag{3.4.22}$$

in general both control qudits are required in order to retrieve this information. Finally, notice that none of the three qudits alone can provide any information about the quantum channel applied on the target, as long as the channel is unital, i.e., $\mathcal{E}(I) = I$.

3.4.4 Comparison to "Choi" and "Choi-Bell" circuits

As it is well-known, there exist other quantum circuits that can encode complete information about a quantum channel onto the output state. First, consider the circuit illustrated in Fig. 3.4.2, which we call "Choi circuit". The name is due to the fact that the output state $C_{\mathcal{E}}$ of the system is proportional to the Choi representation of $\mathcal{E}$, which is a matrix that completely characterizes a quantum

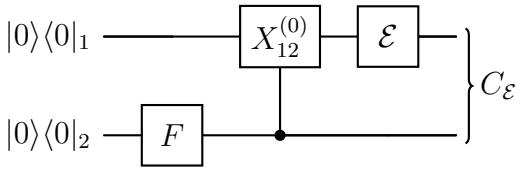

Figure 3.4.2: "Choi circuit".

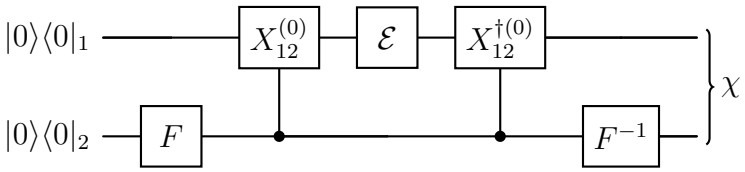

Figure 3.4.3: "Choi-Bell circuit".

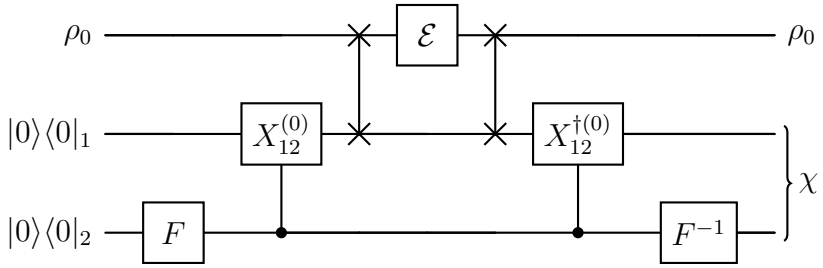

Figure 3.4.4: Choi-Bell circuit with an additional qudit and swap gates.

channel via the Choi-Jamiołkowski isomorphism [186, 187]. As noted in Ref. [188], the process matrix χ relative to the Weyl-Heisenberg basis is equal to the Choi operator written in the Bell basis. This combination gives rise to the circuit that we call "Choi-Bell circuit" (see Fig. 3.4.3), which produces the state χ with less operations than the channel transcription circuit in Fig. 3.4.1, but does not provide information concerning the initial state ρ_0. A proof of the relation between the Choi operator and χ is given in Appendix K using our notation. To recover the initial state ρ_0, we can add a third qubit in an arbitrary initial state and introduce swap operations just before and after the application of $\mathcal{E}$ in Fig. 3.4.3, to obtain a new circuit with exactly the same output state as the channel transcription circuit (see Fig. 3.4.4).

We could still go further and add controlled gates between the two control qudits with the aim of distributing the state ρ_0 among them before the application of $\mathcal{E}$, therefore getting all the features previously described for our circuit. Nevertheless, at this point of the discussion it is clear that both circuits have different structures.

Then, why should one prefer one of them instead of the other? Without intention to give a definite answer to this question, we first note that the circuit in Fig. 3.4.4 requires at least 8 two-qudit controlled gates, compared to the 6 gates required in the circuit in Fig. 3.4.1. In addition, it is worth noting that the circuit in Fig. 3.4.1 is well suited for interferometric arrays using a quantum switch as discussed in Section 3.3.4. This way, our circuit could be fairly implemented with current photonic technology (cf. Ref. [36] and Sec. 3.2.3). Conversely, the Choi-Bell circuit demands non-local operations between the two control qudits, or equivalent non trivial unitary gates acting on the d^2-dimensional control register. Hence, the Choi-Bell circuit seems to be more suitable for platforms where control and target qudits are treated on an equal footing, such as superconducting qubits or ion traps.

3.4.5 Possible applications

The structure of the channel transcription circuit was first utilized in Section 3.3 for the estimation of unitary gates, so it is natural to think that it could find use in quantum process tomography of $\mathcal{E}$ as well. For this task, we could use the circuit to output matrix χ encoded as a quantum state, and then perform quantum state tomography using some available method. Though it is clear that the Choi-Bell circuit (Fig. 3.4.3) is much simpler than ours to this aim, there could still be some place for the application of the transcription circuit in quantum process tomography. Recently, Ref. [189] introduced a similar quantum circuit, highlighting its ability to protect the initial state of the target, but without analyzing the relation of the final state of the control system with the quantum channel applied. Interestingly, the authors realized that the protection of the information is achieved also in scenarios where the control qudits are subject to some classes of noise. It would be interesting to study how robust the transcription of the quantum channel provided by our circuit is against noise, compared to that by the Choi-Bell circuit. We leave this question for future work.

If the transcription circuit does provide some advantage over the Choi-Bell circuit in some scenarios, then it could also become a tool for quantum remote sensing. We could imagine that the control qudits remain in the lab in a low-noise quantum memory, while the target system is sent to some external region to interact with another system (the channel $\mathcal{E}$), and then returned to the lab where the

information about the interaction is retrieved from the control qudits.

Finally, let us note that our circuit can be used to implement a curious version of quantum superdense coding [190, 191]. In the present case, in addition to the 2 dits of information sent in the single target qudit, the target qudit is also sent. Imagine that after the preparation state (Alice), the control qudits are sent to Bob. Indeed, if we consider that the quantum channel is actually Alice implementing one of the d^2 Weyl-Heisenberg operations, then this encodes two dits of information into the target, which is then sent to Bob for completion of the circuit. As no information about the channel is available in the control qudits, they contain no information about the message. These two dits get revealed deterministically by Bob by measuring the control system in the computational basis at the end of the circuit. Moreover, the initial state of the target can be also used to encode information in the computational basis, as in this case all three reduced density matrices are identity. It is still an open question whether the qudit encoded from the beginning in the target system can be useful for some other communication tasks such as quantum signature or author authentication.

3.4.6 Discussion

In this section we showed that the circuit introduced in Section 3.3 outputs the process matrix of an unknown d-dimensional quantum channel while protects the initial state of the target qudit. We also built a variation of the Choi-Bell circuit with the same features of our circuit. The usefulness of our circuit in quantum process tomography and quantum remote sensing remains unclear, although it could be subject to its robustness against noise in the control system, analysis that is left for future work. Also, it is an open question whether our circuit could find some application in quantum communications, with the state of the target system playing a special role. Finally, it would be interesting to take this circuit to the continuous variable regime and compare it with other tools for quantum process characterization.

3.5 Conclusions

In this chapter we have explored the application of the quantum switch for quantum metrology. In particular, we addressed a multiparameter estimation

task consisting in estimating a unitary transformation. Firstly, we proposed a protocol for estimating qubit gates using a $(3, 4)$-switch, which may be easily implemented by modifying the experimental setup of Ref. [36]. Our proposal saturates the quantum Cramér-Rao bound with a lower number of auxiliary gates than related works [142, 180, 181], although does not provide neither metrological nor query advantages. We simulated an equivalent fixed-order circuit in Qiskit using different models of noise. Our simulations show that our procedure outperforms SQPT in a noiseless scenario for every size of the ensemble and also in noisy scenarios with a small ensemble. Then we extended the protocol to higher finite dimensions and showed that it saturates the quantum Cramér-Rao bound for unitary transformations close to the identity. The protocol can be realised as a $(2d-1, d^2)$-switch or an equivalent fixed-order circuit. Replacing the unitary gate by an arbitrary d-dimensional quantum channel, we obtained a quantum circuit that transcribes a quantum channel into the quantum state of an auxiliary system while keeps the target system unaffected by the channel. We compared the circuit with the Choi and Choi-Bell circuits, which have similar features, and mentioned some possible applications.

We have argued at the end of Section 3.2 that indefinite causal order does not play any role in this procedure. Indeed, the most general circuit presented here (see Fig. 3.4.1) is a deterministic supermap, which map an input quantum channel $\mathcal{E}$ to a new quantum channel. This is clearly stated in Eq. 3.4.16, which specifies how the Kraus operators of the input channel are transformed into a new set of Kraus operators. Whether the quantum switch or its fixed-order equivalent is better for experimental implementations, depends exclusively on the technological advancement of the chosen platform. Actually, more research about the performance of our circuit in noisy devices is required. During this chapter, we have learned that multiparameter estimation is a promissory direction for applications of the quantum switch, but with different parameters being encoded in different operations.

The aim of our exploration is to find applications of the quantum switch in CV tasks. The extension of the circuit discussed in Section 3.4 to the CV regime is an interesting future direction, since it could inspire new tomographic methods for characterising CV quantum processes. Notwithstanding, we are interested in applications of indefinite causal order. In this regard, it is important to highlight

that our circuit can be implemented as a quantum switch. If we wish to extend the fixed-order circuit to the CV regime, we may wonder whether the corresponding quantum switch can be extended to the CV regime as well. Notice that the dimension of the control system grows quadratically with the dimension of the target, hence if the target becomes infinite-dimensional, the control system should become infinite-dimensional too. However, the quantum switch has always been defined for a finite number N of operations in up to $N!$ possible orders, implying a finite-dimensional control. In a forthcoming work (see Section 4.3) we will insist in this question: is it possible to extend the definition of the quantum switch to a scenario with a continuous control? If so, is this quantum switch with continuous control a causally non-separable process? And finally, does such a process provide any computational advantage over causally ordered processes as the traditional quantum switch does?

Chapter 4

Conclusions

This final chapter offers a general view of the thesis. In Section 4.1 we summarise our results and discuss the accomplishment of our objectives. In Section 4.2 we insist in some open questions and offer some future directions which may provide further support to our hypothesis. Finally, we offer a sneak peek of an ongoing work in Section 4.3 and close in Section 4.4.

4.1 Summary

In this thesis we explored the application of the quantum switch to quantum information processing, comparing its performance when the target is a CV system versus when it is a finite-dimensional quantum system. In particular, we studied the solution of a family of promise problems and an instance of multiparameter estimation using an (N, p)-switch. We expected the quantum switch to provide broader advantages when the target is a CV quantum system.

In Chapter 2 we were devoted to the study of the Complex Hadamard Promise Problem, a generalized family of promise problems which reduces to the Hadamard and Fourier promise problems as limiting cases. This family has well defined instances in every finite dimension, relaxing the restrictions on the dimension of the control and target systems imposed by previous approaches which focused on the number of gates. Hence, our approach opens the possibility of more flexible experimental realisations of this task. It is important to notice that the whole family of Complex Hadamard promise problems is well defined for a CV target,

while only a particular subset is allowed for each finite dimension of the target. We also showed that every Complex Hadamard promise problem can be solved deterministically using the quantum switch with only one query per gate both in the finite-dimensional and CV cases. Moreover, the best fixed order circuits known to solve the same family of problems require a larger number of queries per gate, which grows with the number N of gates and the dimension p of the control. Thus, the quantum switch provides query advantage in all the cases, independently of the dimension of the target system. For this task, we conclude that using a CV target provides broader advantages than using a finite-dimensional one, accomplishing our first specific objective. This broader advantage is not achieved in terms of the query per gates parameter, but in the amount of problems allowed to be solved, since the CV regime lifts all the restrictions imposed by a finite-dimensional target.

In Chapter 3 we assessed the performance of the quantum switch in a particular multiparameter estimation task consisting in the estimation of a unitary transformation. We proposed a variation of the experimental setup of Ref. [36] for estimating a unitary gate acting on the polarization of a photon. Our proposal saturates the quantum Cramér-Rao bound and uses a lower number of auxiliary gates than related works. Building the equivalent fixed-order circuit, it became clear that indefinite causal order does not provide metrological nor query advantage in our procedure. Our scheme can be generalised to a $(2d-1, d^2)$-switch and the unitary can be replaced by an arbitrary d-dimensional quantum channel. Interestingly, our proposal keeps the target system unaffected by the quantum channel while all the information regarding the channel is encoded in the control register as the χ-matrix of the channel. In order to assess the performance of the quantum switch in this task for CV target systems, a straightforward generalization would demand a quantum switch with a continuous control. Hence, at this point we cannot guarantee that taking our protocol to the CV regime will offer broader advantages as hypothesised. Nevertheless, the quantum switch with continuous control, which is the matter of a work in preparation (see Section 4.3), leads to new effects which are conjectured to lay beyond the process matrices framework, motivating a promising new avenue for research on indefinite causal order.

We have attempted to give new support to the hypothesis that indefinite causal order provides broader advantages when the target system is CV. We have found

those advantages to be a larger family of tasks benefited by the quantum switch when the target system is CV and suggest that new phenomena may arise when the control system becomes infinite-dimensional. Indefinite causal order on CV quantum systems is a topic still quite unexplored and several questions remain open. We discuss a couple of them in the next section.

4.2 Open questions

As we have mentioned in Section 1.2, Ref. [106] demonstrated that the $(2, 2)$-switch with CV target is a causally non-separable process. However, as far as we know, there is no demonstration of causal non-separability in a quantum switch with $p > 2$ orders and CV target. Furthermore, no certification strategy of causal non-separability has been proposed for process matrices with CV target. It would be an interesting future direction to design a CV causal witness, which may be eventually achieved combining methods from Refs. [106] and [192]. Such a causal witness may be used to show that some of the quantum information processing tasks mentioned in Section 1.2, as well as the one introduced in Chapter 2, are indeed instances of indefinite causal order.

Regarding experimental realizations of indefinite causal order on CV systems, we are aware of only two photonic implementations of the quantum switch with a CV target. One of them uses the transverse position of the photon as target [20], while the other applies operations on the orbital angular momentum degree of freedom [24]. Since both experiments use polarization as control, they can combine only two different orders of operations. Therefore, building a quantum switch with CV operations in more than two different orders is still an open challenge. Different degrees of freedom with higher dimension, e.g. frequency and orbital angular momentum, may be used as control to this aim. An experiment like this would be able to implement the most general CHPP discussed in Chapter 2 or an eventual CV causal witness as suggested in the previous paragraph.

4.3 Ongoing work

4.3.1 Quantum switch with continuous control

Following the hint at the end of Chapter 3, we may wonder whether a quantum switch with continuous control can be defined. The traditional approach to the quantum switch and the process matrices framework considers effective transformations performed on the target system, usually illustrated as boxes. As a consequence, the emphasis has always been on the number of agents, each one applying a single quantum instrument on their corresponding input system. If N agents participate in the process, there are up to $N!$ possible orders. Thus, an $N!$-dimensional control system would be enough. However, this operational approach keeps the dynamics hidden. It is well known that the dynamics of a quantum system in standard quantum mechanics is ruled by a differential equation in time, implying that the evolution of a system is continuous in time. Here we propose to redefine the quantum switch by making the dynamics explicit and directly linking the state of the control system to the time ordering of the dynamics. This will allow to extend the quantum switch to a continuous control in a straightforward manner.

To start with, consider the case of two unitary gates U_A and U_B. Each unitary is generated by a Hamiltonian that rules the dynamics of the target system via the Schrödinger equation during a given time frame. From the point of view of the target system, it is indistinct whether one, two or more parties are responsible for the evolution. The target system will evolve according to a time-dependent Hamiltonian $H(t)$ during a total time frame $[t_i, t_f]$. Using the Dyson formula, one of the orders of the unitaries can be written as

$$U_B U_A = \vec{T} \exp\left(-\frac{i}{\hbar}\int_{t_i}^{t_f} H(t)dt\right) , \tag{4.3.1}$$

where $\vec{T}$ is the time-ordering operator. The alternative order does not alter the dynamics behind each unitary nor the total time frame for the evolution. It only affects the time ordering, what can be described by introducing a bijection Λ on the time frame:

$$U_A U_B = \vec{T} \exp\left(-\frac{i}{\hbar}\int_{t_i}^{t_f} H(\Lambda(t))dt\right) . \tag{4.3.2}$$

In this particular case Λ permutes the time frames of the unitaries, but in principle it could be any reshuffling of the total time frame. Consequently, the quantum switch is redefined as a process that couples the state of the control system with the time ordering of the dynamics. Every individual quantum switch is characterised by a *coupling function* which assigns to each state $|k\rangle$ of the control a bijection Λ_k on the total time frame. The overall evolution of the joint system is described by the unitary:

$$U_{switch} = \sum_k |k\rangle\langle k| \otimes \vec{T}\exp\left(-\frac{i}{\hbar}\int_{t_i}^{t_f} H(\Lambda_k(t))dt\right) . \tag{4.3.3}$$

This new definition of the quantum switch, that we will denote generically as *quantum switch with continuous control*, involves at least the following instances:

- **The (N,p)-switch:** The (N,p)-switch is a particular case where the total time frame is partitioned in N parts and the control system has finite dimension p. The coupling function assigns to each state in the computational basis of the control a bijection which is a permutation of the time partition.

- **Superposition of forward and time-reversal dynamics:** Consider a qubit as control and the functions $\Lambda_0(t) = t$ and $\Lambda_1(t) = t_i + t_f - t$ assigned respectively to the states $|0\rangle$ and $|1\rangle$ of the control. If the control is initialized in state $|+\rangle$, then the quantum switch will implement a superposition of forward and time-reversal dynamics. This process resembles a relative of indefinite causal order known as indefinite time direction [193, 194].

- **Continuously cyclic time ordering:** Eq. (4.3.3) can be straightforwardly extended to a continuous-variable control system as

$$U_{switch} = \int d\varphi|\varphi\rangle\langle\varphi| \otimes \vec{T}\exp\left(-\frac{i}{\hbar}\int_{t_i}^{t_f} H(\Lambda_\varphi(t))dt\right) , \tag{4.3.4}$$

  where φ is a continuous variable such as the azimuthal angle of a particle in a ring. A bijection $\Lambda^{(t_0)}$ that cuts the total time frame in a point t_0 and then permutes the two resulting parts (see Fig. 4.3.1) can be assigned to a particular value φ_0 of the control variable. If t_0 can be chosen freely in the total time frame, then a superposition of continuously cyclic time-orderings

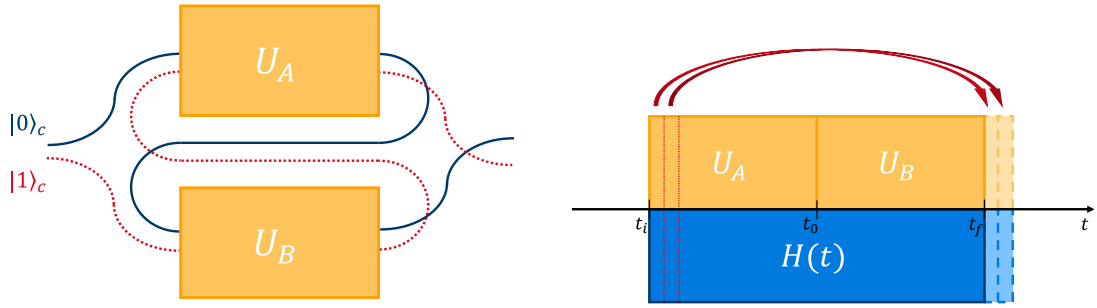

Figure 4.3.1: Quantum switch with continuous control. The quantum switch of two unitary operations (left) can be recast as a single evolution determined by a Hamiltonian $H(t)$ (right). The total time frame is partitioned in two at some instant t_0, which labels the end of one unitary and the beginning of the other. Then the parts are permuted. Forgetting about the original unitaries, the point t_0 could be chosen arbitrarily within the total time frame. Furthermore, each value of t_0 defines a different time ordering on the dynamics, which may be controlled coherently. A quantum switch with continuous control may implement a superposition of continuously cyclic time orderings on the dynamics.

can be achieved.

- **Accelerando/rallentando effect:** In principle, there is no restriction on the functional form of $\Lambda(t)$ as long as it is a bijection. If it is a non-linear continuous function, then the rate of change of the Hamiltonian according to the target system can be modified, altering its overall evolution. This novel effect appears naturally in a variation of the gravitational quantum switch. Indeed, indefinite order of events in the scenario introduced by Ref. [125] is due to gravitational time dilation, which is a non-linear function on the distance to the source of the gravitational field. Therefore, in order to get a non-linear time ordering on the dynamics, it is enough to increase the number of events, which now trigger a change in the Hamiltonian instead of an instantaneous operation.

The quantum switch with continuous control will be further discussed in

- Jorge Escandón-Monardes, Natália S. Móller, Łukasz Rudnicki and Stephen P. Walborn, "Quantum switch with continuous control" (in preparation).

This work is a collaboration with researchers from the International Centre for Theory of Quantum Technologies ICTQT (University of Gdańsk, Poland) and the Research Center for Quantum Information RCQI (Slovak Academy of Sciences,

Slovakia).

4.4 Coda

Indefinite causal order is currently a hot topic within quantum information. It involves several subjects in the field, from a foundational level to applications. It trascends standard quantum mechanics in an attempt to approach quantum gravity, opening several avenues for further research.

This thesis is just a short song within the album of indefinite causal order. Somewhere the main symphony is waiting to be played.

References

[1] L. Hardy, "Towards quantum gravity: a framework for probabilistic theories with non-fixed causal structure", Journal of Physics A: Mathematical and Theoretical **40**, 3081 (2007).

[2] L. Hardy, "Quantum gravity computers: on the theory of computation with indefinite causal structure", in *Quantum reality, relativistic causality, and closing the epistemic circle: essays in honour of abner shimony* (Springer Netherlands, Dordrecht, 2009), pp. 379–401.

[3] G. Chiribella, G. M. D'Ariano, and P. Perinotti, "Transforming quantum operations: quantum supermaps", Europhysics Letters **83**, 30004 (2008).

[4] G. Chiribella, G. M. D'Ariano, and P. Perinotti, "Theoretical framework for quantum networks", Phys. Rev. A **80**, 022339 (2009).

[5] G. Chiribella, G. M. D'Ariano, P. Perinotti, et al., "Quantum computations without definite causal structure", Phys. Rev. A **88**, 022318 (2013).

[6] J. Bavaresco, S. Yoshida, T. Odake, et al., *Can the quantum switch be deterministically simulated?*, arXiv:2409.18202., 2024.

[7] L. M. Procopio, A. Moqanaki, M. Araújo, et al., "Experimental superposition of orders of quantum gates", Nature Communications **6**, 7913 (2015).

[8] G. Rubino, L. A. Rozema, A. Feix, et al., "Experimental verification of an indefinite causal order", Science Advances **3**, e1602589 (2017).

[9] K. Goswami, C. Giarmatzi, M. Kewming, et al., "Indefinite causal order in a quantum switch", Phys. Rev. Lett. **121**, 090503 (2018).

[10] K. Wei, N. Tischler, S.-R. Zhao, et al., "Experimental quantum switching for exponentially superior quantum communication complexity", Phys. Rev. Lett. **122**, 120504 (2019).

[11] K. Goswami, Y. Cao, G. A. Paz-Silva, et al., "Increasing communication capacity via superposition of order", Phys. Rev. Research **2**, 033292 (2020).

[12] Y. Guo, X.-M. Hu, Z.-B. Hou, et al., "Experimental transmission of quantum information using a superposition of causal orders", Phys. Rev. Lett. **124**, 030502 (2020).

[13] G. Rubino, L. A. Rozema, D. Ebler, et al., "Experimental quantum communication enhancement by superposing trajectories", Phys. Rev. Res. **3**, 013093 (2021).

[14] H. Cao, N.-N. Wang, Z. Jia, et al., "Quantum simulation of indefinite causal order induced quantum refrigeration", Phys. Rev. Res. **4**, L032029 (2022).

[15] G. Rubino, L. A. Rozema, F. Massa, et al., "Experimental entanglement of temporal order", Quantum **6**, 621 (2022).
[16] H. Cao, J. Bavaresco, N.-N. Wang, et al., "Semi-device-independent certification of indefinite causal order in a photonic quantum switch", Optica **10**, 561–568 (2023).
[17] W.-Q. Liu, Z. Meng, B.-W. Song, et al., *Experimentally demonstrating indefinite causal order algorithms to solve the generalized deutsch's problem*, arXiv:2305.05416, 2023.
[18] P. Schiansky, T. Strömberg, D. Trillo, et al., "Demonstration of universal time-reversal for qubit processes", Optica **10**, 200–205 (2023).
[19] T. Strömberg, P. Schiansky, R. W. Peterson, et al., "Demonstration of a quantum switch in a sagnac configuration", Phys. Rev. Lett. **131**, 060803 (2023).
[20] P. Yin, X. Zhao, Y. Yang, et al., "Experimental super-heisenberg quantum metrology with indefinite gate order", Nature Physics **19**, 1122–1127 (2023).
[21] G. Zhu, Y. Chen, Y. Hasegawa, et al., "Charging quantum batteries via indefinite causal order: theory and experiment", Phys. Rev. Lett. **131**, 240401 (2023).
[22] M. An, S. Ru, Y. Wang, et al., "Noisy quantum parameter estimation with indefinite causal order", Phys. Rev. A **109**, 012603 (2024).
[23] M. Antesberger, M. T. Quintino, P. Walther, et al., "Higher-order process matrix tomography of a passively-stable quantum switch", PRX Quantum **5**, 010325 (2024).
[24] C.-F. Li, L. Chen, Y.-X. Yang, et al., *Nonlinear enhancement of measurement precision via a hybrid quantum switch*, Preprint available at Research Square., 2024.
[25] H. Tang, Y. Guo, X.-M. Hu, et al., "Demonstration of superior communication through thermodynamically free channels in an optical quantum switch", Phys. Rev. A **110**, 032422 (2024).
[26] X. Nie, X. Zhu, K. Huang, et al., "Experimental realization of a quantum refrigerator driven by indefinite causal orders", Phys. Rev. Lett. **129**, 100603 (2022).
[27] C. Xi, X. Liu, H. Liu, et al., "Experimental validation of enhanced information capacity by quantum switch in accordance with thermodynamic laws", Phys. Rev. Lett. **133**, 040401 (2024).
[28] L. A. Rozema, T. Strömberg, H. Cao, et al., "Experimental aspects of indefinite causal order in quantum mechanics", Nature Reviews Physics **6**, 483–499 (2024).
[29] M. Araújo, F. Costa, and Č. Brukner, "Computational advantage from quantum-controlled ordering of gates", Phys. Rev. Lett. **113**, 250402 (2014).
[30] L. M. Procopio, F. Delgado, M. Enríquez, et al., "Sending classical information via three noisy channels in superposition of causal orders", Phys. Rev. A **101**, 012346 (2020).

[31] S. Sazim, M. Sedlak, K. Singh, et al., "Classical communication with indefinite causal order for N completely depolarizing channels", Phys. Rev. A **103**, 062610 (2021).

[32] M. Wilson and G. Chiribella, "A diagrammatic approach to information transmission in generalised switches", in Proceedings 17th international conference on quantum physics and logic, paris, france, june 2 - 6, 2020, Vol. 340, edited by B. Valiron, S. Mansfield, P. Arrighi, et al., Electronic Proceedings in Theoretical Computer Science (2021), pp. 333–348.

[33] D. Das and S. Bandyopadhyay, "Quantum communication using a quantum switch of quantum switches", Proceedings of the Royal Society A: Mathematical, Physical and Engineering Sciences **478**, 10.1098/rspa.2022.0231 (2022).

[34] S. Kechrimparis, J. Moran, A. Karsa, et al., "Enhancing quantum state discrimination with indefinite causal order", New Journal of Physics **26**, 123030 (2024).

[35] S. Kechrimparis, J. Moran, and H. Kwon, *Probabilistic channel distillation via indefinite causal order*, arXiv:2501.13696, 2025.

[36] M. M. Taddei, J. Cariñe, D. Martínez, et al., "Computational advantage from the quantum superposition of multiple temporal orders of photonic gates", PRX Quantum **2**, 010320 (2021).

[37] G. Chiribella, "Perfect discrimination of no-signalling channels via quantum superposition of causal structures", Phys. Rev. A **86**, 040301 (2012).

[38] M. J. Renner and Č. Brukner, "Computational advantage from a quantum superposition of qubit gate orders", Phys. Rev. Lett. **128**, 230503 (2022).

[39] J. Escandón-Monardes, A. Delgado, and S. P. Walborn, "Practical computational advantage from the quantum switch on a generalized family of promise problems", Quantum **7**, 945 (2023).

[40] D. Trillo, B. Dive, and M. Navascués, "Universal quantum rewinding protocol with an arbitrarily high probability of success", Phys. Rev. Lett. **130**, 110201 (2023).

[41] M. T. Quintino, Q. Dong, A. Shimbo, et al., "Reversing unknown quantum transformations: universal quantum circuit for inverting general unitary operations", Phys. Rev. Lett. **123**, 210502 (2019).

[42] M. T. Quintino, Q. Dong, A. Shimbo, et al., "Probabilistic exact universal quantum circuits for transforming unitary operations", Phys. Rev. A **100**, 062339 (2019).

[43] M. T. Quintino and D. Ebler, "Deterministic transformations between unitary operations: exponential advantage with adaptive quantum circuits and the power of indefinite causality", Quantum **6**, 679 (2022).

[44] P. Ghosal, A. Ghosal, D. Das, et al., "Quantum superposition of causal structures as a universal resource for local implementation of nonlocal quantum operations", Phys. Rev. A **107**, 022613 (2023).

[45] A. A. Abbott, M. Mhalla, and P. Pocreau, "Quantum query complexity of boolean functions under indefinite causal order", Phys. Rev. Res. **6**, L032020 (2024).

[46] N. Ma, P. Z. Zhao, and J. Gong, "Quantum machine learning with indefinite causal order", Phys. Rev. A **110**, 052406 (2024).
[47] Y. Mo, C. Zhu, Z. Liu, et al., "Enhancement of nonstabilizerness within indefinite causal order", Phys. Rev. A **109**, 062428 (2024).
[48] W.-Q. Liu and H.-R. Wei, "Quantum gate teleportation with the superposition of causal order", Phys. Rev. Appl. **23**, 014064 (2025).
[49] A. Feix, M. Araújo, and C. Č. Brukner, "Quantum superposition of the order of parties as a communication resource", Phys. Rev. A **92**, 052326 (2015).
[50] P. A. Guérin, A. Feix, M. Araújo, et al., "Exponential communication complexity advantage from quantum superposition of the direction of communication", Phys. Rev. Lett. **117**, 100502 (2016).
[51] D. Ebler, S. Salek, and G. Chiribella, "Enhanced communication with the assistance of indefinite causal order", Phys. Rev. Lett. **120**, 120502 (2018).
[52] L. M. Procopio, F. Delgado, M. Enríquez, et al., "Communication enhancement through quantum coherent control of n channels in an indefinite causal-order scenario", Entropy **21**, 10.3390/e21101012 (2019).
[53] L. M. Procopio, F. Delgado, M. Enríquez, et al., "Multifold behavior of the information transmission by the quantum 3-switch", Quantum Information Processing **20**, 219 (2021).
[54] G. Chiribella, M. Wilson, and H. F. Chau, "Quantum and classical data transmission through completely depolarizing channels in a superposition of cyclic orders", Phys. Rev. Lett. **127**, 190502 (2021).
[55] F. Delgado and C. Cardoso-Isidoro, "Performance characterization of pauli channels assisted by indefinite causal order and post-measurement", Quantum Inf. Comput. **20**, 1261–1280 (2020).
[56] G. Chiribella, M. Banik, S. S. Bhattacharya, et al., "Indefinite causal order enables perfect quantum communication with zero capacity channels", New Journal of Physics **23**, 033039 (2021).
[57] X. Liu, D. Ebler, and O. Dahlsten, "Thermodynamics of quantum switch information capacity activation", Phys. Rev. Lett. **129**, 230604 (2022).
[58] M. Caleffi, K. Simonov, and A. S. Cacciapuoti, "Beyond shannon limits: quantum communications through quantum paths", IEEE Journal on Selected Areas in Communications **41**, 2707–2724 (2023).
[59] M. Caleffi and A. S. Cacciapuoti, "Quantum switch for the quantum internet: noiseless communications through noisy channels", IEEE Journal on Selected Areas in Communications **38**, 575–588 (2020).
[60] R. Xu, R.-G. Zhou, and Y. Li, "Toward the advantages of quantum trajectories on entanglement distribution in quantum networks", IEEE Transactions on Wireless Communications **22**, 5170–5184 (2023).
[61] C. Mukhopadhyay and A. K. Pati, "Superposition of causal order enables quantum advantage in teleportation under very noisy channels", Journal of Physics Communications **4**, 105003 (2020).
[62] M. Ban, "Continuous variable teleportation with indefinite causal order", Quantum Information Processing **21**, 367 (2022).

[63] I. Dey and N. Marchetti, "Quantum teleportation in higher dimension and entanglement distribution via quantum switches", IET Quantum Communication **6**, e12122 (2025).

[64] D. Chandra, M. Caleffi, and A. S. Cacciapuoti, "The entanglement-assisted communication capacity over quantum trajectories", IEEE Transactions on Wireless Communications **21**, 3632–3647 (2022).

[65] A. Mitra, H. Badhani, and S. Ghosh, "Improvement in quantum communication using quantum switch", Physica Scripta **98**, 045101 (2023).

[66] Z. Wu, J. Fullwood, Z. Ma, et al., "General communication enhancement via the quantum switch", Phys. Rev. A **111**, 012605 (2025).

[67] G. Chiribella and H. Kristjánsson, "Quantum shannon theory with superpositions of trajectories", Proceedings of the Royal Society A: Mathematical, Physical and Engineering Sciences **475**, 20180903 (2019).

[68] A. A. Abbott, J. Wechs, D. Horsman, et al., "Communication through coherent control of quantum channels", Quantum **4**, 333 (2020).

[69] N. Loizeau and A. Grinbaum, "Channel capacity enhancement with indefinite causal order", Phys. Rev. A **101**, 012340 (2020).

[70] A. O. T. Pang, N. Lupu-Gladstein, H. Ferretti, et al., "Experimental communication through superposition of quantum channels", Quantum **7**, 1125 (2023).

[71] P. A. Guérin, G. Rubino, and Č. Brukner, "Communication through quantum-controlled noise", Phys. Rev. A **99**, 062317 (2019).

[72] O. A. D. Molitor, A. H. A. Malavazi, R. D. Baldijão, et al., "Quantum switch instabilities with an open control", Communications Physics **7**, 373 (2024).

[73] S. Koudia, A. S. Cacciapuoti, and M. Caleffi, "Deterministic generation of multipartite entanglement via causal activation in the quantum internet", IEEE Access **11**, 73863–73878 (2023).

[74] Z. Zuo, M. Hanks, and M. S. Kim, "Coherent control of the causal order of entanglement distillation", Phys. Rev. A **108**, 062601 (2023).

[75] H. Spencer-Wood, *Indefinite causal key distribution*, arXiv:2303.03893., 2024.

[76] S. G. Naik, S. Sen, R. K. Patra, et al., *Local-data-hiding and causal inseparability: probing indefinite causal structures with cryptographic primitives*, arXiv:2407.20543., 2024.

[77] D. Felce and V. Vedral, "Quantum refrigeration with indefinite causal order", Phys. Rev. Lett. **125**, 070603 (2020).

[78] M. Frey, "Indefinite causal order aids quantum depolarizing channel identification", Quantum Information Processing **18**, 96 (2019).

[79] C. Mukhopadhyay, M. K. Gupta, and A. K. Pati, *Superposition of causal order as a metrological resource for quantum thermometry*, arXiv:1812.07508., 2018.

[80] X. Zhao, Y. Yang, and G. Chiribella, "Quantum metrology with indefinite causal order", Phys. Rev. Lett. **124**, 190503 (2020).

[81] F. Chapeau-Blondeau, "Noisy quantum metrology with the assistance of indefinite causal order", Phys. Rev. A **103**, 032615 (2021).
[82] F. Chapeau-Blondeau, "Indefinite causal order for quantum metrology with quantum thermal noise", Physics Letters A **447**, 128300 (2022).
[83] F. Chapeau-Blondeau, "Indefinite causal order for quantum phase estimation with pauli noise", Fluctuation and Noise Letters **22**, 10.1142/s0219477523500360 (2023).
[84] Y. Yuan, "Indefinite causal order for parameter estimation of channel with depolarization noise", Physics Letters A **531**, 130163 (2025).
[85] M. Ban, "Quantum fisher information of phase estimation in the presence of indefinite causal order", Physics Letters A **468**, 128749 (2023).
[86] M. Ban, "Phase estimation for a single-mode photon influenced by completely thermalizing channels with indefinite causal order", Physics Letters A **521**, 129744 (2024).
[87] S. M. Barnett, S. Croke, and S. Franke-Arnold, "Measurement with indefinite causal order and the sagnac interferometer", Phil. Trans. R. Soc. A **382**, 20240447 (2024).
[88] A. Z. Goldberg, K. Heshami, and L. L. Sánchez-Soto, "Evading noise in multiparameter quantum metrology with indefinite causal order", Phys. Rev. Res. **5**, 033198 (2023).
[89] S. Koudia and A. Gharbi, "Quantum non-gaussianity from an indefnite causal order of gaussian operations", International Journal of Quantum Information **19**, 2150026 (2021).
[90] N. Gao, D. Li, A. Mishra, et al., "Measuring incompatibility and clustering quantum observables with a quantum switch", Phys. Rev. Lett. **130**, 170201 (2023).
[91] O. Oreshkov, F. Costa, and Č. Brukner, "Quantum correlations with no causal order", Nature Communications **3**, 1092 (2012).
[92] C. Branciard, "Witnesses of causal nonseparability: an introduction and a few case studies", Scientific Reports **6**, 26018 (2016).
[93] M. Araújo, A. Feix, M. Navascués, et al., "A purification postulate for quantum mechanics with indefinite causal order", Quantum **1**, 10 (2017).
[94] O. Oreshkov, "Time-delocalized quantum subsystems and operations: on the existence of processes with indefinite causal structure in quantum mechanics", Quantum **3**, 206 (2019).
[95] T. Purves and A. J. Short, "Quantum theory cannot violate a causal inequality", Phys. Rev. Lett. **127**, 110402 (2021).
[96] J. Wechs, C. Branciard, and O. Oreshkov, "Existence of processes violating causal inequalities on time-delocalised subsystems", Nature Communications **14**, 1471 (2023).
[97] M. Araújo, C. Branciard, F. Costa, et al., "Witnessing causal nonseparability", New Journal of Physics **17**, 102001 (2015).
[98] N. Paunković and M. Vojinović, "Causal orders, quantum circuits and spacetime: distinguishing between definite and superposed causal orders", Quantum **4**, 275 (2020).

[99] V. Vilasini and R. Renner, "Fundamental limits for realizing quantum processes in spacetime", Phys. Rev. Lett. **133**, 080201 (2024).
[100] J. Wechs, H. Dourdent, A. A. Abbott, et al., "Quantum circuits with classical versus quantum control of causal order", PRX Quantum **2**, 030335 (2021).
[101] O. Oreshkov and C. Giarmatzi, "Causal and causally separable processes", New Journal of Physics **18**, 093020 (2016).
[102] A. A. Abbott, J. Wechs, F. Costa, et al., "Genuinely multipartite noncausality", Quantum **1**, 39 (2017).
[103] Ä. Baumeler, A. Feix, and S. Wolf, "Maximal incompatibility of locally classical behavior and global causal order in multiparty scenarios", Phys. Rev. A **90**, 042106 (2014).
[104] Ä. Baumeler and S. Wolf, "The space of logically consistent classical processes without causal order", New Journal of Physics **18**, 013036 (2016).
[105] J. Wechs, A. A. Abbott, and C. Branciard, "On the definition and characterisation of multipartite causal (non)separability", New Journal of Physics **21**, 013027 (2019).
[106] F. Giacomini, E. Castro-Ruiz, and Č. Brukner, "Indefinite causal structures for continuous-variable systems", New Journal of Physics **18**, 113026 (2016).
[107] P. A. Guérin, M. Krumm, C. Budroni, et al., "Composition rules for quantum processes: a no-go theorem", New Journal of Physics **21**, 012001 (2019).
[108] P. Lewandowska, Ł. Pawela, and Z. Puchała, "Strategies for single-shot discrimination of process matrices", Scientific Reports **13**, 3046 (2023).
[109] J. H. Selby, A. B. Sainz, and P. Horodecki, "Revisiting dynamics of quantum causal structures—when can causal order evolve?", Entropy **26**, 10.3390/e26080643 (2024).
[110] P. A. Guérin and Č. Brukner, "Observer-dependent locality of quantum events", New Journal of Physics **20**, 103031 (2018).
[111] J. Wechs and O. Oreshkov, *Subsystem decompositions of quantum evolutions and transformations between causal perspectives*, arXiv:2411.16504., 2024.
[112] O. Gühne and G. Tóth, "Entanglement detection", Physics Reports **474**, 1–75 (2009).
[113] C. Branciard, M. Araújo, A. Feix, et al., "The simplest causal inequalities and their violation", New Journal of Physics **18**, 013008 (2016).
[114] A. A. Abbott, C. Giarmatzi, F. Costa, et al., "Multipartite causal correlations: polytopes and inequalities", Phys. Rev. A **94**, 032131 (2016).
[115] B. S. Cirel'son, "Quantum generalizations of bell's inequality", Letters in Mathematical Physics **4**, 93–100 (1980).
[116] Č. Brukner, "Bounding quantum correlations with indefinite causal order", New Journal of Physics **17**, 083034 (2015).
[117] Z. Liu and G. Chiribella, *Tsirelson bounds for quantum correlations with indefinite causal order*, arXiv:2403.02749, 2024.

[118] T. van der Lugt, J. Barrett, and G. Chiribella, "Device-independent certification of indefinite causal order in the quantum switch", Nature Communications **14**, 5811 (2023).
[119] J. Bavaresco, M. Araújo, Č. Brukner, et al., "Semi-device-independent certification of indefinite causal order", Quantum **3**, 176 (2019).
[120] H. Dourdent, A. A. Abbott, N. Brunner, et al., "Semi-device-independent certification of causal nonseparability with trusted quantum inputs", Phys. Rev. Lett. **129**, 090402 (2022).
[121] H. Dourdent, A. A. Abbott, I. Šupić, et al., "Network-Device-Independent Certification of Causal Nonseparability", Quantum **8**, 1514 (2024).
[122] T. van der Lugt and N. Ormrod, "Possibilistic and maximal indefinite causal order in the quantum switch", Quantum **8**, 1543 (2024).
[123] A. Peres, "Incompatible results of quantum measurements", Physics Letters A **151**, 107–108 (1990).
[124] N. D. Mermin, "Quantum mysteries revisited", American Journal of Physics **58**, 731–734 (1990).
[125] M. Zych, F. Costa, I. Pikovski, et al., "Bell's theorem for temporal order", Nature Communications **10**, 3772 (2019).
[126] N. S. Móller, B. Sahdo, and N. Yokomizo, "Gravitational quantum switch on a superposition of spherical shells", Quantum **8**, 1248 (2024).
[127] E. Castro-Ruiz, F. Giacomini, A. Belenchia, et al., "Quantum clocks and the temporal localisability of events in the presence of gravitating quantum systems", Nature Communications **11**, 2672 (2020).
[128] N. S. Móller, B. Sahdo, and N. Yokomizo, "Quantum switch in the gravity of earth", Phys. Rev. A **104**, 042414 (2021).
[129] A. Dimić, M. Milivojević, D. Gočanin, et al., "Simulating indefinite causal order with rindler observers", Frontiers in Physics **8**, 10.3389/fphy.2020.525333 (2020).
[130] V. Vilasini and R. Renner, "Embedding cyclic information-theoretic structures in acyclic space-times: no-go results for indefinite causality", Phys. Rev. A **110**, 022227 (2024).
[131] M. Salzger and V. Vilasini, "Mapping indefinite causal order processes to composable quantum protocols in a spacetime", New Journal of Physics, 10.1088/1367-2630/ad9d6f (2024).
[132] A.-C. de la Hamette, V. Kabel, M. Christodoulou, et al., *Quantum diffeomorphisms cannot make indefinite causal order definite*, arXiv:2211.15685., 2022.
[133] A.-C. de la Hamette, V. Kabel, and Č. Brukner, *What an event is not: unravelling the identity of events in quantum theory and gravity*, arXiv:2404.00159., 2024.
[134] S. Fedida, A.-C. de la Hamette, V. Kabel, et al., *Knot invariants and indefinite causal order*, arXiv:2409.11448, 2024.
[135] J. Foo, C. S. Arabaci, M. Zych, et al., "Quantum superpositions of minkowski spacetime", Phys. Rev. D **107**, 045014 (2023).

[136] X. Liu, C. Zeng, and J. Wang, *Generation of quantum entanglement in superposed diamond spacetime*, arXiv:2501.00246, 2024.

[137] J. Foo, R. B. Mann, and M. Zych, *Relativity and decoherence of spacetime superpositions*, arXiv:2302.03259, 2023.

[138] D. Xie, C. Xu, and A. Wang, "Quantum metrology with coherent superposition of two different coded channels", Chinese Physics B **30**, 090304, 090304 (2021).

[139] O. A. D. Molitor and Ł. Rudnicki, "Quantum switch as a thermodynamic resource in the context of passive states", Entropy **26**, 10.3390/e26020153 (2024).

[140] A. T. Butson, "Generalized hadamard matrices", Proceedings of the American Mathematical Society **13**, 894–898 (1962).

[141] W. Tadej and K. Życzkowski, "A concise guide to complex hadamard matrices", Open Systems & Information Dynamics **13**, 133–177 (2006).

[142] Z. Hou, J.-F. Tang, H. Chen, et al., "Zero-trade-off multiparameter quantum estimation via simultaneously saturating multiple heisenberg uncertainty relations", Science Advances **7**, eabd2986 (2021).

[143] J. Liu, H. Yuan, X.-M. Lu, et al., "Quantum fisher information matrix and multiparameter estimation", Journal of Physics A: Mathematical and Theoretical **53**, 023001 (2020).

[144] S. Facchini and S. Perdrix, "Quantum circuits for the unitary permutation problem", in Theory and applications of models of computation, edited by R. Jain, S. Jain, and F. Stephan (2015), pp. 324–331.

[145] M. J. Renner and Č. Brukner, "Reassessing the computational advantage of quantum-controlled ordering of gates", Phys. Rev. Research **3**, 043012 (2021).

[146] M. Mirhosseini, O. S. Magaña-Loaiza, M. N. O'Sullivan, et al., "High-dimensional quantum cryptography with twisted light", New Journal of Physics **17**, 033033 (2015).

[147] L. Neves, G. Lima, J. G. Aguirre Gómez, et al., "Generation of entangled states of qudits using twin photons", Phys. Rev. Lett. **94**, 100501 (2005).

[148] S. P. Walborn, D. S. Lemelle, M. P. Almeida, et al., "Quantum key distribution with higher-order alphabets using spatially encoded qudits", Phys. Rev. Lett. **96**, 090501 (2006).

[149] T. Colnaghi, G. M. D'Ariano, S. Facchini, et al., "Quantum computation with programmable connections between gates", Physics Letters A **376**, 2940–2943 (2012).

[150] K.-J. Räihä and E. Ukkonen, "The shortest common supersequence problem over binary alphabet is np-complete", Theoretical Computer Science **16**, 187–198 (1981).

[151] K. Ning and H. W. Leong, "Towards a better solution to the shortest common supersequence problem: the deposition and reduction algorithm", in First international multi-symposiums on computer and computational sciences (imsccs'06), Vol. 1 (2006), pp. 84–90.

[152] P. Koutas and T. Hu, "Shortest string containing all permutations", Discrete Mathematics **11**, 125–132 (1975).
[153] X. S. Liu, G. L. Long, D. M. Tong, et al., "General scheme for superdense coding between multiparties", Phys. Rev. A **65**, 022304 (2002).
[154] M. Reck, A. Zeilinger, H. J. Bernstein, et al., "Experimental realization of any discrete unitary operator", Phys. Rev. Lett. **73**, 58–61 (1994).
[155] A. Crespi, R. Osellame, R. Ramponi, et al., "Suppression law of quantum states in a 3d photonic fast fourier transform chip", Nature Communications **7**, 10469 (2016).
[156] J. Cariñe, G. Cañas, P. Skrzypczyk, et al., "Multi-core fiber integrated multi-port beam splitters for quantum information processing", Optica **7**, 542–550 (2020).
[157] A. M. Pălici, T.-A. Isdrailă, S. Ataman, et al., "OAM tomography with heisenberg–weyl observables", Quantum Science and Technology **5**, 045004 (2020).
[158] O. J. Farías, F. de Melo, P. Milman, et al., "Quantum information processing by weaving quantum talbot carpets", Phys. Rev. A **91**, 062328 (2015).
[159] M. R. Barros, A. Ketterer, O. J. Farías, et al., "Free-space entangled quantum carpets", Phys. Rev. A. **95**, 042311 (2017).
[160] D. S. Tasca, R. M. Gomes, F. Toscano, et al., "Continuous-variable quantum computation with spatial degrees of freedom of photons", Phys. Rev. A **83**, 052325 (2011).
[161] C. H. Baldwin, A. Kalev, and I. H. Deutsch, "Quantum process tomography of unitary and near-unitary maps", Phys. Rev. A **90**, 012110 (2014).
[162] X.-Q. Zhou, H. Cable, R. Whittaker, et al., "Quantum-enhanced tomography of unitary processes", Optica **2**, 510–516 (2015).
[163] I. L. Chuang and M. A. Nielsen, "Prescription for experimental determination of the dynamics of a quantum black box", Journal of Modern Optics **44**, 2455–2467 (1997).
[164] M. Riebe, K. Kim, P. Schindler, et al., "Process tomography of ion trap quantum gates", Phys. Rev. Lett. **97**, 220407 (2006).
[165] R. C. Bialczak, M. Ansmann, M. Hofheinz, et al., "Quantum process tomography of a universal entangling gate implemented with josephson phase qubits", Nature Physics **6**, 409–413 (2010).
[166] A. M. Childs, I. L. Chuang, and D. W. Leung, "Realization of quantum process tomography in nmr", Phys. Rev. A **64**, 012314 (2001).
[167] M. Howard, J. Twamley, C. Wittmann, et al., "Quantum process tomography and linblad estimation of a solid-state qubit", New Journal of Physics **8**, 33 (2006).
[168] C. W. Helstrom, *Quantum detection and estimation theory* (Academic, 1976).
[169] A. S. Holevo, *Probabilistic and statistical aspect of quantum theory* (North-Holland, 1982).
[170] M. Vidrighin, G. Donati, M. G. Genoni, et al., "Joint estimation of phase and phase diffusion for quantum metrology", Nat. Commun. **5**, 3532 (2014).

[171] P. C. Humphreys, M. Barbieri, A. Datta, et al., "Quantum enhanced multiple phase estimation", Phys. Rev. Lett. **111**, 070403 (2013).
[172] S. Ragy, M. Jarzyna, and R. Demkowicz-Dobrzański, "Compatibility in multiparameter quantum metrology", Phys. Rev. A **94**, 052108 (2016).
[173] R. D. Gill and S. Massar, "State estimation for large ensembles", Phys. Rev. A **61**, 042312 (2000).
[174] L. O. Conlon, J. Suzuki, P. K. Lam, et al., "Efficient computation of the nagaoka–hayashi bound for multiparameter estimation with separable measurements", npj Quantum Information **7**, 110 (2021).
[175] M. Hayashi and Y. Ouyang, "Tight Cramér-Rao type bounds for multiparameter quantum metrology through conic programming", Quantum **7**, 1094 (2023).
[176] R. Demkowicz-Dobrzański, W. Górecki, and M. Guţă, "Multi-parameter estimation beyond quantum fisher information", Journal of Physics A: Mathematical and Theoretical **53**, 363001 (2020).
[177] F. Albarelli, M. Barbieri, M. Genoni, et al., "A perspective on multiparameter quantum metrology: from theoretical tools to applications in quantum imaging", Physics Letters A **384**, 126311 (2020).
[178] S. Kurdziałek, W. Górecki, F. Albarelli, et al., "Using adaptiveness and causal superpositions against noise in quantum metrology", Phys. Rev. Lett. **131**, 090801 (2023).
[179] M. A. Nielsen and I. L. Chuang, *Quantum computation and quantum information: 10th anniversary edition* (Cambridge University Press, 2010).
[180] M. A. Ballester, "Estimation of unitary quantum operations", Phys. Rev. A **69**, 022303 (2004).
[181] H. Yuan, "Sequential feedback scheme outperforms the parallel scheme for hamiltonian parameter estimation", Phys. Rev. Lett. **117**, 160801 (2016).
[182] Qiskit contributors, "Qiskit: An Open-source Framework for Quantum Computing" (2023).
[183] M. A. Nielsen, "A simple formula for the average gate fidelity of a quantum dynamical operation", Physics Letters A **303**, 249–252 (2002).
[184] https://github.com/Danuzco/unitary_estimation.
[185] K. Kraus, "General state changes in quantum theory", Annals of Physics **64**, 311–335 (1971).
[186] A. Jamiołkowski, "Linear transformations which preserve trace and positive semidefiniteness of operators", Reports on Mathematical Physics **3**, 275–278 (1972).
[187] M.-D. Choi, "Completely positive linear maps on complex matrices", Linear Algebra and its Applications **10**, 285–290 (1975).
[188] J. de Jong, *Fault-tolerant quantum computation: implementation of a fault-tolerant swap operation on the ibm 5-qubit device*, Master's thesis, Available at https://repository.tudelft.nl/islandora/object/uuid%3A39258a70-a347-40bb-a2f9-9ca301a71652, Jan. 2019.

[189] R. Gangwar, M. L. Bera, G. P. Teja, et al., "Ancilla-assisted protection of information: application to atom–cavity systems", Quantum Information Processing **22**, 425 (2023).

[190] C. H. Bennett and S. J. Wiesner, "Communication via one- and two-particle operators on einstein-podolsky-rosen states", Phys. Rev. Lett. **69**, 2881–2884 (1992).

[191] C. Wang, F.-G. Deng, Y.-S. Li, et al., "Quantum secure direct communication with high-dimension quantum superdense coding", Phys. Rev. A **71**, 044305 (2005).

[192] P. Hyllus and J. Eisert, "Optimal entanglement witnesses for continuous-variable systems", New Journal of Physics **8**, 51 (2006).

[193] G. Rubino, G. Manzano, and Č. Brukner, "Quantum superposition of thermodynamic evolutions with opposing time's arrows", Communications Physics **4**, 251 (2021).

[194] G. Chiribella and Z. Liu, "Quantum operations with indefinite time direction", Communications Physics **5**, 190 (2022).

[195] R. A. Bertlmann and P. Krammer, "Bloch vectors for qudits", Journal of Physics A: Mathematical and Theoretical **41**, 235303 (2008).

Appendix A

Estimation of qubit unitary transformations without prior information

Any qubit unitary gate can be written as (3.2.1), which is expanded as

$$\begin{aligned} U &= \cos(\alpha) I - i \sin(\alpha) \hat{n} \cdot \hat{\sigma} \\ &= c_I I - i c_x X - i c_y Y - i c_z Z \\ &= c_I I - i c_x X + c_y XZ - i c_z Z \ , \end{aligned} \tag{A.1}$$

where $c_I = \cos(\alpha)$ and $c_k = \sin(\alpha) n_k$ for $k \in \{x, y, z\}$, with $\alpha \in [0, \pi/2]$ and $\hat{n} \in \mathbb{R}^3$ a unit vector.

Notice that in the circuit of Fig. 3.2.3, the final joint state is given by

$$|\Phi^{10}\rangle_{012} = |\psi\rangle_0 \otimes |\varphi\rangle_{12} \ . \tag{A.2}$$

Dropping the last X gate on the second control qubit, the quantum state $|\Phi^9\rangle_{012}$ in the previous step of the circuit becomes

$$\begin{aligned} |\Phi^9\rangle_{012} &= |\psi\rangle_0 \otimes \Big(- i c_z |00\rangle_{12} + c_I |01\rangle_{12} + c_y |10\rangle_{12} - i c_x |11\rangle_{12} \Big) \\ &= |\psi\rangle_0 \otimes |\varphi^Z\rangle_{12} \ , \end{aligned} \tag{A.3}$$

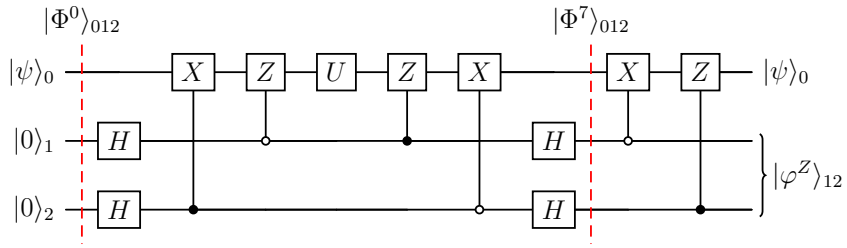

Figure A.1: Measurement of control in Z eigenbasis. The circuit is the same as in Fig. 3.2.3, without the last X gate in the second control qubit.

where $|\varphi^Z\rangle_{12} = -ic_z|00\rangle_{12} + c_I|01\rangle_{12} + c_y|10\rangle_{12} - ic_x|11\rangle_{12}$. Measuring this state in the computational basis (see Fig. A.1) leads to probabilities $P^Z_{00} = |c_z|^2$, $P^Z_{01} = |c_I|^2$, $P^Z_{10} = |c_y|^2$ and $P^Z_{11} = |c_x|^2$.

For measuring the control qubits in the X basis we need to apply a Hadamard gate on each one (see Fig. A.2). We get the new state

$$|\varphi^X\rangle_{12} = \frac{1}{2}\Big[(-ic_z + c_I + c_y - ic_x)|00\rangle_{12} + (-ic_z - c_I + c_y + ic_x)|01\rangle_{12} + (-ic_z + c_I - c_y + ic_x)|10\rangle_{12} + (-ic_z - c_I - c_y - ic_x)|11\rangle_{12}\Big] \ , \quad \text{(A.4)}$$

leading to probabilities

$$\begin{aligned} P^X_{00} &= \frac{1}{4}\Big((c_I + c_y)^2 + (c_x + c_z)^2\Big), \\ P^X_{01} &= \frac{1}{4}\Big((c_I - c_y)^2 + (c_x - c_z)^2\Big), \\ P^X_{10} &= \frac{1}{4}\Big((c_I - c_y)^2 + (c_x - c_z)^2\Big), \\ P^X_{11} &= \frac{1}{4}\Big((c_I + c_y)^2 + (c_x + c_z)^2\Big) \ . \end{aligned} \quad \text{(A.5)}$$

In order to measure the qubits in the Y eigenbasis, we apply a $\pi/2$-phase gate, defined as

$$S = |0\rangle\langle 0| + i|1\rangle\langle 1| \ , \quad \text{(A.6)}$$

followed by a Hadamard gate on each control qubit (see Fig. A.3). We get the

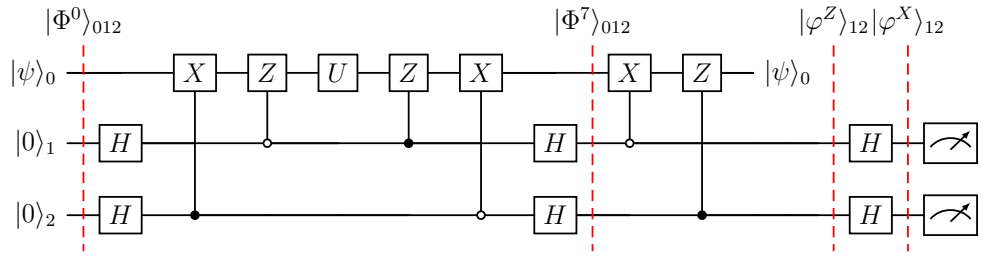

Figure A.2: Measurement of control in X eigenbasis. The circuit is the same as in Fig. 3.2.3, without the last X gate in the second control qubit. Additional rotation is performed in each control qubit in order to measure them in the X eigenbasis.

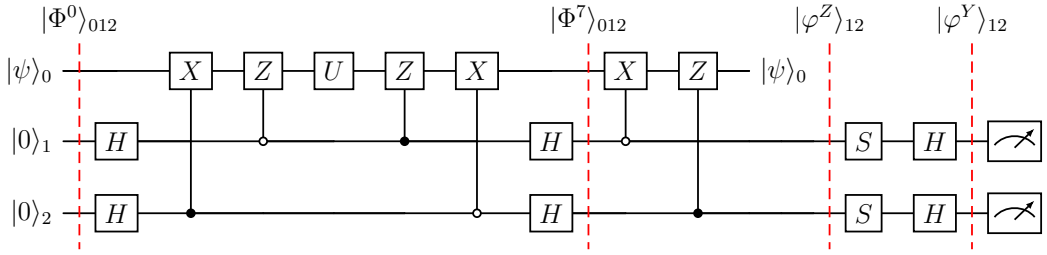

Figure A.3: Measurement of control in Y eigenbasis. The circuit is the same as in Fig. 3.2.3, without the last X gate in the second control qubit. Additional rotation is performed in each control qubit in order to measure them in the Y eigenbasis.

state:

$$|\varphi^Y\rangle_{12} = \frac{i}{2}\Big[(-c_z + c_I + c_y + c_x)|00\rangle_{12} + (-c_z - c_I + c_y - c_x)|01\rangle_{12} + (-c_z + c_I - c_y - c_x)|10\rangle_{12} + (-c_z - c_I - c_y + c_x)|11\rangle_{12}\Big], \tag{A.7}$$

and the outcome probabilities

$$\begin{aligned} P^Y_{00} &= \frac{1}{4}\Big(c_I + c_y + c_x - c_z\Big)^2, \\ P^Y_{01} &= \frac{1}{4}\Big(-c_I + c_y - c_x - c_z\Big)^2, \\ P^Y_{10} &= \frac{1}{4}\Big(c_I - c_y - c_x - c_z\Big)^2, \\ P^Y_{11} &= \frac{1}{4}\Big(-c_I - c_y + c_x - c_z\Big)^2. \end{aligned} \tag{A.8}$$

Since the absolute values of c_I, c_x, c_y and c_z are known from the first experiment, we can now use the outcome probabilities (A.5) and (A.8) to discriminate their signs. We denote $r_i \equiv |c_i|$, $s_i \equiv \mathrm{sgn}(c_i)$ and $s_{xz} = s_x \cdot s_z$. We obtain

$$P_{00}^X + P_{11}^X - P_{00}^Y - P_{11}^Y = 2c_x c_z \ . \tag{A.9}$$

Hence

$$s_{xz} = \mathrm{sgn}(P_{00}^X + P_{11}^X - P_{00}^Y - P_{11}^Y) \ . \tag{A.10}$$

Also, it is easy to show that

$$P_{00}^X + P_{11}^X + P_{00}^Y + P_{11}^Y = 1 + 2c_I c_y \ , \tag{A.11}$$

from where we get

$$s_y = \mathrm{sgn}(P_{00}^X + P_{11}^X + P_{00}^Y + P_{11}^Y - 1) \ , \tag{A.12}$$

where we have used the fact that $c_I^2 + c_x^2 + c_y^2 + c_z^2 = 1$ and $c_I > 0$.

Now we have two ways to obtain s_x. Firstly, noticing that

$$P_{10}^Y + P_{11}^Y = \frac{1}{2} - c_x c_I + c_z c_y \tag{A.13}$$

and that $s_z = s_x s_{xz}$, we can write

$$P_{10}^Y + P_{11}^Y = \frac{1}{2} - s_x r_x r_I + s_x s_{xz} s_y r_z r_y \ , \tag{A.14}$$

from where we get

$$s_x = \frac{P_{10}^Y + P_{11}^Y - 1/2}{s_{xz} s_y r_z r_y - r_x r_I} \ . \tag{A.15}$$

Another possibility is start from

$$P_{10}^Y - P_{11}^Y = c_y c_x - c_z c_I + c_x c_z - c_I c_y \tag{A.16}$$

to get

$$s_x = \frac{P_{10}^Y - P_{11}^Y + s_y r_I r_y - s_{xz} r_x r_z}{s_y r_y r_x - s_{xz} r_I r_z} \ . \tag{A.17}$$

Finally, we obtain $s_z = s_{xz} \cdot s_x$.

Notice that the Eqs. (A.15) and (A.17) are ill defined in some cases. Then, the complete protocol to estimate the unitaries from the outcome probabilities must consider special cases. We summarize the discrimination procedure in the following steps:

1. Get the magnitude of the coefficients r_i from P^Z_{jk}.
2. If three of the r_i are zero, then $U \in \{I, X, Y, Z\}$.
3. If $r_z = r_x = 0$, we only need to find s_y using Eq. (A.12). In case it is exactly zero, it means that either r_I or r_y is close to zero; we choose s_y randomly.
4. If $r_I = r_y = 0$, we get freedom in the global phase. Hence, we choose s_x randomly and calculate s_z from s_{xz} and Eq. (A.10).
5. Otherwise, we calculate s_{xz} and s_x using Eqs. (A.10) and (A.12), respectively. Then we choose Eq. (A.15) or (A.17) according to which expression has the denominator with larger absolute value, in order to diminish the statistical variation on the estimation of s_x. If both denominators are zero, we choose s_x as the numerator of Eq. (A.17).

The codes for this algorithm are shown in github [184].

Appendix B

Noise model for estimation of unitary transformations

We use the `NoiseModel` class from Qiskit to incorporate noise in the simulation of our procedure. The simulation with full noise was accomplished by importing an approximate noise model of the `ibmq_quito` quantum processor of IBM. We consider only qubits 0, 1 and 2 from the five qubits of this processor, assigning qubit 1 for the target qubit in our protocol and qubits 0 and 2 as control register. Tables B.1 and B.2 show the relevant error parameters for this setting, which are relaxation times T1 and T2, single-qubit gates error SX, readout or measurement errors and control-not gates error.

A second noisy simulation was performed considering only control-not gate errors. To this end, we fixed single-qubit gates and readout errors to zero. To avoid relaxation, we kept relaxation times but set the implementation time of each gate to zero. Finally, a full noise simulation but with ideal control-not gate was performed. In this case, only control-not error was consider equal to zero. Table B.3 shows the error parameters considered in these scenarios. These values are the maximum error parameters in `ibmq_quito` at the moment of setting the model and we consider the same values for each qubit.

Error Parameter	Qubit 0	Qubit 1	Qubit 2
Relaxation time T1s [ns]	87.49953×10^3	86.63249×10^3	83.6549×10^3
Relaxation time T2s [ns]	121.65781×10^3	97.53323×10^3	72.867×10^3
Single-qubit gate error (SX)	0.00045	0.0004	0.00027
Readout errors	0.0406	0.0444	0.0841

Table B.1: Error parameters for full noise simulation - Single qubit gates. Error parameters of `ibmq_quito` for each qubit used in the full noise simulation.

Error Parameter	Qubit 01	Qubit 12
Control-not error	0.01021	0.00861

Table B.2: Error parameters for full noise simulation - CNOT gates. Error parameters of `ibmq_quito` for CNOT gates on each pair of qubits used in the full noise simulation.

Error Parameter	Value
Relaxation time T1s [ns]	110×10^3
Dephasing time T2s [ns]	147×10^3
Error probabilities (SX)	0.00045
Readout errors	0.0841
Control-not	0.0142

Table B.3: Error parameters for partial noise simulations. For simulations with noiseless control-not gate we set its value to zero. For simulations considering only a noisy control-not gate we set to zero the other noise sources.

Appendix C

Derivation of the output state of our circuit for estimation of high-dimensional unitary transformations

In this appendix we follow the evolution of the state through the circuit illustrated in Fig. 3.3.1. Before that, let us start with some preliminary definitions.

Let us consider a d-dimensional Hilbert space $\mathcal{H}$ and the d^2-dimensional space $\mathcal{L}(\mathcal{H})$ of linear operators on $\mathcal{H}$. We will denote the d^{th} root of unity as $\omega \equiv \exp(2\pi i/d)$, the addition modulo d as $\oplus$ and the sustraction modulo d as $\ominus$. Some important unitary operations in $\mathcal{L}(\mathcal{H})$ are the following:

1. *Identity*:
$$I := \sum_{k=0}^{d-1} |k\rangle \langle k| \ . \tag{C.1}$$

2. *Shift operator*:
$$X := \sum_{k=0}^{d-1} |k \oplus 1\rangle \langle k| \ . \tag{C.2}$$

3. *Phase operator*:
$$Z := \sum_{k=0}^{d-1} \omega^k |k\rangle \langle k| \ . \tag{C.3}$$

4. *Fourier transform*:

$$F := \frac{1}{\sqrt{d}} \sum_{k=0}^{d-1} \omega^{jk} \left|j\right\rangle \left\langle k\right| \ . \tag{C.4}$$

It can be easily shown that the shift and phase operators satisfy the relation

$$Z^j X^k = \omega^{jk} X^k Z^j \ . \tag{C.5}$$

Also, we use a short notation for the Weyl-Heisenberg operators, defined as

$$D_n \equiv D_{(n_x,n_z)} := X^{n_x} Z^{n_z} \ , \tag{C.6}$$

with $n = (n_x, n_z) \in \mathbb{Z}_d^2$, being $\mathbb{Z}_d = \{0, ..., d-1\}$. The set $\{D_n\}_{n\in\mathbb{Z}_d^2}$ is an orthogonal basis for $\mathcal{L}(\mathcal{H})$; indeed, considering the Hilbert-Schmidt inner product for operators $\langle A, B\rangle = Tr[A^\dagger B]$ and the relation $\sum_{i=0}^{d-1} \omega^{i(j-k)} = d\delta_{jk}$, it is possible to show that

$$\langle D_n, D_m\rangle = d\delta_{nm} \ , \tag{C.7}$$

where $\delta_{nm} = \delta_{n_x m_x}\delta_{n_z m_z}$. Consequently, any operator in $\mathcal{L}(\mathcal{H})$ can be written as a linear combination of Weyl-Heisenberg operators. In particular, an unknown unitary U can be expanded as

$$U = \sum_{n\in\mathbb{Z}_d^2} r_n e^{i\phi_n} D_n = \sum_{n\in\mathbb{Z}_d^2} u_{(n_x,n_z)} X^{n_x} Z^{n_z} \ , \tag{C.8}$$

where $u_n = r_n e^{i\phi_n}$ are complex coefficients with amplitude r_n and phase ϕ_n.

Additionally, we define the controlled unitary operators with shifted control:

$$V_{tc}^{(i)} := \sum_{k=0}^{d-1} V_t^k \otimes \left|k \ominus i\right\rangle_c \left\langle k \ominus i\right| \ , \tag{C.9}$$

where V_t is a unitary gate acting on a target system t controlled by a control system c whose state is shifted by i. For our procedure, we need the following

four controlled operations:

$$X_{02}^{(0)} = \sum_{k=0}^{d-1} X_0^k \otimes |k\rangle_2\langle k| \ , \tag{C.10}$$

$$Z_{01}^{\dagger(1)} = \sum_{k=0}^{d-1} (Z_0^\dagger)^k \otimes |k \ominus 1\rangle_1\langle k \ominus 1| = \sum_{k=0}^{d-1} Z_0^{-k-1} \otimes |k\rangle_1\langle k| \ , \tag{C.11}$$

$$Z_{01}^{(0)} = \sum_{k=0}^{d-1} Z_0^k \otimes |k\rangle_1\langle k| \ , \tag{C.12}$$

$$X_{02}^{\dagger(1)} = \sum_{k=0}^{d-1} (X_0^\dagger)^k \otimes |k \ominus 1\rangle_2\langle k \ominus 1| = \sum_{k=0}^{d-1} X_0^{-k-1} \otimes |k\rangle_2\langle k| \ . \tag{C.13}$$

Now let us proceed with the initial joint state

$$\left|\Phi^0\right\rangle_{012} = |\psi\rangle_0 \otimes |0\rangle_1 \otimes |0\rangle_2 \ , \tag{C.14}$$

where $|\psi\rangle_0$ is an arbitrary pure state. After applying the Fourier gates on the control qudits, it becomes

$$\begin{aligned} \left|\Phi^1\right\rangle_{012} &= (I_0 \otimes F_1 \otimes F_2) \left|\Phi^0\right\rangle_{012} \\ &= \frac{1}{d} \sum_{j_1,j_2=0}^{d-1} |\psi\rangle_0 \otimes |j_1\rangle_1 \otimes |j_2\rangle_2 \ . \end{aligned} \tag{C.15}$$

After the controlled gate $X_{02}^{(0)}$ we have

$$\begin{aligned} \left|\Phi^2\right\rangle_{012} &= (X_{02}^{(0)} \otimes I_1) \left|\Phi^1\right\rangle_{012} \\ &= \frac{1}{d} \sum_{j_1,j_2=0}^{d-1} X_0^{j_2} |\psi\rangle_0 \otimes |j_1\rangle_1 \otimes |j_2\rangle_2 \ . \end{aligned} \tag{C.16}$$

Then,

$$\begin{aligned} \left|\Phi^3\right\rangle_{012} &= (Z_{01}^{\dagger(1)} \otimes I_2) \left|\Phi^2\right\rangle_{012} \\ &= \frac{1}{d} \sum_{j_1,j_2=0}^{d-1} Z_0^{-j_1-1} X_0^{j_2} |\psi\rangle_0 \otimes |j_1\rangle_1 \otimes |j_2\rangle_2 \ . \end{aligned} \tag{C.17}$$

Applying U on the target qudit and using Eq. (C.5), we get

$$\begin{aligned}\left|\Phi^4\right\rangle_{012} &= (U_0 \otimes I_1 \otimes I_2)\left|\Phi^3\right\rangle_{012} \\ &= \frac{1}{d}\sum_{n_x,n_z,j_1,j_2=0}^{d-1} u_{(n_x,n_z)}\omega^{j_2(n_z-j_1-1)}X_0^{n_x+j_2}Z_0^{n_z-j_1-1}\left|\psi\right\rangle_0 \otimes \left|j_1\right\rangle_1 \otimes \left|j_2\right\rangle_2 \ .\end{aligned} \tag{C.18}$$

Following with the next controlled operations we have

$$\begin{aligned}\left|\Phi^5\right\rangle_{012} &= (Z_{01}^{(0)} \otimes I_2)\left|\Phi^4\right\rangle_{012} \\ &= \frac{1}{d}\sum_{n_x,n_z,j_1,j_2=0}^{d-1} u_{(n_x,n_z)}\omega^{j_2(n_z-1)+j_1n_x}X_0^{n_x+j_2}Z_0^{n_z-1}\left|\psi\right\rangle_0 \otimes \left|j_1\right\rangle_1 \otimes \left|j_2\right\rangle_2 \ ,\end{aligned} \tag{C.19}$$

and then

$$\begin{aligned}\left|\Phi^6\right\rangle_{012} &= (X_{02}^{\dagger(1)} \otimes I_1)\left|\Phi^5\right\rangle_{012} \\ &= \frac{1}{d}\sum_{n_x,n_z,j_1,j_2=0}^{d-1} u_{(n_x,n_z)}\omega^{j_2(n_z-1)+j_1n_x}X_0^{n_x-1}Z_0^{n_z-1}\left|\psi\right\rangle_0 \otimes \left|j_1\right\rangle_1 \otimes \left|j_2\right\rangle_2 \\ &= \sum_{n_x,n_z=0}^{d-1} u_{(n_x,n_z)}X_0^{n_x-1}Z_0^{n_z-1}\left|\psi\right\rangle_0 \\ &\quad \otimes \left(\frac{1}{\sqrt{d}}\sum_{j_1=0}^{d-1}\omega^{j_1n_x}\left|j_1\right\rangle_1\right) \otimes \left(\frac{1}{\sqrt{d}}\sum_{j_2=0}^{d-1}\omega^{j_2(n_z-1)}\left|j_2\right\rangle_2\right) \\ &= \sum_{n_x,n_z=0}^{d-1} u_{(n_x,n_z)}X_0^{n_x-1}Z_0^{n_z-1}\left|\psi\right\rangle_0 \otimes F_1\left|n_x\right\rangle_1 \otimes F_2\left|n_z \ominus 1\right\rangle_2 \ .\end{aligned} \tag{C.20}$$

Now we apply the inverse Fourier transform on the control qudits, getting

$$\begin{aligned}\left|\Phi^7\right\rangle_{012} &= (I_0 \otimes F_1^{-1} \otimes F_2^{-1})\left|\Phi^6\right\rangle_{012} \\ &= \sum_{n_x,n_z=0}^{d-1} u_{(n_x,n_z)}X_0^{n_x-1}Z_0^{n_z-1}\left|\psi\right\rangle_0 \otimes \left|n_x\right\rangle_1 \otimes \left|n_z \ominus 1\right\rangle_2 \\ &= \sum_{n_x,n_z=0}^{d-1} u_{(n_x,n_z\oplus 1)}X_0^{n_x-1}Z_0^{n_z}\left|\psi\right\rangle_0 \otimes \left|n_x\right\rangle_1 \otimes \left|n_z\right\rangle_2 \ .\end{aligned} \tag{C.21}$$

In order to disentangle the target from the control qudits, we use the following

controlled gates:

$$X_{01}^{\dagger(-1)} = \sum_{k=0}^{d-1} (X_0^\dagger)^k \otimes |k \oplus 1\rangle_1\langle k \oplus 1| = \sum_{k=0}^{d-1} X_0^{-k+1} \otimes |k\rangle_1\langle k| \ , \tag{C.22}$$

$$Z_{02}^{\dagger(0)} = \sum_{k=0}^{d-1} Z_0^{-k} \otimes |k\rangle_2\langle k| \ . \tag{C.23}$$

Successive steps leads to:

$$\begin{aligned} \left|\Phi^8\right\rangle_{012} &= \left(X_{01}^{\dagger(1)} \otimes I_2\right) \left|\Phi^7\right\rangle_{012} \\ &= \sum_{n_x,n_z=0}^{d-1} u_{(n_x,n_z\oplus 1)} Z_0^{n_z} \left|\psi\right\rangle_0 \otimes \left|n_x\right\rangle_1 \otimes \left|n_z\right\rangle_2 \ , \end{aligned} \tag{C.24}$$

$$\begin{aligned} \left|\Phi^9\right\rangle_{012} &= \left(Z_{02}^{\dagger(0)} \otimes I_1\right) \left|\Phi^8\right\rangle_{012} \\ &= \left|\psi\right\rangle_0 \otimes \left(\sum_{n_x,n_z=0}^{d-1} u_{(n_x,n_z\oplus 1)} \left|n_x\right\rangle_1 \otimes \left|n_z\right\rangle_2 \right) \ , \end{aligned} \tag{C.25}$$

and

$$\begin{aligned} \left|\Phi^{10}\right\rangle_{012} &= (I_0 \otimes I_1 \otimes X_2) \left|\Phi^9\right\rangle_{012} \\ &= \left|\psi\right\rangle_0 \otimes \left(\sum_{n_x,n_z=0}^{d-1} u_{(n_x,n_z)} \left|n_x\right\rangle_1 \otimes \left|n_z\right\rangle_2 \right) \\ &= \left|\psi\right\rangle_0 \otimes \left|\varphi^0\right\rangle_{12} \ , \end{aligned} \tag{C.26}$$

where $|\varphi^0\rangle_{12} = \sum_{n_x,n_z=0}^{d-1} u_{(n_x,n_z)} |n_x\rangle_1 \otimes |n_z\rangle_2$ is the state of the control with exactly the same coefficients of U. For short, we write

$$\left|\varphi^0\right\rangle_{12} = \sum_{n\in\mathbb{Z}_d^2} u_n \left|n\right\rangle = \sum_{n\in\mathbb{Z}_d^2} r_n e^{i\phi_n} \left|n\right\rangle \ , \tag{C.27}$$

which corresponds to Eq. (3.3.8) in the main text.

Appendix D

Unitarity condition of high-dimensional operators

Let us consider the unitary gate U, written in the Weyl-Heisenberg basis as

$$U = \sum_{n \in \mathbb{Z}_d^2} r_n e^{i\phi_n} D_n \ , \tag{D.1}$$

and its adjoint

$$U^\dagger = \sum_{m \in \mathbb{Z}_d^2} r_m e^{-i\phi_m} D_m^\dagger \ , \tag{D.2}$$

where D_n is defined in Eq. (C.6). We have

$$UU^\dagger = \sum_{m,n \in \mathbb{Z}_d^2} r_m r_n e^{i(\phi_n - \phi_m)} D_n D_m^\dagger \ , \tag{D.3}$$

but since U is unitary we also have $UU^\dagger = I$. Noticing that $I = D_0$ and considering Eq. (C.7), we have that unitarity of U implies:

$$Tr[D_p^\dagger U U^\dagger] = d\delta_{p,0} = \begin{cases} d & \text{if } p = (0,0) \\ 0 & \text{if } p \neq (0,0) \end{cases} \ . \tag{D.4}$$

Let us calculate the left hand side of this expression using Eq. (D.3). We have:

$$\begin{aligned} Tr[D_p^\dagger U U^\dagger] &= \sum_{k=0}^{d-1} \langle k| \sum_{m,n\in\mathbb{Z}_d^2} r_m r_n e^{i(\phi_n-\phi_m)} D_p^\dagger D_n D_m^\dagger |k\rangle \\ &= \sum_{m,n\in\mathbb{Z}_d^2} r_m r_n e^{i(\phi_n-\phi_m)} \sum_{k=0}^{d-1} \langle k| D_p^\dagger D_n D_m^\dagger |k\rangle \ , \end{aligned} \tag{D.5}$$

but in terms of the shift and phase operators we also have

$$\begin{aligned} \langle k| D_p^\dagger D_n D_m^\dagger |k\rangle &= \langle k| (X^{p_x} Z^{p_z})^\dagger (X^{n_x} Z^{n_z})(X^{m_x} Z^{m_z})^\dagger |k\rangle \\ &= \langle k| Z^{-p_z} X^{-p_x} X^{n_x} Z^{n_z} Z^{-m_z} X^{-m_x} |k\rangle \\ &= \omega^{-m_x(n_z-m_z)} \omega^{-p_z(n_x-p_x-m_x)} \langle k| X^{n_x-p_x-m_x} Z^{n_z-m_z-p_z} |k\rangle \\ &= \omega^{-m_x(n_z-m_z)} \omega^{-p_z(n_x-p_x-m_x)} \omega^{(n_z-m_z-p_z)k} \langle k| X^{n_x-p_x-m_x} |k\rangle \\ &= \omega^{-m_x(n_z-m_z)} \omega^{-p_z(n_x-p_x-m_x)} \omega^{(n_z-m_z-p_z)k} \langle k| k \oplus n_x \ominus p_x \ominus m_x\rangle \\ &= \omega^{-m_x(n_z-m_z)} \omega^{-p_z(n_x-p_x-m_x)} \omega^{(n_z-m_z-p_z)k} \delta_{n_x,p_x\oplus m_x} \\ &= \omega^{-m_x(n_z-m_z)} \omega^{(n_z-m_z-p_z)k} \delta_{n_x,p_x\oplus m_x} \ , \end{aligned} \tag{D.6}$$

where we have used the commutation relation in Eq. (C.5). Now, summing over k we get

$$\begin{aligned} \sum_{k=0}^{d-1} \langle k| D_p^\dagger D_n D_m^\dagger |k\rangle &= \omega^{-m_x(n_z-m_z)} \left(\sum_{k=0}^{d-1} \omega^{(n_z-m_z-p_z)k} \right) \delta_{n_x,p_x\oplus m_x} \\ &= \omega^{-m_x(n_z-m_z)} d\delta_{n_z,p_z\oplus m_z} \delta_{n_x,p_x\oplus m_x} \\ &= d\omega^{-m_x(n_z-m_z)} \delta_{n,p\oplus m} \ . \end{aligned} \tag{D.7}$$

Replacing Eq. (D.7) in Eq. (D.5), we get

$$\begin{aligned} Tr[D_p^\dagger U U^\dagger] &= d \sum_{m,n\in\mathbb{Z}_d^2} r_m r_n e^{i(\phi_n-\phi_m)} \omega^{-m_x(n_z-m_z)} \delta_{n,p\oplus m} \\ &= d \sum_{m\in\mathbb{Z}_d^2} r_m r_{p\oplus m} e^{i(\phi_{p\oplus m}-\phi_m)} \omega^{-m_x p_z} \ . \end{aligned} \tag{D.8}$$

In particular, for $p = (0, 0)$ in Eq. (D.4) we obtain a normalization condition, which is equivalent to the total probability rule for the outcomes of our circuit:

$$\sum_{m \in \mathbb{Z}_d^2} r_m^2 = 1 \, . \tag{D.9}$$

Besides, for $p \neq (0, 0)$, we have

$$\sum_{m \in \mathbb{Z}_d^2} r_m r_{p \oplus m} e^{i(\phi_{p \oplus m} - \phi_m)} \omega^{-m_x p_z} = 0 \, . \tag{D.10}$$

Eqs. (D.9) and (D.10) appear as Eqs. (3.3.9) and (3.3.10), respectively, in the main text.

Appendix E

Calculation of Quantum Fisher Information Matrix

The entries $\mathcal{F}_{ab}$ of the quantum Fisher information matrix are given by

$$\mathcal{F}_{ab} = 2\langle\Phi|\{H_a, H_b\}|\Phi\rangle - 4\langle\Phi|H_a|\Phi\rangle\langle\Phi|H_b|\Phi\rangle \ , \tag{E.1}$$

with $H_a = i\left(\partial_a U^\dagger\right)U = -iU^\dagger(\partial_a U)$, and $|\Phi\rangle$ the probe state. In our circuit, the probe state is given by Eq. (C.17) as

$$|\Phi\rangle = \left|\Phi^3\right\rangle_{012} = \frac{1}{d}\sum_{j_1,j_2=0}^{d-1} Z_0^{-j_1-1}X_0^{j_2}|\psi\rangle_0 \otimes |j_1\rangle_1 \otimes |j_2\rangle_2 \ , \tag{E.2}$$

where $|\psi\rangle_0$ is the initial state of the target system.

Let us consider again the expansion of the unitary gate

$$U = \sum_{n\in\mathbb{Z}_d^2} r_n e^{i\phi_n} D_n \ , \tag{E.3}$$

where $n = (n_x, n_z)$ is an ordered pair and $D_n = D_{n_x,n_z} = X^{n_x}Z^{n_z}$. The sum can be split using partition (3.3.15) as

$$U = r_0 I + \sum_{f\in S_u} r_f e^{i\phi_f} D_f + \sum_{a\in S_+} r_a\left(e^{i\phi_a}D_a + e^{i\phi_{\ominus a}}D_{\ominus a}\right) , \tag{E.4}$$

where $r_0 = \left(1 - \sum_{n\neq(0,0)} r_n^2\right)^{1/2}$ and we have used $r_a = r_{\ominus a}$ in the last sum. Notice that

$$\begin{aligned} r_0 &= \left(1 - \sum_{f\in S_u} r_f^2 - \sum_{a\in S_+} r_a^2 - \sum_{\ominus a\in S_-} r_{\ominus a}^2\right)^{1/2} \\ &= \left(1 - \sum_{f\in S_u} r_f^2 - 2\sum_{a\in S_+} r_a^2\right)^{1/2} . \end{aligned} \tag{E.5}$$

We can now determine the derivatives of U and therefore the operators H_a that appears in Eq. (E.1). For $f \in S_u$ we have:

$$\partial_{r_f} U = -\frac{r_f}{r_0} I + e^{i\phi_f} D_f \ , \tag{E.6}$$

and therefore

$$\begin{aligned} H_{r_f} &= i\left(\partial_{r_f} U^\dagger\right) U \\ &= i\sum_{n\in\mathbb{Z}_d^2} r_n \left(-\frac{r_f}{r_0} e^{i\phi_n} D_n + e^{i(\phi_n-\phi_f)} D_f^\dagger D_n\right) . \end{aligned} \tag{E.7}$$

Similarly, for $a \in S_+$ we have:

$$\partial_{r_a} U = -2\frac{r_a}{r_0} I + e^{i\phi_a} D_a + e^{i\phi_{\ominus a}} D_{\ominus a} \tag{E.8}$$

and

$$\partial_{\phi_a} U = i r_a (e^{i\phi_a} D_a - e^{i\phi_{\ominus a}} D_{\ominus a}) \ , \tag{E.9}$$

leading to

$$H_{r_a} = i\sum_{n\in\mathbb{Z}_d^2} r_n \left(-2\frac{r_a}{r_0} e^{i\phi_n} D_n + e^{i(\phi_n-\phi_a)} D_a^\dagger D_n + e^{i(\phi_n-\phi_{\ominus a})} D_{\ominus a}^\dagger D_n\right) \tag{E.10}$$

and

$$H_{\phi_a} = \sum_{n\in\mathbb{Z}_d^2} r_a r_n \left(e^{i(\phi_n-\phi_a)} D_a^\dagger D_n - e^{i(\phi_n-\phi_{\ominus a})} D_{\ominus a}^\dagger D_n\right) . \tag{E.11}$$

In order to calculate the anti-commutators in Eq. (E.1), let us note that

$$\begin{aligned}\{H_a, H_b\} &= \left[i\left(\partial_a U^\dagger\right)U\right]\left[-iU^\dagger\left(\partial_b U\right)\right] + \left[i\left(\partial_b U^\dagger\right)U\right]\left[-iU^\dagger\left(\partial_a U\right)\right] \\ &= \left(\partial_a U^\dagger\right)UU^\dagger\left(\partial_b U\right) + \left(\partial_b U^\dagger\right)UU^\dagger\left(\partial_a U\right) \ . \end{aligned} \tag{E.12}$$

By imposing unitarity on U we have that $UU^\dagger = I$ and Eq. (E.12) becomes

$$\{H_a, H_b\} = \left(\partial_a U^\dagger\right)\left(\partial_b U\right) + \left(\partial_b U^\dagger\right)\left(\partial_a U\right) \ . \tag{E.13}$$

We can now replace Eqs. (E.6), (E.8) and (E.9) into (E.13) and get:

$$\begin{aligned}\{H_{r_f}, H_{r_g}\} &= 2\frac{r_f r_g}{r_0^2} I - \frac{r_f}{r_0}\left(e^{i\phi_g} D_g + e^{-i\phi_g} D_g^\dagger\right) - \frac{r_g}{r_0}\left(e^{i\phi_f} D_f + e^{-i\phi_f} D_f^\dagger\right) \\ &\quad + e^{i(\phi_g - \phi_f)} D_f^\dagger D_g + e^{i(\phi_f - \phi_g)} D_g^\dagger D_f \ , \end{aligned} \tag{E.14}$$

$$\begin{aligned}\{H_{r_f}, H_{r_a}\} &= 4\frac{r_f r_a}{r_0^2} I - 2\frac{r_a}{r_0}\left(e^{i\phi_f} D_f + e^{-i\phi_f} D_f^\dagger\right) \\ &\quad - \frac{r_f}{r_0}\left(e^{i\phi_a} D_a + e^{-i\phi_a} D_a^\dagger + e^{i\phi_{\ominus a}} D_{\ominus a} + e^{-i\phi_{\ominus a}} D_{\ominus a}^\dagger\right) \\ &\quad + \left(e^{i(\phi_a - \phi_f)} D_f^\dagger D_a + e^{i(\phi_f - \phi_a)} D_a^\dagger D_f\right) \\ &\quad + \left(e^{i(\phi_{\ominus a} - \phi_f)} D_f^\dagger D_{\ominus a} + e^{i(\phi_f - \phi_{\ominus a})} D_{\ominus a}^\dagger D_f\right) \ , \end{aligned} \tag{E.15}$$

$$\begin{aligned}\{H_{r_f}, H_{\phi_a}\} &= i r_a \Bigg(\frac{r_f}{r_0}\left(-e^{i\phi_a} D_a + e^{-i\phi_a} D_a^\dagger + e^{i\phi_{\ominus a}} D_{\ominus a} - e^{-i\phi_{\ominus a}} D_{\ominus a}^\dagger\right) \\ &\quad + \left(e^{i(\phi_a - \phi_f)} D_f^\dagger D_a - e^{i(\phi_f - \phi_a)} D_a^\dagger D_f\right) \\ &\quad + \left(-e^{i(\phi_{\ominus a} - \phi_f)} D_f^\dagger D_{\ominus a} + e^{i(\phi_f - \phi_{\ominus a})} D_{\ominus a}^\dagger D_f\right)\Bigg) \ , \end{aligned} \tag{E.16}$$

$$\begin{aligned}\{H_{r_a}, H_{r_b}\} &= 8\frac{r_a r_b}{r_0^2} I - 2\frac{r_a}{r_0}\left(e^{i\phi_b} D_b + e^{-i\phi_b} D_b^\dagger + e^{i\phi_{\ominus b}} D_{\ominus b} + e^{-i\phi_{\ominus b}} D_{\ominus b}^\dagger\right) \\ &\quad - 2\frac{r_b}{r_0}\left(e^{i\phi_a} D_a + e^{-i\phi_a} D_a^\dagger + e^{i\phi_{\ominus a}} D_{\ominus a} + e^{-i\phi_{\ominus a}} D_{\ominus a}^\dagger\right) \\ &\quad + \left(e^{i(\phi_b - \phi_a)} D_a^\dagger D_b + e^{i(\phi_a - \phi_b)} D_b^\dagger D_a\right) \\ &\quad + \left(e^{i(\phi_{\ominus b} - \phi_a)} D_a^\dagger D_{\ominus b} + e^{i(\phi_a - \phi_{\ominus b})} D_{\ominus b}^\dagger D_a\right) \\ &\quad + \left(e^{i(\phi_b - \phi_{\ominus a})} D_{\ominus a}^\dagger D_b + e^{i(\phi_{\ominus a} - \phi_b)} D_b^\dagger D_{\ominus a}\right) \\ &\quad + \left(e^{i(\phi_{\ominus b} - \phi_{\ominus a})} D_{\ominus a}^\dagger D_{\ominus b} + e^{i(\phi_{\ominus a} - \phi_{\ominus b})} D_{\ominus b}^\dagger D_{\ominus a}\right) \ , \end{aligned} \tag{E.17}$$

$$\{H_{r_a}, H_{\phi_b}\} = 2i\frac{r_a r_b}{r_0}\left(-e^{i\phi_b}D_b + e^{-i\phi_b}D_b^\dagger + e^{i\phi_{\ominus b}}D_{\ominus b} - e^{-i\phi_{\ominus b}}D_{\ominus b}^\dagger\right)$$
$$+ ir_b\Big(e^{i(\phi_b-\phi_a)}D_a^\dagger D_b - e^{i(\phi_a-\phi_b)}D_b^\dagger D_a - e^{i(\phi_{\ominus b}-\phi_a)}D_a^\dagger D_{\ominus b}$$
$$+ e^{i(\phi_a-\phi_{\ominus b})}D_{\ominus b}^\dagger D_a + e^{i(\phi_b-\phi_{\ominus a})}D_{\ominus a}^\dagger D_b - e^{i(\phi_{\ominus a}-\phi_b)}D_b^\dagger D_{\ominus a}$$
$$+ e^{i(\phi_{\ominus a}-\phi_{\ominus b})}D_{\ominus b}^\dagger D_{\ominus a} - e^{i(\phi_{\ominus b}-\phi_{\ominus a})}D_{\ominus a}^\dagger D_{\ominus b}\Big) \tag{E.18}$$

and

$$\{H_{\phi_a}, H_{\phi_b}\} = r_a r_b\Big(e^{i(\phi_b-\phi_a)}D_a^\dagger D_b + e^{i(\phi_a-\phi_b)}D_b^\dagger D_a - e^{i(\phi_{\ominus b}-\phi_a)}D_a^\dagger D_{\ominus b}$$
$$- e^{i(\phi_a-\phi_{\ominus b})}D_{\ominus b}^\dagger D_a - e^{i(\phi_b-\phi_{\ominus a})}D_{\ominus a}^\dagger D_b - e^{i(\phi_{\ominus a}-\phi_b)}D_b^\dagger D_{\ominus a}$$
$$+ e^{i(\phi_{\ominus a}-\phi_{\ominus b})}D_{\ominus b}^\dagger D_{\ominus a} + e^{i(\phi_{\ominus b}-\phi_{\ominus a})}D_{\ominus a}^\dagger D_{\ominus b}\Big)\,. \tag{E.19}$$

In order to calculate the expectation values $\langle\Phi|\, H_a\,|\Phi\rangle$ and $\langle\Phi|\,\{H_a, H_b\}\,|\Phi\rangle$ in Eq. (E.1), we are going to need $\langle\Phi|\, D_n\,|\Phi\rangle$ and $\langle\Phi|\, D_a^\dagger D_b\,|\Phi\rangle$. We can simplify the notation for our probe state and rewrite Eq. (E.2) as

$$|\Phi\rangle = \frac{1}{d}\sum_{r,s=0}^{d-1} Z^{-1-r}X^s\,|\psi\rangle\,|rs\rangle\ . \tag{E.20}$$

Thus,

$$\begin{aligned}\langle\Phi|\, D_n\,|\Phi\rangle &= \frac{1}{d^2}\sum_{r',s'=0}^{d-1}\sum_{r,s=0}^{d-1}\langle\psi|\,\langle r's'|\, X^{-s'}Z^{1+r'}D_nZ^{-1-r}X^s\,|\psi\rangle\,|rs\rangle\\ &= \frac{1}{d^2}\sum_{r',s'=0}^{d-1}\sum_{r,s=0}^{d-1}\langle r's'|\, rs\rangle\,\langle\psi|\, X^{-s'}Z^{1+r'}D_nZ^{-1-r}X^s\,|\psi\rangle\\ &= \frac{1}{d^2}\sum_{r',s'=0}^{d-1}\sum_{r,s=0}^{d-1}\delta_{r'r}\delta_{s's}\,\langle\psi|\, X^{-s'}Z^{1+r'}D_nZ^{-1-r}X^s\,|\psi\rangle\\ &= \frac{1}{d^2}\sum_{r,s}\langle\psi|\, X^{-s}Z^{1+r}D_nZ^{-1-r}X^s\,|\psi\rangle\ .\end{aligned} \tag{E.21}$$

But $X^{-s}Z^{1+r}D_nZ^{-1-r}X^s = X^{-s}Z^{1+r}(X^{n_x}Z^{n_z})Z^{-1-r}X^s = X^{n_x}Z^{n_z}\omega^{rn_x}\omega^{sn_z}\omega^{n_x}$.

Thus,

$$\begin{aligned}\langle\Phi|\, D_n\, |\Phi\rangle &= \frac{1}{d^2}\,\langle\psi|\, X^{n_x} Z^{n_z}\, |\psi\rangle\, \omega^{n_x} \sum_r \omega^{r n_x} \sum_s \omega^{s n_z} \\ &= \frac{1}{d^2}\,\langle\psi|\, D_n\, |\psi\rangle\, \omega^{n_x} d^2 \delta_{n_x,0}\delta_{n_z,0} \\ &= \langle\psi|\, D_n\, |\psi\rangle\, \omega^{n_x}\delta_{n_x,0}\delta_{n_z,0}\ . \end{aligned} \tag{E.22}$$

Note that Eq. (E.22) is different to zero only when $n_x = 0$ and $n_z = 0$, in which case $D_n = D_0 = I$. Hence,

$$\langle\Phi|\, D_n\, |\Phi\rangle = \delta_{n,0}\ . \tag{E.23}$$

Also,

$$\begin{aligned} D_a^\dagger D_b &= Z^{-a_z} X^{-a_x} X^{b_x} Z^{b_z} \\ &= Z^{-a_z} X^{b_x - a_x} Z^{b_z} \\ &= \omega^{-a_z(b_x-a_x)} X^{b_x-a_x} Z^{b_z-a_z} \\ &= \omega^{-a_z(b_x-a_x)} D_{b-a}\ . \end{aligned} \tag{E.24}$$

Thus, $\langle\Phi|\, D_a^\dagger D_b\, |\Phi\rangle = \omega^{-a_z(b_x-a_x)}\,\langle\Phi|\, D_{b-a}\, |\Phi\rangle$. Replacing D_{b-a} into (E.23) we obtain

$$\begin{aligned}\langle\Phi|\, D_a^\dagger D_b\, |\Phi\rangle &= \omega^{-a_z(b_x-a_x)}\,\langle\Phi|\, D_{b-a}\, |\Phi\rangle \\ &= \omega^{-a_z(b_x-a_x)}\delta_{a_x,b_x}\delta_{a_z,b_z} \\ &= \delta_{a,b} \end{aligned} \tag{E.25}$$

We can now find each $\langle\Phi|\, H_a\, |\Phi\rangle$. By using Eq. (E.7),

$$\langle\Phi|\, H_{r_f}\, |\Phi\rangle = i \sum_n \left(-\frac{r_f r_n}{r_0} e^{i\phi_n}\,\langle\Phi|\, D_n\, |\Phi\rangle + r_n e^{i(\phi_n-\phi_f)}\,\langle\Phi|\, D_f^\dagger D_n\, |\Phi\rangle \right)\ . \tag{E.26}$$

From Eqs.(E.23) and (E.25) we see that the first term in Eq.(E.26) is non-zero only for $n = 0$, whereas the second term is non-zero only for $n = f$. Therefore,

$$\langle\Phi|\, H_{r_f}\, |\Phi\rangle = -i\frac{r_f r_0}{r_0} + i r_f = 0\ . \tag{E.27}$$

Similarly, using Eq. (E.10) we have

$$\begin{aligned}\langle\Phi|\, H_{r_a}\,|\Phi\rangle &= i\sum_{n\in\mathbb{Z}_d^2} r_n\Big(-2\frac{r_a}{r_0}e^{i\phi_n}\,\langle\Phi|\, D_n\,|\Phi\rangle + e^{i(\phi_n-\phi_a)}\,\langle\Phi|\, D_a^\dagger D_n\,|\Phi\rangle \\ &\qquad + e^{i(\phi_n-\phi_{\ominus a})}\,\langle\Phi|\, D_{\ominus a}^\dagger D_n\,|\Phi\rangle\Big) \\ &= i\left(-2\frac{r_a r_0}{r_0} + r_a + r_{\ominus a}\right) \\ &= 0\,, \end{aligned} \tag{E.28}$$

and using Eq. (E.11) we get

$$\begin{aligned}\langle\Phi|\, H_{\phi_a}\,|\Phi\rangle &= \sum_{n\in\mathbb{Z}_d^2} r_a r_n\left(e^{i(\phi_n-\phi_a)}\,\langle\Phi|\, D_a^\dagger D_n\,|\Phi\rangle - e^{i(\phi_n-\phi_{\ominus a})}\,\langle\Phi|\, D_{\ominus a}^\dagger D_n\,|\Phi\rangle\right) \\ &= r_a^2 - r_a r_{\ominus a} \\ &= 0\,. \end{aligned} \tag{E.29}$$

Now let us determine the expectation values of the form $\langle\Phi|\,\{H_a, H_b\}\,|\Phi\rangle$. From (E.14) and using Eqs.(E.23) and (E.25) we get

$$\begin{aligned}\langle\Phi|\,\{H_{r_f}, H_{r_g}\}\,|\Phi\rangle = 2\frac{r_f r_g}{r_0^2} &- \frac{r_f}{r_0}(e^{i\phi_g}+e^{-i\phi_g})\delta_{g,0} - \frac{r_g}{r_0}(e^{i\phi_f}+e^{-i\phi_f})\delta_{f,0} \\ &+ (e^{i(\phi_g-\phi_f)}+e^{i(\phi_f-\phi_g)})\delta_{f,g}\,. \end{aligned} \tag{E.30}$$

Given the partition (3.3.15), we have $f, g \in S_u$. It follows that $f \neq 0$ and $g \neq 0$, hence the second and third term vanish. Thus,

$$\langle\Phi|\,\{H_{r_f}, H_{r_g}\}\,|\Phi\rangle = 2\frac{r_f r_g}{r_0^2} + 2\delta_{f,g}\,. \tag{E.31}$$

By replacing Eqs. (E.27) and (E.31) into (E.1), we obtain the entries of the first block of $\mathcal{F}$:

$$\mathbf{A}_{f,g} := \mathcal{F}_{r_f r_g} = 4\frac{r_f r_g}{r_0^2} + 4\delta_{f,g}\,. \tag{E.32}$$

In the same way, from Eq. (E.15), we have

$$\begin{aligned}\langle\Phi|\left\{H_{r_f},H_{r_a}\right\}|\Phi\rangle = 4\frac{r_f r_a}{r_0^2} - 2\frac{r_a}{r_0}\left(e^{i\phi_f}+e^{-i\phi_f}\right)\delta_{f,0} \\ - \frac{r_f}{r_0}\left(e^{i\phi_a}\delta_{a,0}+e^{-i\phi_a}\delta_{a,0}+e^{i\phi_{\ominus a}}\delta_{\ominus a,0}+e^{-i\phi_{\ominus a}}\delta_{\ominus a,0}\right) \\ + \left(e^{i(\phi_a-\phi_f)}+e^{i(\phi_f-\phi_a)}\right)\delta_{f,a}+\left(e^{i(\phi_{\ominus a}-\phi_f)}+e^{i(\phi_f-\phi_{\ominus a})}\right)\delta_{f,\ominus a}\,.\end{aligned} \tag{E.33}$$

Notice that all the Kronecker deltas in this equation are null because their indexes belong to different sets of the partition (3.3.15). Thus,

$$\langle\Phi|\left\{H_{r_f},H_{r_a}\right\}|\Phi\rangle = 4\frac{r_f r_a}{r_0^2}\,, \tag{E.34}$$

and we get the second block of $\mathcal{F}$:

$$\mathbf{B}_{f,a} := \mathcal{F}_{r_f r_a} = 8\frac{r_f r_a}{r_0^2}\,. \tag{E.35}$$

From Eq. (E.16), we have

$$\begin{aligned}\langle\Phi|\left\{H_{r_f},H_{\phi_a}\right\}|\Phi\rangle = ir_a\Bigg(\frac{r_f}{r_0}\left(-e^{i\phi_a}\delta_{a,0}+e^{-i\phi_a}\delta_{a,0}+e^{i\phi_{\ominus a}}\delta_{\ominus a,0}-e^{-i\phi_{\ominus a}}\delta_{\ominus a,0}\right) \\ + \left(e^{i(\phi_a-\phi_f)}-e^{i(\phi_f-\phi_a)}\right)\delta_{f,a} \\ + \left(-e^{i(\phi_{\ominus a}-\phi_f)}+e^{i(\phi_f-\phi_{\ominus a})}\right)\delta_{f,\ominus a}\Bigg)\,.\end{aligned} \tag{E.36}$$

Again, the Kronecker deltas are always zero because of the partition, hence

$$\langle\Phi|\left\{H_{r_f},H_{\phi_a}\right\}|\Phi\rangle = 0\,, \tag{E.37}$$

and thus

$$\mathcal{F}_{r_f\phi_a} = 0\,. \tag{E.38}$$

From Eq. (E.17) we have

$$\begin{aligned}\langle\Phi|\left\{H_{r_a},H_{r_b}\right\}|\Phi\rangle = 8\frac{r_a r_b}{r_0^2} &- 2\frac{r_a}{r_0}\left(e^{i\phi_b}\delta_{b,0}+e^{-i\phi_b}\delta_{b,0}+e^{i\phi_{\ominus b}}\delta_{\ominus b,0}+e^{-i\phi_{\ominus b}}\delta_{\ominus b,0}\right)\\ &- 2\frac{r_b}{r_0}\left(e^{i\phi_a}\delta_{a,0}+e^{-i\phi_a}\delta_{a,0}+e^{i\phi_{\ominus a}}\delta_{\ominus a,0}+e^{-i\phi_{\ominus a}}\delta_{\ominus a,0}\right)\\ &+ \left(e^{i(\phi_b-\phi_a)}+e^{i(\phi_a-\phi_b)}\right)\delta_{a,b}+\left(e^{i(\phi_{\ominus b}-\phi_a)}+e^{i(\phi_a-\phi_{\ominus b})}\right)\delta_{a,\ominus b}\\ &+ \left(e^{i(\phi_b-\phi_{\ominus a})}+e^{i(\phi_{\ominus a}-\phi_b)}\right)\delta_{\ominus a,b}\\ &+ \left(e^{i(\phi_{\ominus b}-\phi_{\ominus a})}+e^{i(\phi_{\ominus a}-\phi_{\ominus b})}\right)\delta_{a,b}\ ,\end{aligned} \tag{E.39}$$

Now, the only Kronecker deltas that do not vanish are $\delta_{a,b}$. Thus,

$$\langle\Phi|\left\{H_{r_a},H_{r_b}\right\}|\Phi\rangle = 8\frac{r_a r_b}{r_0^2}+4\delta_{a,b} \tag{E.40}$$

and

$$\mathbf{C}_{a,b} := \mathcal{F}_{r_a r_b} = 16\frac{r_a r_b}{r_0^2}+8\delta_{a,b}\ . \tag{E.41}$$

From Eq. (E.18),

$$\begin{aligned}\langle\Phi|\left\{H_{r_a},H_{\phi_b}\right\}|\Phi\rangle = 2i\frac{r_a r_b}{r_0} &\left(-e^{i\phi_b}\delta_{b,0}+e^{-i\phi_b}\delta_{b,0}+e^{i\phi_{\ominus b}}\delta_{\ominus b,0}-e^{-i\phi_{\ominus b}}\delta_{\ominus b,0}\right)\\ &+ ir_b\Big(e^{i(\phi_b-\phi_a)}\delta_{a,b}-e^{i(\phi_a-\phi_b)}\delta_{a,b}-e^{i(\phi_{\ominus b}-\phi_a)}\delta_{a,\ominus b}\\ &+ e^{i(\phi_a-\phi_{\ominus b})}\delta_{a,\ominus b}+e^{i(\phi_b-\phi_{\ominus a})}\delta_{\ominus a,b}-e^{i(\phi_{\ominus a}-\phi_b)}\delta_{\ominus a,b}\\ &+ e^{i(\phi_{\ominus a}-\phi_{\ominus b})}\delta_{a,b}-e^{i(\phi_{\ominus b}-\phi_{\ominus a})}\delta_{a,b}\Big)\ ,\end{aligned} \tag{E.42}$$

but some Kronecker deltas are null because of the partition, while the terms in $\delta_{a,b}$ cancel out. Thus,

$$\langle\Phi|\left\{H_{r_a},H_{\phi_b}\right\}|\Phi\rangle = 0 \tag{E.43}$$

and

$$\mathcal{F}_{r_a\phi_b} = 0\ . \tag{E.44}$$

Finally, from Eq. (E.19), we have

$$\begin{aligned}\langle\Phi|\left\{H_{\phi_a},H_{\phi_b}\right\}|\Phi\rangle &= r_a r_b\Big(e^{i(\phi_b-\phi_a)}\delta_{a,b}+e^{i(\phi_a-\phi_b)}\delta_{a,b}-e^{i(\phi_{\ominus b}-\phi_a)}\delta_{a,\ominus b}\\ &\quad -e^{i(\phi_a-\phi_{\ominus b})}\delta_{a,\ominus b}-e^{i(\phi_b-\phi_{\ominus a})}\delta_{\ominus a,b}-e^{i(\phi_{\ominus a}-\phi_b)}\delta_{\ominus a,b}\\ &\quad +e^{i(\phi_{\ominus a}-\phi_{\ominus b})}\delta_{a,b}+e^{i(\phi_{\ominus b}-\phi_{\ominus a})}\delta_{a,b}\Big)\\ &= 4r_a r_b\delta_{a,b}\\ &= 4r_a^2\delta_{a,b}\end{aligned} \tag{E.45}$$

and

$$\mathbf{D}_{a,b} := \mathcal{F}_{\phi_a\phi_b} = 8r_a^2\delta_{a,b}\ . \tag{E.46}$$

Summarizing, the quantum Fisher information matrix for estimating a unitary gate close-to-the-identity in dimension even is

$$\mathcal{F}_{even} = \begin{pmatrix}\mathbf{A} & \mathbf{B} & \mathbf{0}\\ \mathbf{B}^T & \mathbf{C} & \mathbf{0}\\ \mathbf{0} & \mathbf{0} & \mathbf{D}\end{pmatrix}\ , \tag{E.47}$$

with $\mathbf{A}$, $\mathbf{B}$, $\mathbf{C}$, and $\mathbf{D}$ being the blocks defined in Eqs. (E.32), (E.35), (E.41) and (E.46), respectively. This matrix corresponds to the block matrix in Eq. (3.3.24).

Appendix F

Calculation of Classical Fisher Information Matrix

The classical Fisher information matrix is given by

$$\mathcal{I}_{ab} = \sum_y \frac{1}{P(y|\mathbf{t})} \left[\frac{\partial P(y|\mathbf{t})}{\partial t_a}\right] \left[\frac{\partial P(y|\mathbf{t})}{\partial t_b}\right] \ . \tag{F.1}$$

We can expand the sum using the partition (3.3.15):

$$\begin{aligned}\mathcal{I}_{ab} = &\frac{1}{P_0} \left[\frac{\partial P_0}{\partial t_a}\right] \left[\frac{\partial P_0}{\partial t_b}\right] + \sum_{h\in S_u} \frac{1}{P_h} \left[\frac{\partial P_h}{\partial t_a}\right] \left[\frac{\partial P_h}{\partial t_b}\right] \\ &+ \sum_{c\in S_+} \left(\frac{1}{P_c} \left[\frac{\partial P_c}{\partial t_a}\right] \left[\frac{\partial P_c}{\partial t_b}\right] + \frac{1}{P_{\ominus c}} \left[\frac{\partial P_{\ominus c}}{\partial t_a}\right] \left[\frac{\partial P_{\ominus c}}{\partial t_b}\right] \right) \ . \end{aligned} \tag{F.2}$$

Deriving the probablities in Eqs. (3.3.20) we get:

$$\frac{\partial P_0}{\partial r_f} = \frac{\partial}{\partial r_f} \left(1 - \sum_{h\in S_s} r_h^2 - 2 \sum_{c\in S_+} r_c^2 \right) = -2r_f \ , \tag{F.3}$$

$$\frac{\partial P_0}{\partial r_a} = \frac{\partial}{\partial r_a} \left(1 - \sum_{h\in S_s} r_h^2 - 2 \sum_{c\in S_+} r_c^2 \right) = -4r_a \ , \tag{F.4}$$

$$\frac{\partial P_0}{\partial \phi_a} = \frac{\partial}{\partial \phi_a}\left(1 - \sum_{h\in S_s} r_h^2 - 2\sum_{c\in S_+} r_c^2\right) = 0\ . \tag{F.5}$$

$$\frac{\partial P_h}{\partial r_f} = \frac{\partial}{\partial r_f} r_h^2 = 2 r_h \delta_{h,f}\ . \tag{F.6}$$

$$\frac{\partial P_h}{\partial r_a} = 0\ . \tag{F.7}$$

$$\frac{\partial P_h}{\partial \phi_a} = 0\ . \tag{F.8}$$

$$\frac{\partial P_c}{\partial r_f} = \frac{\partial}{\partial r_f} r_c^2\,(1+\cos(\Delta_c)) = 0\ . \tag{F.9}$$

$$\frac{\partial P_c}{\partial r_a} = \frac{\partial}{\partial r_a} r_c^2\,(1+\cos(\Delta_c)) = 2 r_c \delta_{a,c}\,(1+\cos(\Delta_c))\ . \tag{F.10}$$

Considering Eq. (3.3.21),

$$\frac{\partial P_c}{\partial \phi_a} = \frac{\partial}{\partial \phi_a} r_c^2\,(1+\cos(\Delta_c)) = -2 r_c^2 \sin(\Delta_c)\delta_{a,c}\ . \tag{F.11}$$

$$\frac{\partial P_{\ominus c}}{\partial r_f} = \frac{\partial}{\partial r_f} r_c^2\,(1-\cos(\Delta_c)) = 0\ . \tag{F.12}$$

$$\frac{\partial P_{\ominus c}}{\partial r_a} = \frac{\partial}{\partial r_a} r_c^2\,(1-\cos(\Delta_c)) = 2 r_c \delta_{a,c}\,(1-\cos(\Delta_c))\ . \tag{F.13}$$

$$\frac{\partial P_{\ominus c}}{\partial \phi_a} = \frac{\partial}{\partial \phi_a} r_c^2\,(1-\cos(\Delta_c)) = 2 r_c^2 \sin(\Delta_c)\delta_{a,c}\ . \tag{F.14}$$

Putting all these derivatives in Eq. (F.2), we can calculate $\mathcal{I}$ by blocks. We have:

$$\begin{aligned}\mathbf{A}_{f,g} &:= \mathcal{I}_{r_f r_g} \\ &= 4\frac{r_f r_g}{r_0^2} + \sum_{h\in S_s} \frac{1}{r_h^2} 4 r_g r_f \delta_{h,f}\delta_{h,g} + 0 \\ &= 4\frac{r_f r_g}{r_0^2} + \frac{1}{r_f^2} 4 r_g r_f \delta_{f,g} \\ &= 4\frac{r_f r_g}{r_0^2} + 4\delta_{f,g}\ . \end{aligned} \tag{F.15}$$

Also,

$$\mathbf{B}_{f,a} := \mathcal{I}_{r_f r_a} = 8\frac{r_f r_a}{r_0^2} + 0 + 0 = 8\frac{r_f r_a}{r_0^2}\ , \tag{F.16}$$

and

$$\mathcal{I}_{r_f \phi_a} = 0 + 0 + 0 = 0\ , \tag{F.17}$$

similarly

$$\begin{aligned}\mathbf{C}_{a,b} &:= \mathcal{I}_{r_a r_b} \\ &= 16\frac{r_a r_b}{r_0^2} + 0 + \sum_{c\in S_+} \left(\frac{1}{r_c^2(1+\cos\Delta_c)} 4 r_c^2 (1+\cos\Delta_c)^2 \delta_{a,c}\delta_{b,c} \right. \\ &\quad \left. + \frac{1}{r_c^2(1-\cos\Delta_c)} 4 r_c^2 (1-\cos\Delta_c)^2 \delta_{a,c}\delta_{b,c} \right) \\ &= 16\frac{r_a r_b}{r_0^2} + \left(4(1+\cos\Delta_a) + 4(1-\cos\Delta_a)\right)\delta_{a,b} \\ &= 16\frac{r_a r_b}{r_0^2} + 8\delta_{a,b}\ , \end{aligned} \tag{F.18}$$

and

$$\begin{aligned}\mathcal{I}_{r_a \phi_b} &= 0 + 0 + \sum_{c\in S_+} \left(\frac{-4}{r_c^2(1+\cos\Delta)} r_c^3 (1+\cos\Delta_c)\sin\Delta_c \delta_{a,c}\delta_{b,c} \right. \\ &\quad \left. + \frac{4}{r_c^2(1-\cos\Delta_c)} r_c^3 (1-\cos\Delta_c)\sin\Delta_c \delta_{a,c}\delta_{b,c} \right) \\ &= \sum_{c\in S_+} \left(-4 r_c \sin\Delta_c + 4 r_c \sin\Delta_c\right)\delta_{a,c}\delta_{b,c} \\ &= 0\ , \end{aligned} \tag{F.19}$$

finally

$$
\begin{aligned}
\mathbf{D}_{a,b} &:= \mathcal{I}_{\phi_a \phi_b} \\
&= 0 + 0 + \sum_{c \in S_+} \left(\frac{4}{r_c^2 (1 + \cos \Delta_c)} r_c^4 \sin^2 \Delta_c \delta_{a,c} \delta_{b,c} \right. \\
&\quad \left. + \frac{4}{r_c^2 (1 - \cos \Delta_c)} r_c^4 \sin^2 \Delta_c \delta_{a,c} \delta_{b,c} \right) \\
&= \sum_{c \in S_+} 4 r_c^2 \sin^2 \Delta_c \delta_{a,c} \delta_{b,c} \left(\frac{1}{1 + \cos \Delta_c} + \frac{1}{1 - \cos \Delta_c} \right) \\
&= \sum_{c \in S_+} 4 r_c^2 \sin^2 \Delta_c \delta_{a,c} \delta_{b,c} \left(\frac{1 - \cos \Delta_c}{1 - \cos^2 \Delta_c} + \frac{1 + \cos \Delta_c}{1 - \cos^2 \Delta_c} \right) \\
&= \sum_{c \in S_+} 8 r_c^2 \delta_{a,c} \delta_{b,c} \\
&= 8 r_a^2 \delta_{a,b} \, .
\end{aligned} \tag{F.20}
$$

Summarizing, we obtained the following classical Fisher information matrix for our procedure:

$$
\mathcal{I} = \begin{pmatrix} \mathbf{A} & \mathbf{B} & \mathbf{0} \\ \mathbf{B}^T & \mathbf{C} & \mathbf{0} \\ \mathbf{0} & \mathbf{0} & \mathbf{D} \end{pmatrix} \, , \tag{F.21}
$$

where each block has the same definition of the corresponding block in the quantum Fisher information matrix in Eq. (E.47).

Appendix G

Comparison of classical and quantum Fisher information matrices slightly away from the identity

G.1 Alternative Parametrization of U: Gell-Mann matrices

In order to compare the classical and quantum Fisher information matrices, we firstly need to guarantee the unitarity of U while mantaining the independence of the parameters. A suitable way to do this is by writing an arbitrary unitary gate as the exponential of a Hermitian operator H:

$$U = \exp(iH) \ . \tag{G.1.1}$$

We can always write H as

$$H = \sum_{j=1}^{d^2-1} \lambda_j T_j \ , \tag{G.1.2}$$

where T_j are the generalized Gell-Mann matrices and λ_j are d^2-1 real parameters (see definition in Ref. [195]).

The set $\{T_j\}$ of the d^2-1 generalized Gell-Mann matrices plus the operator $\sqrt{2/d}\ I$

is a set of d^2 linear operators satisfying the orthogonality relation $Tr[T_i^\dagger T_j] = 2\delta_{i,j}$, with $\delta_{i,j}$ being the Kronecker delta. Hence, this set is an orthogonal basis for the space of d-dimensional linear operators. As a consequence, any operator U can be spanned as:

$$U = \sum_{k=1}^{d^2} u_k^{(GM)} T_k \ , \tag{G.1.3}$$

where $u_k^{(GM)}$ are complex coefficients. In order to relate this expansion with the one in the main text, we will rewrite here Eq. (3.3.1) as:

$$U = \sum_{k=1}^{d^2} u_k^{(WH)} D_k \ , \tag{G.1.4}$$

where $u_k^{(WH)}$ are complex coefficients and D_k are the Weyl-Heisenberg operators.

Notice that every Gell-Mann matrix can also be spaned in the Weyl-Heisenberg basis. We can write

$$T_k = \sum_{j=1}^{d^2} t_j^{(k)} D_j \ , \tag{G.1.5}$$

where the j-th component $t_j^{(k)}$ of the k-th Gell-Mann matrix can be calculated as

$$t_i^{(k)} = \frac{1}{d} Tr[D_i^\dagger T_k] \ . \tag{G.1.6}$$

Let us highlight that now we have two orthogonal bases in the space of d-dimensional operators. Moreover, we know from Eq. (3.3.9) that every unitary transformation is associated to a unitary vector when it is expanded in the Weyl-Heisenberg basis. This is not the case if we use the Gell-Mann basis, as can be easily seen by taking the identity, which in the Gell-Mann basis has a unique component different from zero with value $\sqrt{d/2}$. We would like to normalize Gell-Mann matrices in such a way that any unitary operator is still associated to a unitary vector. To this end, we define the normalized Gell-Mann matrices as

$$\tilde{T}_k = \sqrt{\frac{d}{2}} T_k \ , \tag{G.1.7}$$

whose components in the Weyl-Heisenberg basis are

$$\tilde{t}_i^{(k)} = \frac{1}{d} Tr[D_i^\dagger \tilde{T}_k] = \sqrt{\frac{d}{2}} t_i^{(k)} \ . \tag{G.1.8}$$

These components define the vectors of an alternative orthonormal basis in a d^2-dimensional vector space. Indeed, let us calculate the inner product of the k-th vector by the j-th vector:

$$\begin{aligned}
\sum_i \tilde{t}_i^{(k)} \cdot \tilde{t}_i^{(j)*} &= \sum_i \frac{1}{d^2} \cdot Tr[D_i^\dagger \tilde{T}_k] \cdot Tr[D_i^\dagger \tilde{T}_j]^* \\
&= \sum_i \frac{1}{d^2} \cdot \frac{d}{2} \cdot Tr[D_i^\dagger T_k] \cdot Tr[D_i^\dagger T_j]^* \\
&= \frac{1}{2d} \sum_{i,m,n} \langle m|D_i^\dagger T_k|m\rangle \langle n|D_i^\dagger T_j|n\rangle^* \\
&= \frac{1}{2d} \sum_{i,m,n} \langle m|D_i^\dagger T_k|m\rangle \langle n|T_j^\dagger D_i|n\rangle \\
&= \frac{1}{2d} \sum_{i,m,n} \langle n|T_j^\dagger D_i|n\rangle \langle m|D_i^\dagger T_k|m\rangle \\
&= \frac{1}{2d} \sum_{m,n} \langle n|T_j^\dagger \sum_i \left(D_i|n\rangle\langle m|D_i^\dagger \right) T_k|m\rangle \ .
\end{aligned} \tag{G.1.9}$$

But notice that

$$\begin{aligned}
\sum_i \left(D_i|n\rangle\langle m|D_i^\dagger \right) &= \sum_{i_x,i_z} \left(X^{i_x} Z^{i_z}|n\rangle\langle m|Z^{-i_z} X^{-i_x} \right) \\
&= \sum_{i_x,i_z} \omega^{i_z(n-m)} |n \oplus i_x\rangle\langle m \oplus i_x| \\
&= \sum_{i_x} d \cdot \delta_{m,n} |n \oplus i_x\rangle\langle m \oplus i_x| \ .
\end{aligned} \tag{G.1.10}$$

Then,

$$\begin{aligned}\sum_i \tilde{t}_i^{(k)} \cdot \tilde{t}_i^{(j)*} &= \frac{1}{2d} \sum_{m,n,i_x} d \cdot \delta_{m,n} \langle n|T_j^\dagger|n \oplus i_x\rangle\langle m \oplus i_x|T_k|m\rangle \\ &= \frac{1}{2} \sum_m \langle m|T_j^\dagger \sum_{i_x} \left(|m \oplus i_x\rangle\langle m \oplus i_x|\right) T_k|m\rangle \\ &= \frac{1}{2} \sum_m \langle m|T_j^\dagger T_k|m\rangle \\ &= \frac{1}{2} \cdot Tr[T_j^\dagger T_k] \\ &= \frac{1}{2} \cdot 2\delta_{j,k} \\ &= \delta_{j,k} \ . \end{aligned} \tag{G.1.11}$$

In the next subsection, we will use $\{\tilde{t}^{(k)}\}$ as the measurement basis for the control system in our circuit.

G.2 Estimating the parameteres of U (first order)

Let us consider an arbitrary unitary transformation U close to the identity. If we expand Eq. (G.1.1) to first order, we get

$$U \approx I + iH \ . \tag{G.2.1}$$

Using Eq. (G.1.2),

$$U \approx I + i \sum_{j=1}^{d^2-1} \lambda_j T_j \ . \tag{G.2.2}$$

Considering the normalized Gell-Mann matrices, we have

$$U \approx I + i\sqrt{\frac{2}{d}} \sum_{j=1}^{d^2-1} \lambda_j \tilde{T}_j \ , \tag{G.2.3}$$

and we can rewrite Eq. (G.1.3) as

$$\begin{aligned} U &= \sqrt{\frac{2}{d}} \sum_{k=1}^{d^2} u_k^{(GM)} \tilde{T}_k \\ &= \sum_{k=1}^{d^2} \tilde{u}_k^{(GM)} \tilde{T}_k \ , \end{aligned} \tag{G.2.4}$$

with $\tilde{u}_k^{(GM)} = \sqrt{2/d} \cdot u_k^{(GM)}$ being the components of the unitary vector representing U in the normalized Gell-Mann basis. Thus, we have:

$$\tilde{u}_0^{(GM)} \approx 1 \ , \tag{G.2.5}$$

$$\tilde{u}_j^{(GM)} \approx i\sqrt{\frac{2}{d}} \lambda_j \ , \text{ for } 1 \leq j \leq d^2 - 1 \ . \tag{G.2.6}$$

Now let us consider again our circuit. By measuring the final state of the control system in the basis induced by the normalized Gell-Mann matrices, we get outcome probabilities

$$p_0 = |\tilde{u}_0^{(GM)}|^2 \approx 1 \ , \tag{G.2.7}$$

$$p_j = |\tilde{u}_j^{(GM)}|^2 \approx \frac{2\lambda_j^2}{d} \ , \text{ for } 1 \leq j \leq d^2 - 1 \ , \tag{G.2.8}$$

from where we get an estimation of the parameters. Assuming $\lambda_j \geq 0$, we have

$$\lambda_j \approx \sqrt{\frac{d \cdot p_j}{2}} \ . \tag{G.2.9}$$

Now we can use this estimator to assess the quality of the approximation when we go slightly away from the identity, and also compare numerically the classical and quantum Fisher information matrices.

G.3 Quality of the estimation

We assessed numerically the accuracy of the parameter estimation using Eq. (G.2.9). For each dimension $d = 2, 3, 4$ and 5 we created 10000 random unitary transformations close to the identity. Hamiltonian parameters were chosen randomly within a variable range up to $[0, 0.1]$, in such a way that we could scan

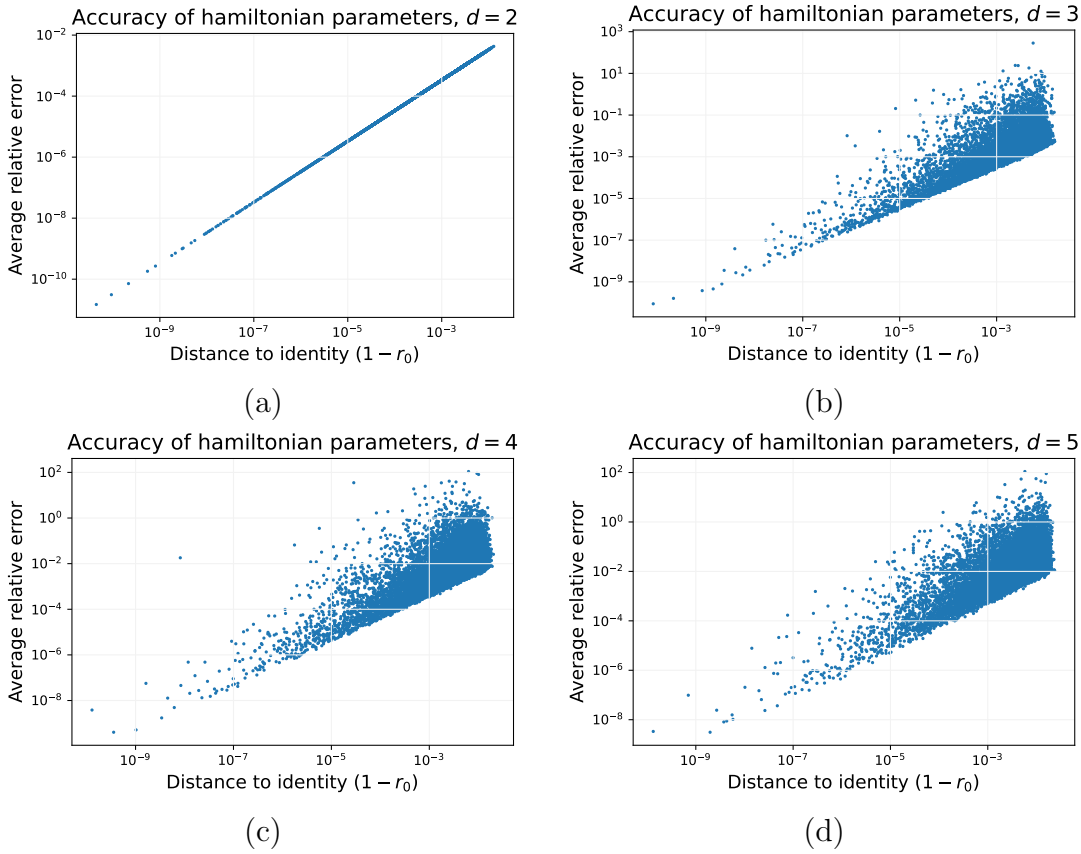

Figure G.3.1: Average relative error of estimated Hamiltonian parameters using first order approximation. Figures (a), (b), (c) and (d) show unitary transformations close to the identity in dimensions 2, 3, 4 and 5, respectively.

different distances to the identity. Although it is not properly a distance, we used $1 - r_0$ as a measure of how close is U to the identity operator, with r_0 being the component of U in the Weyl-Heisenberg basis as in the main text (we also tried with the trace distance, obtaining equivalent results). For each unitary transformation, we estimated the parameters in the asymptotic limit using Eq. (G.2.9). The average relative error of the estimated parameters for each unitary is shown in Fig. G.3.1. As expected, the accuracy of the estimation gets worse as U is further from the identity. For dimensions 3, 4 and 5 the approximation leads to an average relative error easily surpassing 1% when $1 - r_0 > 1 \times 10^{-3}$, i.e. for $r_0 < 0.999$. For dimension $d = 2$, the average relative error remains below 1% in the range of parameters considered.

G.4 Classical and quantum Fisher Information comparison

For the same unitaries as the previous section, we numerically calculated the quantum Fisher information matrix respect to the Hamiltonian parameters and the classical Fisher information matrix for two different measurement schemes: 1) when the control system of our circuit is measured in the computational basis (corresponding to the Weyl-Heisenberg basis in the space of linear operators) and 2) in the basis induced by the normalized Gell-Mann matrices. We used the trace distance between the quantum an classical Fisher information matrices as figure of merit. Fig G.4.1 shows that for dimensions 3, 4 and 5 the classical Fisher information matrix is closer to the quantum Fisher information matrix when the control system is measured in the basis induced by Gell-Mann matrices. Moreover, this distance approaches to zero as U approaches the identity, while the distance between the classical Fisher information using the computational basis and quantum Fisher information matrices remains constant when U approaches to identity. In the case of dimension $d = 2$, where both bases are the same, the trace distance achieves lower values than in higher dimensions.

G.5 Far from the identity

The estimation of parameters performed above only considers a first order approximation of U around the identity. It would be interesting to go beyond this approximation to estimate parameters far from the identity. For example, we could approximate U to second order and calculate the Hamiltonian parameters from the outcome probabilities by using equations similar to Eq. (G.2.9). However, we could not find neither analytical nor numerical solutions for the nonlinear equations system not even in dimension $d = 3$. An alternative approach consists in having a good guess for the unitary gate (let us call it $\tilde{U}$) and expand U to first order around $\tilde{U}$. However, this approach is not straightforward, since it involves derivatives of operators which do not necessarily commute. Finally, it would be interesting to explore different parametrizations for unitary operators, what we let for future work.

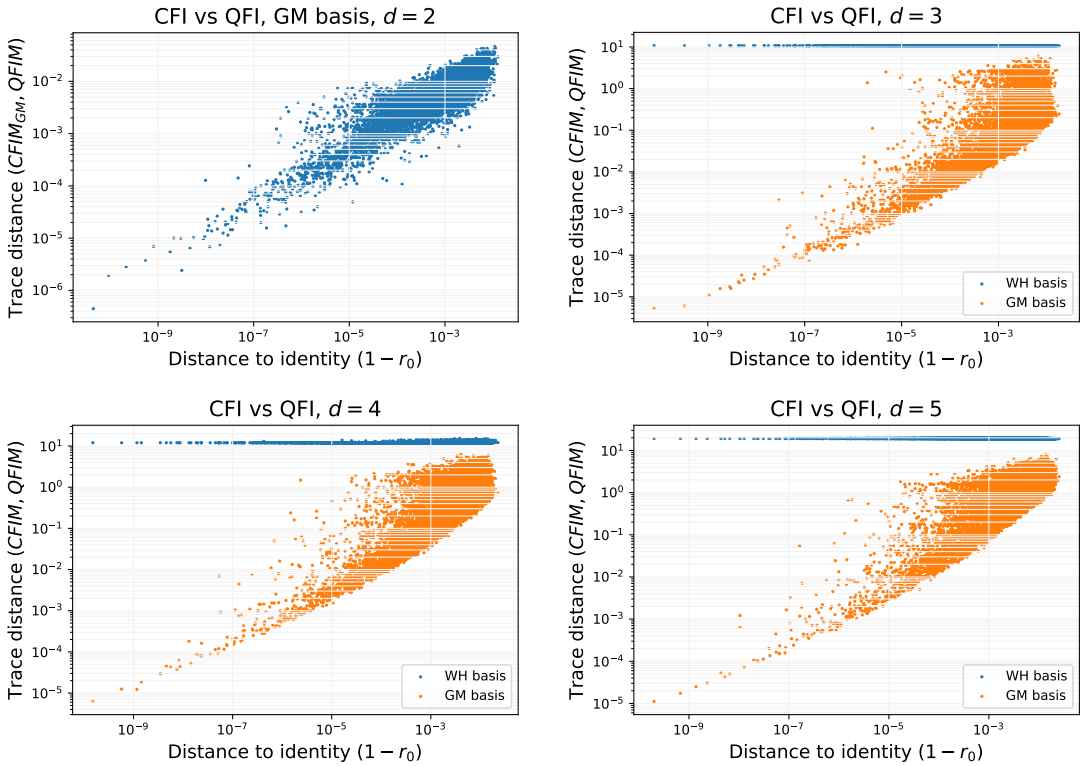

Figure G.4.1: Trace distance between classical Fisher information (CFI) and quantum Fisher information (QFI) matrices. For dimension 3, 4 and 5, classical Fisher information is computed from probabilities obtained by measuring the control system in two different bases: the computational basis (WH, blue dots) and the basis induced by normalized Gell-Mann matrices (GM, orange dots). For dimension $d = 2$ both bases are exactly the same.

Appendix H

Process matrix representation of a quantum channel

Let $\mathcal{H}$ be a d-dimensional Hilbert space, $\mathcal{L}(\mathcal{H})$ the space of linear operators on $\mathcal{H}$ and $\mathcal{E} : \mathcal{L}(\mathcal{H}) \to \mathcal{L}(\mathcal{H})$ an arbitrary quantum channel (or CPTP linear map). The action of $\mathcal{E}$ on an input state ρ can be written in the Kraus representation [179, 185] as

$$\mathcal{E}(\rho) = \sum_i E_i \rho E_i^\dagger \ , \tag{H.1}$$

where the E_i are linear operators on $\mathcal{H}$ satisfying the completeness relation

$$\sum_i E_i^\dagger E_i = I \ , \tag{H.2}$$

with I the identity operator.

An alternative representation of a quantum channel is known as the *process matrix* or *chi matrix* representation [163]. Given a basis $\mathcal{B} = \{\tilde{E}_j\}_{j=1}^{d^2}$ for the space $\mathcal{L}(\mathcal{H})$ of linear operators on $\mathcal{H}$, the Kraus operators can be spanned as the linear combination

$$E_i = \sum_j e_{ij} \tilde{E}_j \ , \tag{H.3}$$

where e_{ij} are complex coefficients. Then, the action of the channel can be written

as

$$\begin{aligned}\mathcal{E}(\rho) &= \sum_i \Big(\sum_j e_{ij}\tilde{E}_j \Big) \rho \Big(\sum_k e_{ik}^* \tilde{E}_k^\dagger \Big) \\ &= \sum_{jk} \Big(\sum_i e_{ij} e_{ik}^* \Big) \tilde{E}_j \rho \tilde{E}_k^\dagger \\ &= \sum_{jk} \chi_{jk} \tilde{E}_j \rho \tilde{E}_k^\dagger \, , \end{aligned} \tag{H.4}$$

where

$$\chi_{jk} := \sum_i e_{ij} e_{ik}^* \tag{H.5}$$

are the elements of a $d^2 \times d^2$ matrix χ. Thus, χ completely describes the action of $\mathcal{E}$ provided a basis for $\mathcal{L}(\mathcal{H})$.

The matrix χ becomes a particularly interesting representation of a quantum channel when the operators $\tilde{E}_j \in \mathcal{B}$ satisfy the orthogonality relation

$$Tr[\tilde{E}_j{}^\dagger \tilde{E}_k] = d\delta_{jk} \, , \tag{H.6}$$

where $\langle A, B \rangle = Tr[A^\dagger B]$ is the Hilbert-Schmidt inner product of A and B on $\mathcal{L}(\mathcal{H})$. Indeed, in that case χ is a density matrix since it has the following properties:

1. *Positive semi-definite:*

   If we consider an orthonormal basis $\{|j\rangle\}$ for a d^2-dimensional space, then we can write χ as:

$$\begin{aligned}\chi &= \sum_{jk} \chi_{jk} |j\rangle\langle k| \\ &= \sum_{ijk} e_{ij} e_{ik}^* |j\rangle\langle k| \\ &= \sum_i \Big(\sum_j e_{ij} \, |j\rangle \Big) \Big(\sum_k \langle k| \, e_{ik}^* \Big) \\ &= \sum_i |e_i\rangle\langle e_i| \, , \end{aligned} \tag{H.7}$$

   with

$$|e_i\rangle := \sum_j e_{ij} \, |j\rangle \ . \tag{H.8}$$

Therefore, given an arbitrary d^2-dimensional state $|\psi\rangle$, we have:

$$\begin{aligned}\langle\psi|\,\chi\,|\psi\rangle &= \sum_i \langle\psi|\,e_i\rangle\langle e_i\,|\psi\rangle \\ &= \sum_i |\,\langle e_i|\,\psi\rangle|^2 \\ &\geq 0\,. \end{aligned} \tag{H.9}$$

2. *Unitary trace:*

We have

$$\begin{aligned} Tr[\chi] &= \sum_n \langle n|\,\chi\,|n\rangle \\ &= \sum_{ijkn} e_{ij}e_{ik}^*\langle n|j\rangle\langle k|n\rangle \\ &= \sum_{ijkn} e_{ij}e_{ik}^*\delta_{nj}\delta_{kn} \\ &= \sum_{in} e_{in}e_{in}^* \\ &= \sum_{in} |e_{in}|^2\,. \end{aligned} \tag{H.10}$$

But from the completeness relation of the Kraus operators,

$$\begin{aligned} &\sum_i E_i^\dagger E_i = I \\ \Rightarrow\ &\sum_i\sum_j e_{ij}^*\tilde{E}_j^\dagger \sum_k e_{ik}\tilde{E}_k = I \\ \Rightarrow\ &\sum_{ijk} e_{ij}^* e_{ik}\tilde{E}_j^\dagger\tilde{E}_k = I\,. \end{aligned} \tag{H.11}$$

Tracing both sides of the equation we get:

$$\begin{aligned} \Rightarrow\ & Tr\left[\sum_{ijk} e_{ij}^* e_{ik}\tilde{E}_j^\dagger\tilde{E}_k\right] = Tr\big[I\big] \\ \Rightarrow\ &\sum_{ijk} e_{ij}^* e_{ik} Tr[\tilde{E}_j^\dagger\tilde{E}_k] = d\,. \end{aligned} \tag{H.12}$$

Using the relation (H.6), we have

$$\begin{aligned} & \sum_{ijk} e_{ij}^* e_{ik} d\delta_{jk} = d \\ \Rightarrow \quad & \sum_{ij} e_{ij}^* e_{ij} = 1 \\ \Rightarrow \quad & \sum_{ij} |e_{ij}|^2 = 1 \ , \end{aligned} \tag{H.13}$$

and replacing in Eq. (H.10), we get

$$Tr[\chi] = 1 \ . \tag{H.14}$$

Thus, when the elements of B satisfy Eq. (H.6), χ is a density matrix. Consequently, any quantum channel $\mathcal{E}$ acting on a d-dimensional space $\mathcal{H}$ can be represented by a quantum state χ of dimension d^2.

Notice that χ can be used to obtain back a set of Kraus operators for $\mathcal{E}$. Indeed, if the elements of $\mathcal{B}$ satisfy Eq. (H.6), then we can choose the basis $|j\rangle = \left|\tilde{E}_j\right\rangle$ where the ket $|A\rangle$ denotes a vector with the same coefficients of the operator A in the basis $\mathcal{B}$. Hence, in Eq. (H.8) $|e_i\rangle = |E_i\rangle$, and therefore Eq. (H.7) shows a direct relation between the Kraus operators and an ensemble of quantum states leading to χ. It is known that the Kraus representation of a quantum channel is not unique; here we see that any ensemble compatible with χ is related to a Kraus representation of $\mathcal{E}$.

Appendix I

Derivation of the output state of our circuit for an arbitrary quantum channel

Here we describe and calculate the evolution of an input state ρ_{in} going through the circuit in Fig. 3.4.1. The circuit consists in one target and two control qudits initialized in the state

$$\rho_{in} = \rho_0 \otimes |0\rangle\langle 0|_1 \otimes |0\rangle\langle 0|_2 \,, \tag{I.1}$$

where ρ_0 is an arbitrary initial state for the target qudit. Firstly, Fourier transforms

$$F = \frac{1}{\sqrt{d}} \sum_{j,k=0}^{d-1} \omega^{jk} |j\rangle\langle k| \tag{I.2}$$

act on the control qudits, letting them in a maximally coherent state. Then, controlled operations $X_{02}^{(0)}$ and $Z_{01}^{\dagger(1)}$ are applied creating entanglement between the target and control systems. These controlled operations are particular cases of what we call *controlled operators with shifted control*, which are generally defined as

$$V_{tc}^{(i)} := \sum_{k=0}^{d-1} V_t^k \otimes |k \ominus i\rangle_c\langle k \ominus i| \,. \tag{I.3}$$

In particular,

$$X_{02}^{(0)} = \sum_{k=0}^{d-1} X_0^k \otimes |k\rangle_2\langle k| \,, \tag{I.4}$$

$$Z_{01}^{\dagger(1)} = \sum_{k=0}^{d-1} (Z_0^\dagger)^k \otimes |k \ominus 1\rangle_1\langle k \ominus 1| = \sum_{k=0}^{d-1} Z_0^{-k-1} \otimes |k\rangle_1\langle k| \,. \tag{I.5}$$

Then, an arbitrary quantum channel

$$\mathcal{E}(\rho) = \sum_i E_i \rho E_i^\dagger \tag{I.6}$$

is applied on the target system followed by controlled operations

$$Z_{01}^{(0)} = \sum_{k=0}^{d-1} Z_0^k \otimes |k\rangle_1\langle k| \,, \tag{I.7}$$

$$X_{02}^{\dagger(1)} = \sum_{k=0}^{d-1} (X_0^\dagger)^k \otimes |k \ominus 1\rangle_2\langle k \ominus 1| = \sum_{k=0}^{d-1} X_0^{-k-1} \otimes |k\rangle_2\langle k| \,. \tag{I.8}$$

Inverse Fourier transforms act on the control qudits bringing them back to the computational basis. At this point, the joint state of the system may remain entangled, so new controlled operations

$$X_{01}^{\dagger(-1)} = \sum_{k=0}^{d-1} (X_0^\dagger)^k \otimes |k \oplus 1\rangle_1\langle k \oplus 1| = \sum_{k=0}^{d-1} X_0^{-k+1} \otimes |k\rangle_1\langle k| \,, \tag{I.9}$$

$$Z_{02}^{\dagger(0)} = \sum_{k=0}^{d-1} Z_0^{-k} \otimes |k\rangle_2\langle k| \tag{I.10}$$

are implemented in order to separate the target from the control. Finally an X gate is conveniently applied to the second control qudit for pairing the coefficients that characterize the quantum channel with the computational basis of the control register.

Now let us calculate the output of the circuit. Firstly, notice that the evolution of the joint system before the application of $\mathcal{E}$ is unitary. Hence, we can group the operations preceding $\mathcal{E}$ as

$$V = (Z_{01}^{\dagger(1)} \otimes I_2)(X_{02}^{(0)} \otimes I_1)(I_0 \otimes F_1 \otimes F_2) \,. \tag{I.11}$$

Similarly, we can group the unitary operations applied after $\mathcal{E}$ in the gate

$$W = (I_0 \otimes I_1 \otimes X_2)(Z_{02}^{\dagger(0)} \otimes I_1)(X_{01}^{\dagger(-1)} \otimes I_2)(I_0 \otimes F_1^\dagger \otimes F_2^\dagger)(X_{02}^{\dagger(1)} \otimes I_1)(Z_{01}^{(0)} \otimes I_2) \ . \tag{I.12}$$

Thus, the action of the circuit can be written shortly as

$$\rho_{out} = \sum_i W E_i V \rho_{in} V^\dagger E_i^\dagger W^\dagger \ , \tag{I.13}$$

or

$$\rho_{out} = \sum_i K_i \rho_{in} K_i^\dagger \ , \tag{I.14}$$

with

$$K_i = W E_i V \ . \tag{I.15}$$

In other words, we can consider our circuit as transforming a d-dimensional quantum channel with Kraus operators E_i into a d^3-dimensional quantum channel with Kraus operators $K_i = W E_i V$.

Let us calculate the Kraus operators K_i of the resulting channel. Firstly, we have

$$I_0 \otimes F_1 \otimes F_2 = \frac{1}{d} \sum_{j_1,j_2,k_1,k_2=0}^{d-1} \omega^{j_1 k_1} \omega^{j_2 k_2} I_0 \otimes |j_1\rangle\langle k_1|_1 \otimes |j_2\rangle\langle k_2|_2 \ . \tag{I.16}$$

Then,

$$\begin{aligned} &(X_{02}^{(0)} \otimes I_1)(I_0 \otimes F_1 \otimes F_2) = \\ &= \frac{1}{d} \sum_{j_1,j_2,k_1,k_2=0}^{d-1} \omega^{j_1 k_1} \omega^{j_2 k_2} \sum_{k=0}^{d-1} X_0^k \otimes |j_1\rangle\langle k_1|_1 \otimes |k\rangle \langle k|j_2\rangle \langle k_2|_2 \\ &= \frac{1}{d} \sum_{j_1,j_2,k_1,k_2=0}^{d-1} \omega^{j_1 k_1} \omega^{j_2 k_2} X_0^{j_2} \otimes |j_1\rangle\langle k_1|_1 \otimes |j_2\rangle \langle k_2|_2 \end{aligned} \tag{I.17}$$

and V becomes

$$\begin{aligned} V &= (Z_{01}^{\dagger(1)} \otimes I_2)(X_{02}^{(0)} \otimes I_1)(I_0 \otimes F_1 \otimes F_2) \\ &= \frac{1}{d} \sum_{j_1,j_2,k_1,k_2=0}^{d-1} \omega^{j_1 k_1} \omega^{j_2 k_2} \sum_{k=0}^{d-1} Z_0^{-k-1} X_0^{j_2} \otimes |k\rangle \langle k|j_1\rangle \langle k_1|_1 \otimes |j_2\rangle \langle k_2|_2 \end{aligned}$$

$$= \frac{1}{d} \sum_{j_1,j_2,k_1,k_2=0}^{d-1} \omega^{j_1 k_1} \omega^{j_2 k_2} Z_0^{-j_1-1} X_0^{j_2} \otimes |j_1\rangle \langle k_1|_1 \otimes |j_2\rangle \langle k_2|_2$$

$$= \frac{1}{d} \sum_{j_1,j_2,k_1,k_2=0}^{d-1} \omega^{j_1 k_1} \omega^{j_2 k_2} \omega^{-j_2(j_1+1)} X_0^{j_2} Z_0^{-j_1-1} \otimes |j_1\rangle \langle k_1|_1 \otimes |j_2\rangle \langle k_2|_2 \quad \text{(I.18)}$$

Expanding the Kraus operators of $\mathcal{E}$ in the Weyl-Heisenberg basis as

$$E_i = \sum_{n \in \mathbb{Z}_d^2} e_{in} X_0^{n_x} Z_0^{n_z} \ , \quad \text{(I.19)}$$

we have

$$\begin{aligned} E_i V &= \frac{1}{d} \sum_{n \in \mathbb{Z}_d^2} e_{in} \sum_{j_1,j_2,k_1,k_2=0}^{d-1} \omega^{j_1 k_1} \omega^{j_2 k_2} \omega^{-j_2(j_1+1)} X_0^{n_x} Z_0^{n_z} X_0^{j_2} Z_0^{-j_1-1} \\ &\quad \otimes |j_1\rangle\langle k_1|_1 \otimes |j_2\rangle\langle k_2|_2 \\ &= \frac{1}{d} \sum_{n \in \mathbb{Z}_d^2} e_{in} \sum_{j_1,j_2,k_1,k_2=0}^{d-1} \omega^{j_1 k_1} \omega^{j_2 k_2} \omega^{-j_2(j_1+1)} \omega^{j_2 n_z} X_0^{n_x+j_2} Z_0^{n_z-j_1-1} \\ &\quad \otimes |j_1\rangle\langle k_1|_1 \otimes |j_2\rangle\langle k_2|_2 \ . \end{aligned} \quad \text{(I.20)}$$

Following with the operations of W, we get

$$\begin{aligned} &(Z_{01}^{(0)} \otimes I_2) E_i V = \\ &= \frac{1}{d} \sum_{n \in \mathbb{Z}_d^2} e_{in} \sum_{j_1,j_2,k_1,k_2=0}^{d-1} \omega^{j_1 k_1} \omega^{j_2 k_2} \omega^{-j_2(j_1+1)} \omega^{j_2 n_z} \sum_{k=0}^{d-1} Z_0^k X_0^{n_x+j_2} Z_0^{n_z-j_1-1} \\ &\quad \otimes |k\rangle \langle k|j_1\rangle \langle k_1|_1 \otimes |j_2\rangle \langle k_2|_2 \\ &= \frac{1}{d} \sum_{n \in \mathbb{Z}_d^2} e_{in} \sum_{j_1,j_2,k_1,k_2=0}^{d-1} \omega^{j_1 k_1} \omega^{j_2 k_2} \omega^{-j_2(j_1+1)} \omega^{j_2 n_z} Z_0^{j_1} X_0^{n_x+j_2} Z_0^{n_z-j_1-1} \\ &\quad \otimes |j_1\rangle \langle k_1|_1 \otimes |j_2\rangle \langle k_2|_2 \\ &= \frac{1}{d} \sum_{n \in \mathbb{Z}_d^2} e_{in} \sum_{j_1,j_2,k_1,k_2=0}^{d-1} \omega^{j_1 k_1} \omega^{j_2 k_2} \omega^{-j_2(j_1+1)} \omega^{j_2 n_z} \omega^{j_1(n_x+j_2)} X_0^{n_x+j_2} Z_0^{n_z-1} \\ &\quad \otimes |j_1\rangle \langle k_1|_1 \otimes |j_2\rangle \langle k_2|_2 \end{aligned}$$

$$= \frac{1}{d} \sum_{n \in \mathbb{Z}_d^2} e_{in} \sum_{j_1,j_2,k_1,k_2=0}^{d-1} \omega^{j_1(k_1+n_x)} \omega^{j_2(k_2-1+n_z)} X_0^{n_x+j_2} Z_0^{n_z-1} \otimes |j_1\rangle \langle k_1|_1 \otimes |j_2\rangle \langle k_2|_2 \ . \tag{I.21}$$

Then,

$$\begin{aligned}
&(X_{02}^{\dagger(1)} \otimes I_1)(Z_{01}^{(0)} \otimes I_2) E_i V = \\
&= \frac{1}{d} \sum_{n \in \mathbb{Z}_d^2} e_{in} \sum_{j_1,j_2,k_1,k_2=0}^{d-1} \omega^{j_1(k_1+n_x)} \omega^{j_2(k_2-1+n_z)} \sum_{k=0}^{d-1} X_0^{-k-1} X_0^{n_x+j_2} Z_0^{n_z-1} \\
&\quad \otimes |j_1\rangle \langle k_1|_1 \otimes |k\rangle \langle k|j_2\rangle \langle k_2|_2 \\
&= \frac{1}{d} \sum_{n \in \mathbb{Z}_d^2} e_{in} \sum_{j_1,j_2,k_1,k_2=0}^{d-1} \omega^{j_1(k_1+n_x)} \omega^{j_2(k_2-1+n_z)} X_0^{-j_2-1} X_0^{n_x+j_2} Z_0^{n_z-1} \\
&\quad \otimes |j_1\rangle \langle k_1|_1 \otimes |j_2\rangle \langle k_2|_2 \\
&= \frac{1}{d} \sum_{n \in \mathbb{Z}_d^2} e_{in} \sum_{j_1,j_2,k_1,k_2=0}^{d-1} \omega^{j_1(k_1+n_x)} \omega^{j_2(k_2-1+n_z)} X_0^{n_x-1} Z_0^{n_z-1} \otimes |j_1\rangle \langle k_1|_1 \otimes |j_2\rangle \langle k_2|_2 \ .
\end{aligned} \tag{I.22}$$

Reordering the sums and noticing that

$$F |k \oplus n\rangle = \frac{1}{\sqrt{d}} \sum_{j=0}^{d-1} \omega^{j(k+n)} |j\rangle \ , \tag{I.23}$$

we can write

$$\begin{aligned}
&(X_{02}^{\dagger(1)} \otimes I_1)(Z_{01}^{(0)} \otimes I_2) E_i V = \\
&= \sum_{n \in \mathbb{Z}_d^2} e_{in} X_0^{n_x-1} Z_0^{n_z-1} \otimes \left(\frac{1}{\sqrt{d}} \sum_{j_1,k_1=0}^{d-1} \omega^{j_1(k_1+n_x)} |j_1\rangle \langle k_1|_1 \right) \\
&\quad \otimes \left(\frac{1}{\sqrt{d}} \sum_{j_2,k_2=0}^{d-1} \omega^{j_2(k_2-1+n_z)} |j_2\rangle \langle k_2|_2 \right) \\
&= \sum_{n \in \mathbb{Z}_d^2} e_{in} X_0^{n_x-1} Z_0^{n_z-1} \otimes \sum_{k_1=0}^{d-1} F |k_1 \oplus n_x\rangle \langle k_1|_1 \otimes \sum_{k_2=0}^{d-1} F |k_2 \oplus n_z \ominus 1\rangle \langle k_2|_2 \ .
\end{aligned} \tag{I.24}$$

Applying the Fourier inverse on the control qudits,

$$
\begin{aligned}
&(I_0 \otimes F_1^\dagger \otimes F_2^\dagger)(X_{02}^{\dagger(1)} \otimes I_1)(Z_{01}^{(0)} \otimes I_2)E_i V = \\
&= \sum_{n\in\mathbb{Z}_d^2} \sum_{k_1,k_2=0}^{d-1} e_{in} X_0^{n_x-1} Z_0^{n_z-1} \otimes |k_1 \oplus n_x\rangle \langle k_1|_1 \otimes |k_2 \oplus n_z \ominus 1\rangle \langle k_2|_2 \ . \qquad \text{(I.25)}
\end{aligned}
$$

It follows that

$$
\begin{aligned}
&(X_{01}^{\dagger(-1)} \otimes I_2)(I_0 \otimes F_1^\dagger \otimes F_2^\dagger)(X_{02}^{\dagger(1)} \otimes I_1)(Z_{01}^{(0)} \otimes I_2)E_i V = \\
&= \sum_{n\in\mathbb{Z}_d^2} \sum_{k_1,k_2=0}^{d-1} \sum_{k=0}^{d-1} e_{in} X_0^{-k+1} X_0^{n_x-1} Z_0^{n_z-1} \\
&\quad \otimes |k\rangle \langle k|k_1 \oplus n_x\rangle \langle k_1|_1 \otimes |k_2 \oplus n_z \ominus 1\rangle \langle k_2|_2 \\
&= \sum_{n\in\mathbb{Z}_d^2} \sum_{k_1,k_2=0}^{d-1} e_{in} X_0^{-k_1} Z_0^{n_z-1} \otimes |k_1 \oplus n_x\rangle \langle k_1|_1 \otimes |k_2 \oplus n_z \ominus 1\rangle \langle k_2|_2 \ , \qquad \text{(I.26)}
\end{aligned}
$$

then

$$
\begin{aligned}
&(Z_{02}^{\dagger(0)} \otimes I_1)(X_{01}^{\dagger(-1)} \otimes I_2)(I_0 \otimes F_1^\dagger \otimes F_2^\dagger)(X_{02}^{\dagger(1)} \otimes I_1)(Z_{01}^{(0)} \otimes I_2)E_i V = \\
&= \sum_{n\in\mathbb{Z}_d^2} \sum_{k_1,k_2=0}^{d-1} \sum_{k=0}^{d-1} e_{in} Z_0^{-k} X_0^{-k_1} Z_0^{n_z-1} \otimes |k_1 \oplus n_x\rangle \langle k_1|_1 \otimes |k\rangle \langle k|k_2 \oplus n_z \ominus 1\rangle \langle k_2|_2 \\
&= \sum_{n\in\mathbb{Z}_d^2} \sum_{k_1,k_2=0}^{d-1} e_{in} Z_0^{-k_2-n_z+1} X_0^{-k_1} Z_0^{n_z-1} \otimes |k_1 \oplus n_x\rangle \langle k_1|_1 \otimes |k_2 \oplus n_z \ominus 1\rangle \langle k_2|_2 \\
&= \sum_{n\in\mathbb{Z}_d^2} \sum_{k_1,k_2=0}^{d-1} e_{in} \omega^{k_1(k_2+n_z-1)} X_0^{-k_1} Z_0^{-k_2} \otimes |k_1 \oplus n_x\rangle \langle k_1|_1 \otimes |k_2 \oplus n_z \ominus 1\rangle \langle k_2|_2 \ ,
\end{aligned}
\qquad \text{(I.27)}
$$

and finally

$$
\begin{aligned}
K_i &= (I_0 \otimes I_1 \otimes X_2)(Z_{02}^{\dagger(0)} \otimes I_1)(X_{01}^{\dagger(-1)} \otimes I_2)(I_0 \otimes F_1^\dagger \otimes F_2^\dagger)(X_{02}^{\dagger(1)} \otimes I_1) \\
&\quad \cdot (Z_{01}^{(0)} \otimes I_2)E_i V \\
&= \sum_{n\in\mathbb{Z}_d^2} \sum_{k_1,k_2=0}^{d-1} e_{in} \omega^{k_1(k_2+n_z-1)} X_0^{-k_1} Z_0^{-k_2} \otimes |k_1 \oplus n_x\rangle \langle k_1|_1 \otimes |k_2 \oplus n_z\rangle \langle k_2|_2 \ .
\end{aligned}
\qquad \text{(I.28)}
$$

Now let us consider the initial state

$$\rho_{in} = \rho_0 \otimes |0\rangle\langle 0|_1 \otimes |0\rangle\langle 0|_2 \,, \tag{I.29}$$

where ρ_0 is an arbitrary state for the target qudit. The output of our circuit will be the state

$$\begin{aligned}
\rho_{out} =& \sum_i K_i \rho_{in} K_i^\dagger \\
=& \sum_i \Bigg(\sum_{n\in\mathbb{Z}_d^2} \sum_{k_1,k_2=0}^{d-1} e_{in}\omega^{k_1(k_2+n_z-1)} X_0^{-k_1} Z_0^{-k_2} \\
& \otimes |k_1 \oplus n_x\rangle \langle k_1|_1 \otimes |k_2 \oplus n_z\rangle \langle k_2|_2 \Bigg) \Big(\rho_0 \otimes |0\rangle\langle 0|_1 \otimes |0\rangle\langle 0|_2 \Big) \\
& \Bigg(\sum_{m\in\mathbb{Z}_d^2} \sum_{j_1,j_2=0}^{d-1} e_{im}^* \omega^{-j_1(j_2+m_z-1)} Z_0^{j_2} X_0^{j_1} \otimes |j_1\rangle \langle j_1 \oplus m_x|_1 \otimes |j_2\rangle \langle j_2 \oplus m_z|_2 \Bigg) \\
=& \sum_i \sum_{n,m\in\mathbb{Z}_d^2} \sum_{k_1,k_2,j_1,j_2=0}^{d-1} e_{in} e_{im}^* \omega^{k_1(k_2+n_z-1)} \omega^{-j_1(j_2+m_z-1)} \\
& \cdot \Big(X_0^{-k_1} Z_0^{-k_2} \rho_0 Z_0^{j_2} X_0^{j_1} \Big) \otimes \Big(|k_1 \oplus n_x\rangle \langle k_1|0\rangle\langle 0|j_1\rangle \langle j_1 \oplus m_x|_1 \Big) \\
& \otimes \Big(|k_2 \oplus n_z\rangle \langle k_2|0\rangle\langle 0|j_2\rangle \langle j_2 \oplus m_z|_2 \Big) \\
=& \sum_i \sum_{n,m\in\mathbb{Z}_d^2} \sum_{k_1,k_2,j_1,j_2=0}^{d-1} e_{in} e_{im}^* \omega^{k_1(k_2+n_z-1)} \omega^{-j_1(j_2+m_z-1)} \Big(X_0^{-k_1} Z_0^{-k_2} \rho_0 Z_0^{j_2} X_0^{j_1} \Big) \\
& \otimes \delta_{k_1,0}\delta_{j_1,0}\delta_{k_2,0}\delta_{j_2,0} \Big(|k_1 \oplus n_x\rangle \langle j_1 \oplus m_x|_1 \Big) \otimes \Big(|k_2 \oplus n_z\rangle \langle j_2 \oplus m_z|_2 \Big) \\
=& \sum_i \sum_{n,m\in\mathbb{Z}_d^2} e_{in} e_{im}^* \rho_0 \otimes |n_x\rangle \langle m_x|_1 \otimes |n_z\rangle \langle m_z|_2 \\
=& \sum_{n,m\in\mathbb{Z}_d^2} \Big(\sum_i e_{in} e_{im}^* \Big) \rho_0 \otimes |n_x\rangle \langle m_x|_1 \otimes |n_z\rangle \langle m_z|_2 \\
=& \sum_{n,m\in\mathbb{Z}_d^2} \chi_{nm} \rho_0 \otimes |n\rangle \langle m|_{12} \\
=& \rho_0 \otimes \Bigg(\sum_{n,m\in\mathbb{Z}_d^2} \chi_{nm} |n\rangle \langle m|_{12} \Bigg) \\
=& \rho_0 \otimes \chi_{12} \,,
\end{aligned} \tag{I.30}$$

where $|n\rangle_{12} = |n_x\rangle_1 \otimes |n_z\rangle_2$.

Thus, we have showed that for the input state in Eq. (I.1), the circuit keeps the initial target state invariant and outputs the process matrix χ associated to $\mathcal{E}$ as the state of the control system.

Appendix J

Reduced density matrix right before and after $\mathcal{E}$ in our circuit

J.1 Before $\mathcal{E}$

Firstly, let us calculate the joint state of the system right *before* the application of $\mathcal{E}$. It is given by

$$\rho^{(3)} = V \rho_{in} V^\dagger \,, \tag{J.1.1}$$

where

$$V = \frac{1}{d} \sum_{j_1,j_2,k_1,k_2=0}^{d-1} \omega^{j_1 k_1} \omega^{j_2 k_2} \omega^{-j_2(j_1+1)} X_0^{j_2} Z_0^{-j_1-1} \otimes |j_1\rangle \langle k_1|_1 \otimes |j_2\rangle \langle k_2|_2 \tag{J.1.2}$$

is the composition of all the unitaries in the circuit before $\mathcal{E}$ (cf. Eq. (I.18)) and

$$\rho_{in} = \rho_0 \otimes |0\rangle\langle 0|_1 \otimes |0\rangle\langle 0|_2 \tag{J.1.3}$$

is the initial state of the circuit according to Eq. (3.4.8). Thus,

$$
\begin{aligned}
\rho^{(3)} &= \frac{1}{d^2}\left(\sum_{j_1,j_2,k_1,k_2=0}^{d-1} \omega^{j_1k_1}\omega^{j_2k_2}\omega^{-j_2(j_1+1)} X_0^{j_2} Z_0^{-j_1-1} \otimes |j_1\rangle\langle k_1|_1 \otimes |j_2\rangle\langle k_2|_2\right) \\
&\quad \left(\rho_0 \otimes |0\rangle\langle 0|_1 \otimes |0\rangle\langle 0|_2\right) \\
&\quad \left(\sum_{p_1,p_2,q_1,q_2=0}^{d-1} \omega^{-p_1q_1}\omega^{-p_2q_2}\omega^{+p_2(p_1+1)} Z_0^{p_1+1} X_0^{-p_2} \otimes |q_1\rangle\langle p_1|_1 \otimes |q_2\rangle\langle p_2|_2\right) \\
&= \frac{1}{d^2}\sum_{j_1,j_2,k_1,k_2,p_1,p_2,q_1,q_2=0}^{d-1} \omega^{j_1k_1}\omega^{j_2k_2}\omega^{-j_2(j_1+1)}\omega^{-p_1q_1}\omega^{-p_2q_2}\omega^{+p_2(p_1+1)} \\
&\quad \left(X_0^{j_2} Z_0^{-j_1-1}\rho_0 Z_0^{p_1+1} X_0^{-p_2}\right) \otimes |j_1\rangle\langle k_1|0\rangle\langle 0|q_1\rangle\langle p_1|_1 \otimes |j_2\rangle\langle k_2|0\rangle\langle 0|q_2\rangle\langle p_2|_2 \\
&= \frac{1}{d^2}\sum_{j_1,j_2,p_1,p_2=0}^{d-1} \omega^{-j_2(j_1+1)}\omega^{+p_2(p_1+1)}\left(X_0^{j_2} Z_0^{-j_1-1}\rho_0 Z_0^{p_1+1} X_0^{-p_2}\right) \\
&\quad \otimes |j_1\rangle\langle p_1|_1 \otimes |j_2\rangle\langle p_2|_2 \ . \qquad \text{(J.1.4)}
\end{aligned}
$$

Now let us calculate the reduced density matrices:

J.1.1 Reduced density matrix of the target:

$$
\begin{aligned}
\rho_0^{(3)} &= Tr_{12}\left[\rho^{(3)}\right] \\
&= \frac{1}{d^2}\sum_{j_1,j_2,p_1,p_2=0}^{d-1} \omega^{-j_2(j_1+1)}\omega^{+p_2(p_1+1)}\left(X_0^{j_2} Z_0^{-j_1-1}\rho_0 Z_0^{p_1+1} X_0^{-p_2}\right) \\
&\quad Tr\left[\,|j_1\rangle\langle p_1|\,\right] Tr\left[\,|j_2\rangle\langle p_2|\,\right] \\
&= \frac{1}{d^2}\sum_{j_1,j_2,p_1,p_2=0}^{d-1} \omega^{-j_2(j_1+1)}\omega^{+p_2(p_1+1)}\left(X_0^{j_2} Z_0^{-j_1-1}\rho_0 Z_0^{p_1+1} X_0^{-p_2}\right)\delta_{j_1p_1}\delta_{j_2p_2} \\
&= \frac{1}{d^2}\sum_{j_1,j_2=0}^{d-1} \omega^{-j_2(j_1+1)}\omega^{+j_2(j_1+1)}\left(X_0^{j_2} Z_0^{-j_1-1}\rho_0 Z_0^{j_1+1} X_0^{-j_2}\right) \\
&= \frac{1}{d^2}\sum_{j_1,j_2=0}^{d-1} X_0^{j_2} Z_0^{-j_1-1}\rho_0 Z_0^{j_1+1} X_0^{-j_2} \qquad \text{(J.1.5)}
\end{aligned}
$$

Writing ρ_0 as

$$\rho_0 = \sum_{m,n=0}^{d-1} \rho_{m,n} |m\rangle\langle n| \,, \tag{J.1.6}$$

we have

$$\begin{aligned}
\rho_0^{(3)} &= \frac{1}{d^2} \sum_{j_1,j_2,m,n=0}^{d-1} \rho_{m,n} X_0^{j_2} Z_0^{-j_1-1} |m\rangle\langle n| Z_0^{j_1+1} X_0^{-j_2} \\
&= \frac{1}{d^2} \sum_{j_1,j_2,m,n=0}^{d-1} \rho_{m,n} \omega^{(n-m)(j_1+1)} X_0^{j_2} |m\rangle\langle n| X_0^{-j_2} \\
&= \frac{1}{d^2} \sum_{j_2,m,n=0}^{d-1} \rho_{m,n} \sum_{j_1=0}^{d-1} \left(\omega^{(n-m)(j_1+1)}\right) |m \oplus j_2\rangle\langle n \oplus j_2| \\
&= \frac{1}{d^2} \sum_{j_2,m,n=0}^{d-1} \rho_{m,n} d\delta_{m,n} |m \oplus j_2\rangle\langle n \oplus j_2| \\
&= \frac{1}{d} \sum_{j_2,m=0}^{d-1} \rho_{m,m} |m \oplus j_2\rangle\langle m \oplus j_2| \\
&= \frac{1}{d} \left(\sum_{m=0}^{d-1} \rho_{m,m}\right) \left(\sum_{j=0}^{d-1} |j\rangle\langle j|\right) \\
&= \frac{I}{d} \,,
\end{aligned} \tag{J.1.7}$$

where we changed the summation index j_2 by $j = m \oplus j_2$ and used the fact that $Tr[\rho_0] = \sum_m \rho_{m,m} = 1$.

J.1.2 Reduced density matrix of the control:

$$\begin{aligned}
\rho_{12}^{(3)} &= Tr_0[\rho^{(3)}] \\
&= \frac{1}{d^2} \sum_{j_1,j_2,p_1,p_2=0}^{d-1} \omega^{-j_2(j_1+1)} \omega^{+p_2(p_1+1)} Tr\left[X_0^{j_2} Z_0^{-j_1-1} \rho_0 Z_0^{p_1+1} X_0^{-p_2}\right] \\
&\quad |j_1\rangle\langle p_1|_1 \otimes |j_2\rangle\langle p_2|_2 \\
&= \frac{1}{d^2} \sum_{j_1,j_2,p_1,p_2,m,n=0}^{d-1} \rho_{m,n} \omega^{-j_2(j_1+1)} \omega^{+p_2(p_1+1)} Tr\left[X_0^{j_2} Z_0^{-j_1-1} |m\rangle\langle n| Z_0^{p_1+1} X_0^{-p_2}\right] \\
&\quad |j_1\rangle\langle p_1|_1 \otimes |j_2\rangle\langle p_2|_2
\end{aligned}$$

$$
\begin{aligned}
&= \frac{1}{d^2} \sum_{j_1,j_2,p_1,p_2,m,n=0}^{d-1} \rho_{m,n} \omega^{-(j_2+m)(j_1+1)} \omega^{(p_2+n)(p_1+1)} Tr\left[|j_2 \oplus m\rangle\langle p_2 \oplus n|\right] \\
&\quad |j_1\rangle \langle p_1|_1 \otimes |j_2\rangle \langle p_2|_2 \\
&= \frac{1}{d^2} \sum_{j_1,j_2,p_1,p_2,m,n=0}^{d-1} \rho_{m,n} \omega^{-(j_2+m)(j_1+1)} \omega^{(p_2+n)(p_1+1)} \delta_{j_2\oplus m, p_2 \oplus n} \\
&\quad |j_1\rangle \langle p_1|_1 \otimes |j_2\rangle \langle p_2|_2 \\
&= \frac{1}{d^2} \sum_{j_1,j_2,p_1,p_2,m=0}^{d-1} \rho_{m,m\oplus j_2 \ominus p_2} \omega^{(j_2+m)(p_1-j_1)} |j_1\rangle \langle p_1|_1 \otimes |j_2\rangle \langle p_2|_2 \ . \qquad \text{(J.1.8)}
\end{aligned}
$$

If we change the index $j_2' = j_2 \oplus m$ and then $p_2' = j_2' \ominus p_2$, we get

$$
\rho_{12}^{(3)} = \frac{1}{d^2} \sum_{j_1,j_2',p_1,p_2',m=0}^{d-1} \rho_{m,p_2'} \omega^{j_2'(p_1-j_1)} |j_1\rangle \langle p_1|_1 \otimes |j_2' \ominus m\rangle \langle j_2' \ominus p_2'|_2 \ , \qquad \text{(J.1.9)}
$$

or equivalently,

$$
\rho_{12}^{(3)} = \frac{1}{d^2} \sum_{p,q,m,n,k=0}^{d-1} \rho_{m,n} \omega^{k(q-p)} |p\rangle \langle q|_1 \otimes |k \ominus m\rangle \langle k \ominus n|_2 \ . \qquad \text{(J.1.10)}
$$

J.1.3 Reduced density matrix of control 1:

$$
\begin{aligned}
\rho_1^{(3)} &= Tr_2\left[\rho_{12}^{(3)}\right] \\
&= \frac{1}{d^2} \sum_{p,q,m,n,k=0}^{d-1} \rho_{m,n} \omega^{k(q-p)} |p\rangle \langle q|_1 \delta_{m,n} \\
&= \frac{1}{d^2} \sum_{p,q=0}^{d-1} \left(\sum_{m=0}^{d-1} \rho_{m,m} \right) \left(\sum_{k=0}^{d-1} \omega^{k(q-p)} \right) |p\rangle \langle q|_1 \\
&= \frac{1}{d^2} \sum_{p,q=0}^{d-1} d\delta_{p,q} |p\rangle \langle q|_1 \\
&= \frac{I}{d} \ . \qquad \text{(J.1.11)}
\end{aligned}
$$

J.1.4 Reduced density matrix of control 2:

$$\begin{aligned}
\rho_2^{(3)} &= Tr_1\left[\rho_{12}^{(3)}\right] \\
&= \frac{1}{d^2}\sum_{p,q,m,n,k=0}^{d-1}\rho_{m,n}\omega^{k(q-p)}\delta_{p,q}\left|k\ominus m\right\rangle\left\langle k\ominus n\right|_2 \\
&= \frac{1}{d^2}\sum_{p,m,n,k=0}^{d-1}\rho_{m,n}\left|k\ominus m\right\rangle\left\langle k\ominus n\right|_2 \\
&= \frac{1}{d}\sum_{m,n,k=0}^{d-1}\rho_{m,n}\left|k\ominus m\right\rangle\left\langle k\ominus n\right|_2 \\
&= \frac{1}{d}\sum_{m,n=0}^{d-1}\rho_{m,n}\left(\sum_{k=0}^{d-1}\left|k\ominus m\right\rangle\left\langle k\ominus n\right|_2\right) \\
&= \frac{1}{d}\sum_{m,n=0}^{d-1}\rho_{m,n}X^{n-m}\ . \qquad \text{(J.1.12)}
\end{aligned}$$

J.2 After $\mathcal{E}$

Now we can easily calculate the reduced density matrices immediately *after* the application of $\mathcal{E}$.

J.2.1 Reduced density matrix of the target:

$$\begin{aligned}
\rho_0^{(4)} &= Tr_{12}\left[(\mathcal{E}\otimes\mathcal{I}_{12})(\rho^{(3)})\right] \\
&= \mathcal{E}\left(Tr_{12}[\rho^{(3)})]\right) \\
&= \mathcal{E}\left(\rho_0^{(3)})\right) \\
&= \frac{1}{d}\mathcal{E}\left(I\right)\ . \qquad \text{(J.2.1)}
\end{aligned}$$

Here we have used the fact that $\mathcal{E}$ is applied only on the target system, so it commutes with the partial trace applied on the control system. Notice that, in particular,

$$\rho_0^{(4)} = \frac{I}{d} \qquad \text{(J.2.2)}$$

when $\mathcal{E}$ is unital.

J.2.2 Reduced density matrix of the control:

$$\begin{aligned}\rho_{12}^{(4)} &= Tr_0\left[(\mathcal{E}\otimes\mathcal{I}_{12})(\rho^{(3)})\right]\\ &= Tr_0\left[\rho^{(3)}\right]\\ &= \rho_{12}^{(3)}\,,\end{aligned} \tag{J.2.3}$$

where we have used the fact that $\mathcal{E}$ is trace-preserving, so $Tr_0\circ\mathcal{E} = Tr_0$. Consequently, according to Eqs. (J.1.8), (J.1.11) and (J.1.12), we have:

$$\rho_{12}^{(4)} = \frac{1}{d^2}\sum_{p,q,m,n,k=0}^{d-1}\rho_{m,n}\omega^{k(q-p)}\left|p\right\rangle\left\langle q\right|_1\otimes\left|k\ominus m\right\rangle\left\langle k\ominus n\right|_2\,, \tag{J.2.4}$$

$$\rho_1^{(4)} = \frac{I}{d}\,, \tag{J.2.5}$$

$$\rho_2^{(4)} = \frac{1}{d}\sum_{m,n=0}^{d-1}\rho_{m,n}X^{n-m}\,. \tag{J.2.6}$$

We can see that the information about the initial state ρ_0 of the target system is present in the control system and it can be partially recovered from $\rho_2^{(4)}$ alone. The amount of information in the second control depends on which is the state ρ_0. Here we specify two cases:

- If ρ_0 is diagonal, then $\rho_{m,n}=0$ for $m\neq n$. Hence,

$$\begin{aligned}\rho_2^{(4)} &= \frac{1}{d}\sum_{m=0}^{d-1}\rho_{m,m}X^0\\ &= \frac{I}{d}\,.\end{aligned} \tag{J.2.7}$$

  In this case, no information about ρ_0 is available in the second control alone.

- If ρ_0 is an eigenstate of X, i.e., if

$$\rho_0=\sigma_k:=\left|\phi_k\right\rangle\left\langle\phi_k\right|\,,\text{for } k=0,...d-1\,, \tag{J.2.8}$$

with $|\phi_k\rangle$ satisfying

$$X\,|\phi_k\rangle = \alpha_k\,|\phi_k\rangle \ , \tag{J.2.9}$$

with $\alpha_k \in \mathbb{C}$, then we can show that $\rho_2^{(4)}$ is another eigenstate of X. Firstly, we will show that the eigenvectors of X have the form

$$|\phi_k\rangle = F\,|k\rangle \ \text{, with } k = 0, ..., d-1 \ , \tag{J.2.10}$$

with corresponding eigenvalues

$$\alpha_k = \omega^{-k} \ . \tag{J.2.11}$$

Indeed,

$$\begin{aligned}
X\,|\phi_n\rangle &= XF\,|n\rangle \\
&= X\frac{1}{\sqrt{d}}\sum_{j,k=0}^{d-1}\omega^{jk}\,|j\rangle\,\langle k|n\rangle \\
&= X\frac{1}{\sqrt{d}}\sum_{j=0}^{d-1}\omega^{jn}\,|j\rangle \\
&= \frac{1}{\sqrt{d}}\sum_{j=0}^{d-1}\omega^{jn}\,|j\oplus 1\rangle \\
&= \frac{1}{\sqrt{d}}\sum_{j=0}^{d-1}\omega^{(j-1)n}\,|j\rangle \\
&= \omega^{-n}\frac{1}{\sqrt{d}}\sum_{j=0}^{d-1}\omega^{jn}\,|j\rangle \\
&= \omega^{-n}F\,|n\rangle \\
&= \omega^{-n}\,|\phi_n\rangle \ .
\end{aligned} \tag{J.2.12}$$

Now, for the state σ_k, we have

$$\begin{aligned}
\rho_2^{(4)} &= \frac{1}{d}\sum_{m,n=0}^{d-1}\langle m|\,\sigma_k\,|n\rangle\,X^{n-m} \\
&= \frac{1}{d}\sum_{m,n=0}^{d-1}\langle m|\phi_k\rangle\langle\phi_k|n\rangle X^{n-m}
\end{aligned}$$

$$
\begin{aligned}
&= \frac{1}{d}\sum_{m,n=0}^{d-1} \langle m|\phi_k\rangle \langle\phi_k| X^{n-m} |m\rangle X^{n-m} \\
&= \frac{1}{d}\sum_{m,n=0}^{d-1} \langle\phi_k| X^{n-m} |m\rangle \langle m|\phi_k\rangle X^{n-m} \\
&= \frac{1}{d}\sum_{m,j=0}^{d-1} \langle\phi_k| X^{j} |m\rangle \langle m|\phi_k\rangle X^{j} \\
&= \frac{1}{d}\sum_{j=0}^{d-1} \langle\phi_k| X^{j} |\phi_k\rangle X^{j} \\
&= \frac{1}{d}\sum_{j=0}^{d-1} \omega^{-kj} X^{j} \ . \qquad \text{(J.2.13)}
\end{aligned}
$$

Noticing that X can be written in its diagonal form as

$$X = \sum_{m=0}^{d-1} \omega^{-m} |\phi_m\rangle\langle\phi_m| \ , \qquad \text{(J.2.14)}$$

hence

$$X^j = \sum_{m=0}^{d-1} \omega^{-jm} |\phi_m\rangle\langle\phi_m| \ , \qquad \text{(J.2.15)}$$

we have

$$
\begin{aligned}
\rho_2^{(4)} &= \frac{1}{d}\sum_{j,m=0}^{d-1} \omega^{-j(k+m)} |\phi_m\rangle\langle\phi_m| \\
&= \frac{1}{d}\sum_{m=0}^{d-1} d\delta_{m,\ominus k} |\phi_m\rangle\langle\phi_m| \\
&= |\phi_{\ominus k}\rangle\langle\phi_{\ominus k}| \\
&= \sigma_{\ominus k} \ . \qquad \text{(J.2.16)}
\end{aligned}
$$

Thus, if ρ_0 is an eigenstate of X, the reduced state of control 2 will be another eigenstate of X, specifically the one with conjugate eigenvalue.

Appendix K

Relation between the Choi operator and the process matrix of a quantum channel.

Given a quantum channel $\mathcal{E}$, its Choi operator is defined as

$$\tilde{C}_{\mathcal{E}} := \mathcal{E} \otimes \mathcal{I}(|\tilde{\Phi}\rangle\langle\tilde{\Phi}|) \,, \tag{K.1}$$

where

$$\left|\tilde{\Phi}\right\rangle = \sum_{i=0}^{d-1} |i\rangle \otimes |i\rangle \ . \tag{K.2}$$

We can also normalize $\left|\tilde{\Phi}\right\rangle$ in order to make it a quantum state, as

$$|\Phi\rangle = \frac{1}{\sqrt{d}} \sum_{i=0}^{d-1} |i\rangle \otimes |i\rangle \ , \tag{K.3}$$

and get a normalized Choi operator

$$C_{\mathcal{E}} = \frac{1}{d} \sum_{i,j=0}^{d-1} \mathcal{E}(|i\rangle\langle j|) \otimes |i\rangle\langle j| \,. \tag{K.4}$$

The most relevant characteristic of the Choi operator is that it completely represents a quantum channel, since it is a block matrix indicating the action of the channel on any element $|i\rangle\langle j|$ of the standard basis of the space of operators.

Now let us consider the Choi circuit showed in Fig. 3.4.2. The outcome state is exactly the normalized Choi operator. We can complement this result and complete the Bell-Choi circuit in Fig. 3.4.3. Firstly, we expand Eq. (K.4) in terms of the elements of the χ matrix, following Eq. (3.4.4):

$$C_{\mathcal{E}} = \frac{1}{d} \sum_{i,j=0}^{d-1} \sum_{m,n=0}^{d^2-1} \chi_{mn} \tilde{E}_m |i\rangle\langle j| \tilde{E}_n^\dagger \otimes |i\rangle\langle j| \ . \tag{K.5}$$

Using the Weyl-Heisenberg basis in Eq. (3.4.7), and writing

$$\tilde{E}_n = X^{n_x} Z^{n_z} \ , \tag{K.6}$$

we have

$$C_{\mathcal{E}} = \frac{1}{d} \sum_{i,j,m_x,m_z,n_x,n_z=0}^{d-1} \chi_{m_x m_z n_x n_z} X^{m_x} Z^{m_z} |i\rangle\langle j| Z^{-n_z} X^{-n_x} \otimes |i\rangle\langle j| \ . \tag{K.7}$$

Then, following the Choi-Bell circuit:

$$\begin{aligned}
C'_{\mathcal{E}} &= X_{12}^{\dagger(0)} C_{\mathcal{E}} X_{12}^{(0)} \\
&= \left(\sum_{k_1=0}^{d-1} X^{-k_1} \otimes |k_1\rangle\langle k_1| \right) \\
&\quad \left(\frac{1}{d} \sum_{i,j,m_x,m_z,n_x,n_z=0}^{d-1} \chi_{m_x m_z n_x n_z} X^{m_x} Z^{m_z} |i\rangle\langle j| Z^{-n_z} X^{-n_x} \otimes |i\rangle\langle j| \right) \\
&\quad \left(\sum_{k_2=0}^{d-1} X^{k_2} \otimes |k_2\rangle\langle k_2| \right) \\
&= \frac{1}{d} \sum_{k_1,k_2,i,j,m_x,m_z,n_x,n_z=0}^{d-1} \chi_{m_x m_z n_x n_z} X^{m_x - k_1} Z^{m_z} |i\rangle\langle j| Z^{-n_z} X^{-n_x + k_2} \\
&\quad \otimes |k_1\rangle \langle k_1|i\rangle\langle j|k_2\rangle \langle k_2| \\
&= \frac{1}{d} \sum_{i,j,m_x,m_z,n_x,n_z=0}^{d-1} \chi_{m_x m_z n_x n_z} X^{m_x - i} Z^{m_z} |i\rangle\langle j| Z^{-n_z} X^{-n_x + j} \otimes |i\rangle \langle j| \ .
\end{aligned} \tag{K.8}$$

Finally, applying the Fourier inverse on the second qudit,

$$
\begin{aligned}
C''_{\mathcal{E}} &= (I \otimes F^{-1}) C'_{\mathcal{E}} (I \otimes F) \\
&= \frac{1}{d} \sum_{i,j,m_x,m_z,n_x,n_z=0}^{d-1} \chi_{m_x m_z n_x n_z} X^{m_x - i} Z^{m_z} |i\rangle\langle j| Z^{-n_z} X^{-n_x + j} \otimes F^{-1} |i\rangle \langle j| F \\
&= \frac{1}{d} \sum_{i,j,m_x,m_z,n_x,n_z=0}^{d-1} \chi_{m_x m_z n_x n_z} \omega^{m_z i - n_z j} |m_x\rangle\langle n_x| \\
&\quad \otimes \frac{1}{d} \sum_{k_1=0}^{d-1} \omega^{-k_1 i} |k_1\rangle \langle k_2| \sum_{k_2=0}^{d-1} \omega^{k_2 j} \\
&= \frac{1}{d^2} \sum_{k_1,k_2,i,j,m_x,m_z,n_x,n_z=0}^{d-1} \chi_{m_x m_z n_x n_z} \omega^{m_z i - n_z j - k_1 i + k_2 j} |m_x\rangle\langle n_x| \otimes |k_1\rangle \langle k_2| \\
&= \frac{1}{d^2} \sum_{k_1,k_2,m_x,m_z,n_x,n_z=0}^{d-1} \chi_{m_x m_z n_x n_z} \left(\sum_{i=0}^{d-1} \omega^{i(m_z - k_1)} \right) \left(\sum_{j=0}^{d-1} \omega^{j(k_2 - n_z)} \right) \\
&\quad |m_x\rangle\langle n_x| \otimes |k_1\rangle \langle k_2| \\
&= \frac{1}{d^2} \sum_{k_1,k_2,m_x,m_z,n_x,n_z=0}^{d-1} \chi_{m_x m_z n_x n_z} d^2 \delta_{m_z,k_1} \delta_{k_2,n_z} |m_x\rangle\langle n_x| \otimes |k_1\rangle \langle k_2| \\
&= \sum_{m_x,m_z,n_x,n_z=0}^{d-1} \chi_{m_x m_z n_x n_z} |m_x\rangle\langle n_x| \otimes |m_z\rangle \langle n_z| \\
&= \sum_{m,n=0}^{d-1} \chi_{mn} |m\rangle\langle n| \\
&= \chi \,, \qquad \text{(K.9)}
\end{aligned}
$$

where we have used $|m\rangle = |m_x\rangle \otimes |m_z\rangle$.

Thus, the Choi-Bell circuit leads to a final state which is equal to the χ matrix of $\mathcal{E}$ when the Weyl-Heisenberg basis is considered.